UNIVERSITY OF CALIFORNIA
RIVERSIDE

Exploring the Dynamics of Fluorescence Staining of Bacteria with Cyanine Dyes for the Development of Kinetic Assays

A Dissertation submitted in partial satisfaction
of the requirement for the Degree of

Doctor of Philosophy

in

Bioengineering

by

Marlon Sheldon Thomas

August 2010

Dissertation Committee:
- Dr. Valentine Vullev, Chairperson
- Dr. Victor Rodgers
- Dr. Jerome Schultz
- Dr. Neal Schiller

The Dissertation of Marlon Sheldon Thomas is approved:

Committee Chairperson: Valentine I. Vullev

University of California, Riverside

ABSTRACT OF THE DISSERTATION

Exploring the Dynamics of Fluorescence Staining of Bacteria with Cyanine Dyes for the Development of Kinetic Assays

by

Marlon Sheldon Thomas

Doctor of Philosophy, Graduate Program in Bioengineering
University of California, Riverside, August 2010
Dr. Valentine Vullev, Chairperson

Bacterial infections continue to be one of the major health risks in the United States. The common occurrence of such infection is one of the major contributors to the high cost of health care and significant patient mortality. The work presented in this thesis describes spectroscopic studies that will contribute to the development of a fluorescent assay that may allow the rapid identification of bacterial species. Herein, the optical interactions between six bacterial species and a series of thiacyanine dyes are investigated. The interactions between the dyes and the bacterial species are hypothesized to be species-specific. For this thesis, two Gram-negative strains, *Escherichia coli (E. coli)* TOP10 and *Enterobacter aerogenes*; two Gram-positive bacterial strains, *Bacillus sphaericus* and *Bacillus subtilis;* and two *Bacillus* endospores, *B. globigii* and *B. thuringiensis*, were used to test the proposed hypothesis. A series of three thiacyanine dyes—3,3'-diethylthiacyanine iodide

(THIA), 3,3'-diethylthiacarbocyanine iodide (THC) and thiazole orange (THO)—were used as fluorescent probes. The basis of our spectroscopic study was to explore the bacterium-induced interactions of the bacterial cells with the individual thiacyanine dyes or with a mixture of the three dyes. Steady-state absorption spectroscopy revealed that the different bacterial species altered the absorption properties of the dyes. Mixed-dye solutions gave unique absorption patterns for each bacteria tested, with competitive binding observed between the bacteria and spectrophotometric probes (thiacyanine dyes). Emission spectroscopy recorded changes in the emission spectra of THIA following the introduction of bacterial cells. Experimental results revealed that the emission enhancement of the dyes resulted from increases in the emission quantum yield of the thiacyanine dyes upon binding to the bacteria cellular components. The recorded emission enhancement data were fitted to an exponential (mono-exponential or bi-exponential) function, and time constants were extracted by regressing on the experimental data. The addition of the TWEEN surfactants decreased the rate at which the dyes interacted with the bacterial cells, which typically resulted in larger time constants derived from an exponential fit. ANOVA analysis of the time constants confirmed that the values of the time constants clustered in a narrow range and were independent of dye concentration and weakly dependent on cell density.

Table of contents

List of Schemes

List of Tables

List of Figures

List of Equations

Chapter 1

Absorption and Fluorescence Properties of Cyanine Dyes in the Presence of Bacteria

Abstract

The Gram staining technique, developed over a century ago, led to colorimetric and fluorescence staining becoming the foundation for a bacterial detection. The dynamics of such staining processes, however, remain largely unexplored. This chapter investigated the bacterium-induced changes to the steady-state absorption and the steady-state emission spectra of thiacyanine dyes. The dyes examined in this study were: 3,3'-diethylthiacyanine iodide (THIA), 3,3'-diethylthiacarbocyanine iodide (THC) and thiazole orange (THO). The addition of bacterial cells to each of the three dye solutions resulted in an uptake of the dye by the cells, with the process reaching saturation within approximately 10 minutes. THIA was used as a model dye because it had a large molar extinction coefficient of approximately 120,000 $cm^{-1}M^{-1}$. THIA also displayed the greatest sensitivity to the addition of the bacterial cells with emission enhancements of up to 1 count per second (CPS) per cell. In this chapter, we will analyze the steady-state absorption and emission spectra of THIA with and without the addition of two Gram-negative bacteria, *Escherichia coli* (*E. coli*) TOP10 and *Enterobacter aerogenes (E. aerogenes)*; and two Gram-positive vegetative bacterial species, *Bacillus subtilis (B. subtilis)* and *Bacillus sphaericus (B. sphaericus)*, as model organisms. Bacterium-induced changes to the steady-state

absorption spectra of THIA were also monitored, with and without the introduction of endospores from *B. globigii* and *B. thuringiensis*. The *Bacillus* endospores displayed orders-of-magnitude emission enhancement when introduced to each of the thiacyanine dye solutions. Furthermore, we determined that the observed emission enhancement was a corollary from an increase in the fluorescence quantum yield of THIA, which resulted from an increase in the rigidity of the molecular microenvironment.

1.1. Introduction

This chapter describes the photo-physical investigation of the interaction between thiacyanine dyes and a series of model bacterial species. Here we use absorption and emission spectroscopy to evaluate bacterium-induced changes of the spectral properties of the dyes. We observed a decrease of up to 50% in the molar extinction coefficients of the cyanine dyes upon binding to bacterial cells.[1] Concurrently, the uptake by the bacteria caused a significant increase in the fluorescence intensity of the dyes. Based on the observed absorption and emission trends, we ascribed the bacterium-induced enhancement of the fluorescence to an increase in the fluorescence quantum yield of the thiacyanine dyes when taken up by the cells.

1.1.1. Background and motivation.

Bacterial infections are common and are responsible for thousands of fatalities annually in the United States.[1] The ability to detect and identify bacteria rapidly is important for diagnosis and treatment for bacteria-induced infectious diseases.[2] A report published by the United States Centers for Disease Control and Prevention (CDC) in the New England Journal of Medicine indicated that nearly 19,000 fatalities occurred in the United States in 2005 due to infections from virulent drug-resistant bacteria.[1, 3, 4] The CDC also reported that approximately 1.7 million cases of bacteria-related healthcare infections occurred in the United States in 2002; of these illnesses, approximately 100,000 resulted in fatalities.[3, 4]

Even well equipped laboratories can take up to 72 hours to positively identify an unknown microbial pathogen.[5] Patients are often treated with inappropriate antibiotics while the infections persist.[6] Besides having no benefit for the patient's health, such treatments may lead to the buildup of antibiotic-resistant strains. For example, the percentage of healthcare-associated *Staphylococcus aureus* (staph) infections caused by Methicillin-resistant *S. aureus* increased from 2% in 1974 to 64% in 2008.[1, 7, 8] Increases in the frequency of drug-resistant bacterial strains have been largely attributed to the over-prescription of antibiotics.[9-18] Rapid yet accurate identification of bacterial species has the potential to improve the diagnosis and treatment of bacterial infections by ensuring that doctors have the appropriate level of information prior to making their diagnosis.

1.1.2. Bacteria species: vegetative cells and endospores.

Bacteria are members of the prokaryotes (along with archaea), which are single-cell organisms that lack cell nuclei or organelles.[19] Bacteria are traditionally classified into two groups on the basis of their cell wall structure: Gram-negative and Gram-positive.[19] Gram-negative bacterial cells have two cell membranes, while Gram-positive bacterial cells only have a single membrane with a thick cell wall (Scheme 1).[19] Observing the appearance of the cells after Gram staining has traditionally been the method for differentiation between these two types of bacterial cells.[19] Cells that appear red are classified as Gram-negative while cells that appear violet are considered Gram-positive.[20] The Gram-staining technique uses crystal violet (a purple colored dye) to stain all cells in the sample.[20] Gram-positive cells are able to resist decoloration by alcohol.[20] Gram-negative cells, however, are decolored and can then be restained with a counter-stain, typically safarin.[20]

Scheme 1. Cell-wall structure of (a) Gram-positive and (b) Gram-negative bacterial cells.

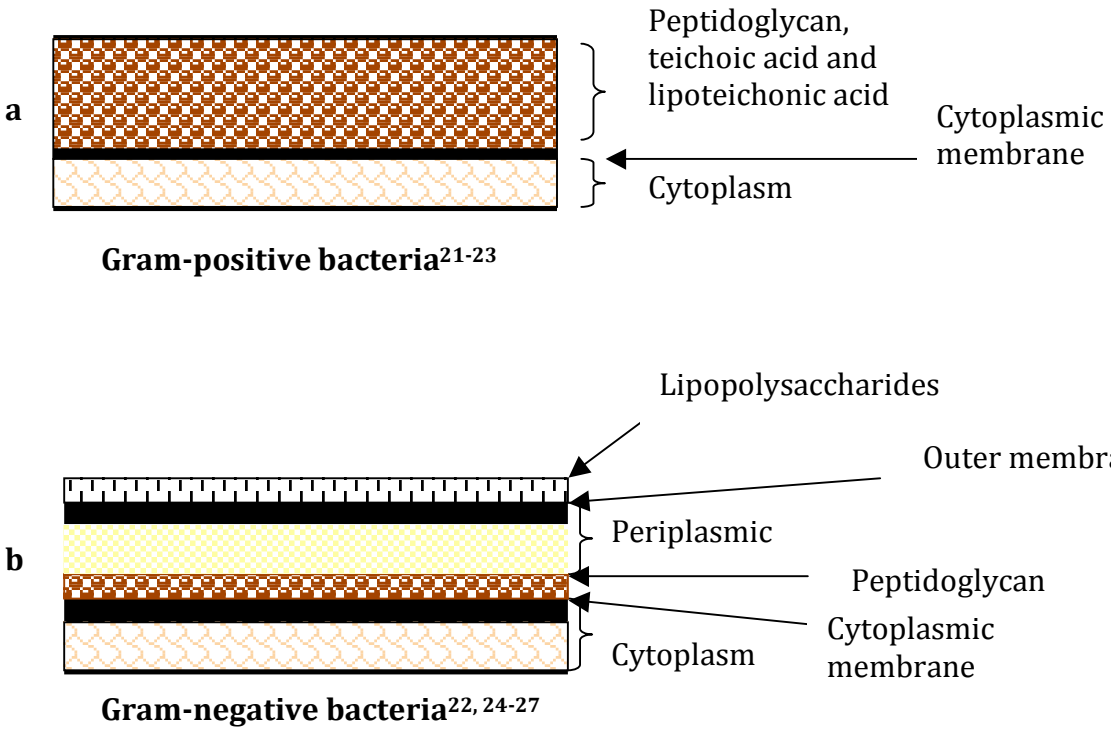

Several Gram-positive bacteria, including but not limited to cells from the genus *Bacillus* and genus *Clostridium*, can exist as either vegetative cells or as endospores.[28] The morphology, size, shape and endogenous metabolism are different between endospores and vegetative cells (Scheme 2.).[29] *Bacillus* are a family of rod-like bacteria that typically measure 1–3 μM in length and are approximately 0.5 μM in width.[30] The typical cell wall of the vegetative cells for *Bacillus* bacteria is 20–40 nm thick.[31] These cells are not particularly rugged and are

easily lysed.[32-34] Consequently, these cells are often used as a recombinant host for producing proteins.[35] Several Gram-positive bacterial cells, including many *Bacillus* species, form endospores when they encounter adverse conditions.[30, 36] Endospores from many *Bacillus* strains can handle extreme conditions.[30] Endospores from pathogenic strains are capable of causing severe illnesses.[37] For example, endospores from the bio-terrorist agent *Bacillus anthracis* can be lethal.[38] The process of a *vegetative bacterial cell* forming an endospore is called "sporulation" while the process of endospores forming vegetative bacterial cells is germenation.[39]

Scheme 2. Schematic of the size, shape and layers of *Bacillus* cells: (a) endospore and (b) vegetative cell.

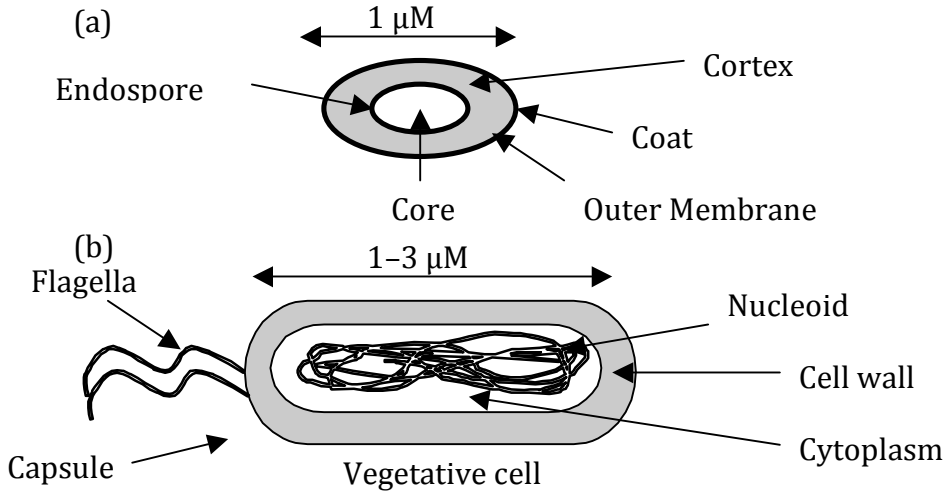

1.1.3. Techniques for identification of bacterial cells.

In the modern healthcare setting, techniques used to identify unknown bacterial species range from culture and biochemical tests to molecular markers (such as real-time PCR, DNA sequencing, and immuno-assays) to cell staining methods that utilize optical microscopy or fluorescence spectroscopy.[2, 40-43] Observation of the cell morphology along with simple or differential staining has been done for over a hundred years.[44] Several general groups of bacteria have been formulated by simple observation of cell shape, size or ability to form bacterial endospores.

Advances in the area of molecular biology have led to the development of molecular techniques for genotyping bacteria.[44] Polymerase chain reaction (PCR) is a powerful tool for identification of bacterial species. PCR involves multiple steps of duplication of the DNA molecule, hence, the targeted sequence are amplified.[2, 45] Amplified DNA can be analyzed via electrophoresis, mass spectrometric other techniques.[8, 46-48] Another state-of-the-art analytical techniques that have been applied to the field of bacteriology are Matrix Assisted Laser Desorption Ionization (MALDI) and Electro-spray Ionization (ESI) mass spectrometry (MS). These mild ionization MS techniques are used for analyzing the bacteria cell-wall composition and allow either lysed bacterial cells or whole organisms to be used for such analysis.[49, 50]

Ever since the development of the Gram staining technique, which was first reported by Carl Friedländer in 1883[51] and detailed a year later by Hans Christian Gram,[51, 52] bio-analytical methodologies for cellular observation and identification have placed principal emphasis on the initial and final appearance of the analyzed cells. Hence, the staining analyses produce only Boolean outcomes, i.e., the reagents either stain or do not stain the analyzed bacteria. As a result, each analysis affords a classification of species only into two groups. Similarly, Boolean assays with improved specificity (such as immuno-fluorescence staining)[40, 42, 53, 54] are informative solely about species that are sought, allowing for analytes that are present in the sample but not targeted by the particular stain to remain undetected.

While the cell-staining methods are economical and produce expedient results, particularly when coupled with morphological examination of the bacterial samples, current methods for cell staining are inherently limited, as they produce only Boolean outcomes (e.g., “stains” vs. “does not stain”). Staining provides limited information about species identification and specifically detects only the species that are sought.[55] Here we demonstrate the spectral features observed upon interaction of cyanine dyes with bacterial cells that may have the potential for the development of rapid non-Boolean method for identification of viable cells by fluorescence staining.[56, 57]

1.1.4. Absorption and fluorescence spectroscopy.

Fluorescence is a type of light emission (i.e., luminescence) resultant from radiative deactivation of the lowest singlet excited state to the singlet ground state of the excited species.[58, 59] Unlike phosphorescence, fluorescence do not involve spin-forbidden transitions: i.e., changes in multiplicity. Therefore, the rate constants of this first-order process (i.e., of fluorescence) are rarely smaller than 10^8 s^{-1}.[58, 59] Via the rate constants of fluorescence, k_f, and the rate constants of the competing non-radiative decays, k_{nd}, the kinetics of deactivation of the excited state are related to the fluorescence quantum yield, Φ_f, which represents the relative number of emitted photons in comparison with the number of absorbed photons (i.e., of generated photo-excited species).

$$\Phi_f = \frac{number\ \ of\ \ emitted\ \ photons}{number\ \ of\ \ absorbed\ \ photons} = \frac{k_f}{k_f + k_{nd}} = \tau\ k_f \qquad \textbf{Equation 1.}$$

The fluorescence lifetime, τ, represents the average time a molecule spends in its excited state from which the radiative decay occurs: $\tau = (k_f + k_{nd})^{-1}$.[58, 59] The fluorescence rate constant, k_f, for organic chromophores depends on their molecular structures and is not sensitive to their environment.[58, 59] However, the rate constant for non-radiative deactivation, represented by k_{nd}, can be highly influenced by the

media. Therefore, it is the k_{nd} that is responsible for emission enhancement or quenching resultant from quantum-yield alterations.[60-62]

In fluorescence imaging, only the light emitted by the samples is collected and the background light does not pass to the detector. Therefore, fluorescence imaging has been established as one of the most sensitive techniques and extensively used for characterization of biological samples.[100]

When performing fluorescent imaging of biological samples, changes in photo-physical properties of the staining chromophores leading to an increase in the fluorescence intensity are immensely beneficial for achieving relatively large contrast ratios.[62-64] The inherent contrast of bacterial cells using brightfield microscopy is poor without using any type of staining because of the similarity in the refractive index of the biological sample and the aqueous-based media used to culture most cells.[64] Since significant changes in the refractive index are needed to achieve high contrast ratios in unstained images, staining techniques have been developed to help researchers observe the heterogeneity of cells.[64] For this reason, fluorescence imaging has been extensively used to label biological samples.[62] One important parameter that influences the fluorescence-image contrast is the partition of the staining agent and its local concentration in the viewed cells.[64] The efficient accumulation of a dye increases its local concentration, C, in the imaged regions and hence increases the amount of light absorbed and emitted from such regions. The amount of absorbed light is directly proportional to the concentration of the stain and is described by Bouguer-Lambert-Beer's law:[58]

$\mathbf{A(\lambda) = \varepsilon(\lambda)\, L\, C}$ **Equation 2.**

Where A is the absorbance of the dye molecules in solution; C is the concentration of the stain; ε is the molar extinction coefficient at the wavelength, l; and L is the thickness of the photo-excited sample (A and ε are wavelength-dependent).[58, 59]

Experiments described in this thesis focus on characterizing the photo-physical properties of a series of thiacyanine dyes upon their interactions with bacterial cells. Our findings revealed that it was the increase in the fluorescence quantum yield (rather than an increase in extinction coefficient at the excitation wavelength) that led to the observed emission enhancement (section 3). Furthermore, we ascribed the increase in the quantum yield to the decrease in k_{nd} (Equation 1.).[60, 65-68] Decrease in the k_{nd} of cyanine dyes, resulting from binding to DNA or proteins, have been reported elsewhere.[61, 69, 70]

A Jablonski diagram provides visualization of the photo-physical transitions of the dyes used, including the process of light absorption and emission (Scheme 3). Vibrational relaxation of conformers achieved via molecular rotation about the vinyl group, separating the two aromatic ring system in each of these dyes, presents an alternative non-radiative pathway for each molecule to decay back to its ground state.[65, 71, 72] In order to decrease the probability of nonradiative decay of the molecule from its singlet excited state and increase the probability of fluorescence, molecular rotation should be restricted. Such molecular modes of motion can be

suppressed by: (1) increasing the solvent viscosity, (2) chemically modifying the molecular structure to increase rigidity or (3) physically restricting the molecular motion by physical interaction (non-covalent bonding) with a substrate.

Scheme 3. Jablonski diagram representing the electronic transitions during the photo-activation and the excited-state deactivation of organic chromophores such as THIA.

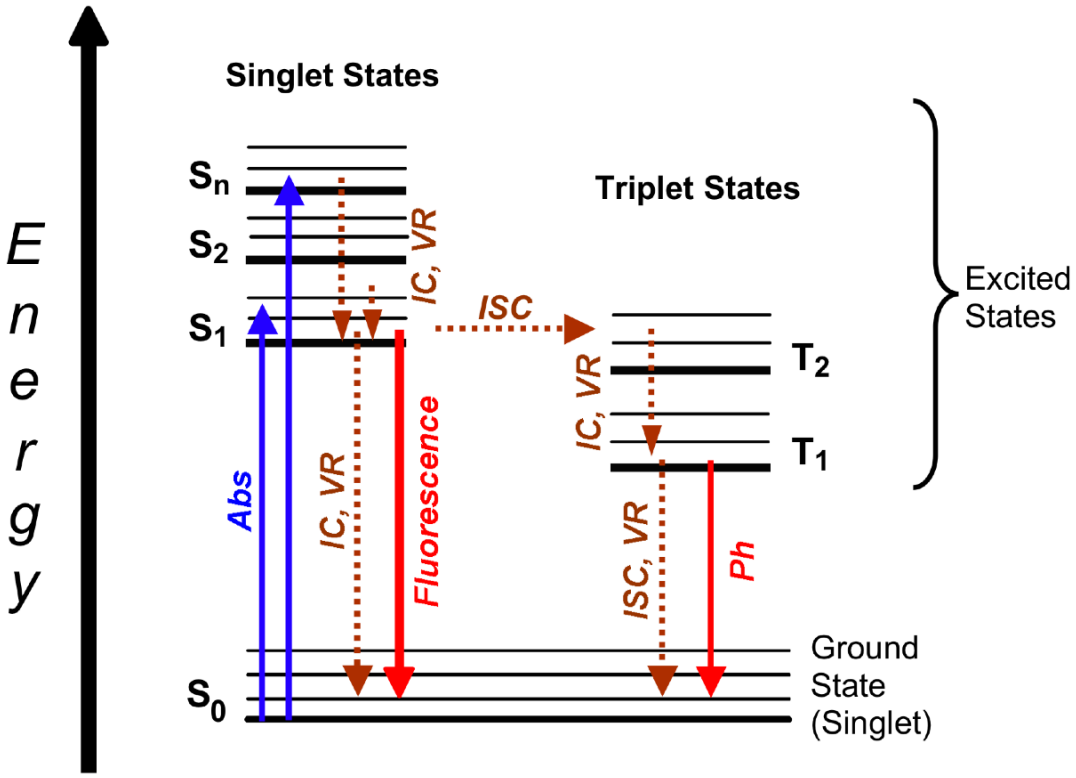

Radiative transitions. Involve photon-electron interactions. The energy of the system changes without changing the nuclear coordinates (transitions between electronic states):
Abs = absorption.
Fluorescence, light emission without a change in the multiplicity (i.e., without a spin flip).
Ph = phosphorescence: light emission with a multiplicity change.

Non-radiative transitions. Do not involve light waves:
VR = vibrational relaxation: relaxation of the system within an electronic state; involves a decrease in energy without a transition to a different electronic state.
IC = internal conversion: a transition to a different electronic state with the same multiplicity without a change in the energy.
ISC = intersystem crossing: a transition to an electronic state with a different multiplicity (i.e., involves a spin flip).

Fluorescence transitions normally occur from the lowest vibrational levels of the lowest excited electronic states but may involve upper vibrational levels of the ground states resulting in, on average, smaller energy changes than the absorption transitions. Therefore, the fluorescence bands always appear at longer wavelengths in comparison with the corresponding absorption bands.[59] The Stokes shift, expressed as the wavelength difference between the absorption and emission maxima, represents the extent of the vibrational relaxation of the ground and excited states, between which the radiative transitions take place.[58] The Stokes shift and extinction coefficient for each thiacyanine dye used in this study were determined (Table 1.).

1.1.5. Thiacyanine dyes.

Herein, we report the investigation of the staining dynamics of several bacterial species with the thiacyanine dyes 3,3'-diethylthiacyanine iodide (THIA), 3,3'-diethylthiacarbocyanine iodide (THC) and thiazole orange (THO).

Several reports have described the emission enhancement of cyanine dyes due to the rigidification of the molecule's environment, for example, by binding to a substrate such as DNA or proteins.[61, 70, 73] Cyanine dyes have a large binding affinity for negatively charged macromolecules with hydrophobic sites.[78-85] The reports attribute the emission enhancement to restriction of the molecular rotation, which has the effect of decreasing the non-radiative relaxation pathways (internal

conversion) from the single excited state.[60, 66-68, 70, 71] We believe that such binding interactions are responsible for the enhancement of thiacyanine dyes upon the addition of bacterial cells.

We focused our studies on THIA, as it has the largest molar extinction coefficient and the greatest emission enhancement of the dyes explored. The molecular structure of each of the three thiacyanine dyes used in this study is.

Scheme 4. The molecular structure of the thiacyanine dyes used in this study: (a) 3,3'-diethylthiacyanine iodide (THIA), (b) 3,3'-diethylthiacarbocyanine iodide (THC) and (c) Thiazole orange (THO).

(a)

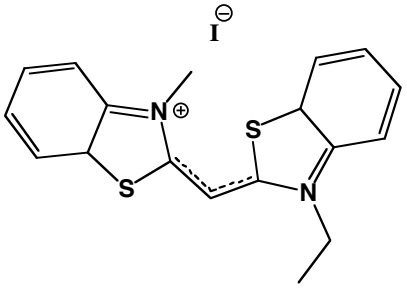

(b)

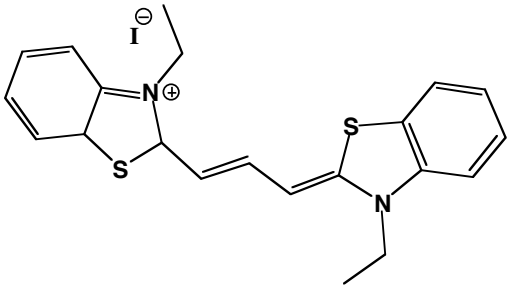

(c)

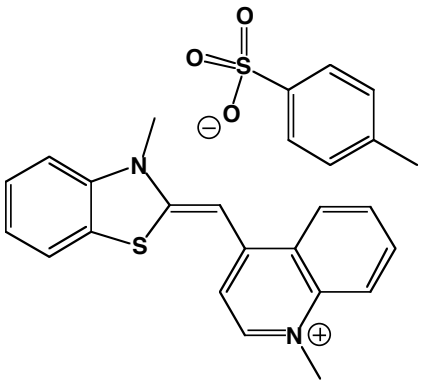

Table 1. Optical properties of the thiacyanine dyes used in this study.

Dyes	Extinction coefficient (cm^{-1} M^{-1})	λ_{abs} (nm)	λ_{em} (nm)	Stokes shift (nm)[a]
THIA	120,000	424	475	51
THC	120,000	510	577	67
THO	43,750	480	531	101

a. The Stokes shift is the difference between the location of λ_{ex} and λ_{em}

1.1.6. Choice of bacterial species for this study.

Six model bacterial species were selected, including two Gram-negative and two Gram-positive bacteria along with two *Bacillus* endospores. These bacterial species were chosen for several reasons, including the fact that much is known about each species. The handling of the species we used for this study required solely Biological Safety Level I (BSL-I). Furthermore, cultures for the investigated species are all commercially available.

The Gram-negative strains included *Escherichia coli* (*E. coli*) TOP10, which is the most widely used gene expression system in research laboratories;[74] and *Enterobacter aerogenes* (*E. aerogenes*), which is a commonly occurring bacterium classified as an opportunistic pathogen.[75] Healthy humans with fully functional immune systems are typically not affected by *E. aerogenes*.[75] Individuals who have open wounds or compromised immune systems, however, can develop an

infection.[75, 76] The Gram-positive bacterial strains selected were *Bacillus subtilis (B. subtilis)*, which is a ubiquitous soil bacteria, and *Bacillus sphaericus (B. sphaericus),* which is also a commonly occurring soil bacteria.[23, 44] *B. subtilis* is one of the most well understood bacterium in terms of molecular biology and cell biology.[77, 78] *B. subtilis* has excellent genetic amenability, and its large size has made it a popular choice for researchers.[79] *B. sphaericus* is a bacterium extensively studied around the world because it produces a toxin used as an effective method for controlling several common pests, including mosquito populations.[80] Neither *B. subtilis* nor *B. sphaericus* are considered pathogenic strains for humans; hence, they are not expected to colonize the human body for extended periods.[81] The two *Bacillus* endospores selected were *Bacillus thuringiensis* (*B. thuringiensis)* and *Bacillus globigii (B. globigii)*. These non-pathogenic *Bacillus* species have long been used as models for studying methods for detection of and protecting against endospores of as simulants for the bioterrorist organism *B. anthracis*, which causes anthrax.[82-84]

B. thuringiensis is a rod-shaped soil bacterium that is commonly used as a pesticide.[85] The endospore of *B. thuringiensis* is similar to the endospores of *B. anthracis*.[85] *B. globigii* is a rod-shaped soil bacteria that forms a protected endospore that can tolerate extreme conditions.[86]

THIA was effective at rapidly staining both the endospores and the vegetative bacterial cells from all six model systems.[56, 87] While some of these organisms are potential pathogens, none of these bacterial species are considered dangerous, as evident by their classification at BSL I.[33, 44]

1.2. Results and Discussion

1.2.1. Absorption spectra of cyanine dyes.

When taken up by bacterial cells, thiacyanine dyes exhibited a decrease in the molar extinction coefficient and changes in the spectral shape of their longest wavelength absorption band (Figures 1–6). The absorption spectra of each of the thiacyanine dyes were recorded with and without the addition of bacterial cells (Figures 1-6). All dye solutions used to perform absorption spectroscopy contained 565 μM TWEEN 40, except where otherwise stated. The absorbance at the spectral maxima dramatically reduced after dye uptake (by up to approximately two-fold reduction after 15 minutes) and the shapes of the absorption spectra were perturbed.

Bacterium-induced changes in the absorption properties of the three thiacyanine dyes, manifested patterns that were different for the different species. For quantification of the observed spectral changes of the three dyes in the presence of the six species, we used the relative change, ΔA, of the absorbance at dye spectral maxima measures at different times, t.

$$\Delta A(t) = \frac{A(0) - A(t)}{A(0)} \qquad \textbf{Equation 3.}$$

Where *A(t)* is the absorbance at time *t*, and *A(0)* is the initial absorbance prior to mixing with bacterial cells.

We recorded the dye spectra prior to addition of the bacteria; immediately upon injecting the bacterial suspension; and every fine minutes following the injection. Because of the time it takes to record a whole spectrum in the working wavelength span, the roperted times are within uncertainty of approximately one fifteen seconds.

1.2.1.1. Absorption of cyanine dyes in the presence of *E. coli*.

The addition of *E. coli* cells to the different dye solutions resulted in a decrease in their absorption peaks (Figure 1). For THO and THC, we also observed peaks broadening (Figure 1). The absorption of THIA were reduced by approximately 40% after 15 minutes while the absorption spectra of THO were reduced by approximately 40%, almost immediately upon addition of the *E. coli* suspension. On the absorption of the most red-shifted dye, THC, however, the bacteria induced a less than 20% gradual decrease over 15 minutes (Figure 1). The difference between THIA and THC is only in the length of the π-conjugation link between THIA and THC is only in the length of the π-conjugating link between the two aromatic ring systems. The relatively small difference in size between the two dye molecules implies that the observed differences in the rate of uptake cannot be sought solely by size.

While THIA and THO have similar size and charge, they have suttle structural differences. Unlike THIA, THO is a thiacyanine dye with an asymmetric molecular structure (Scheme 4). The difference in the uptake behavior of these two dyes, therefore, implies differences in the molecular-level interaction with components of the bacterial cells.

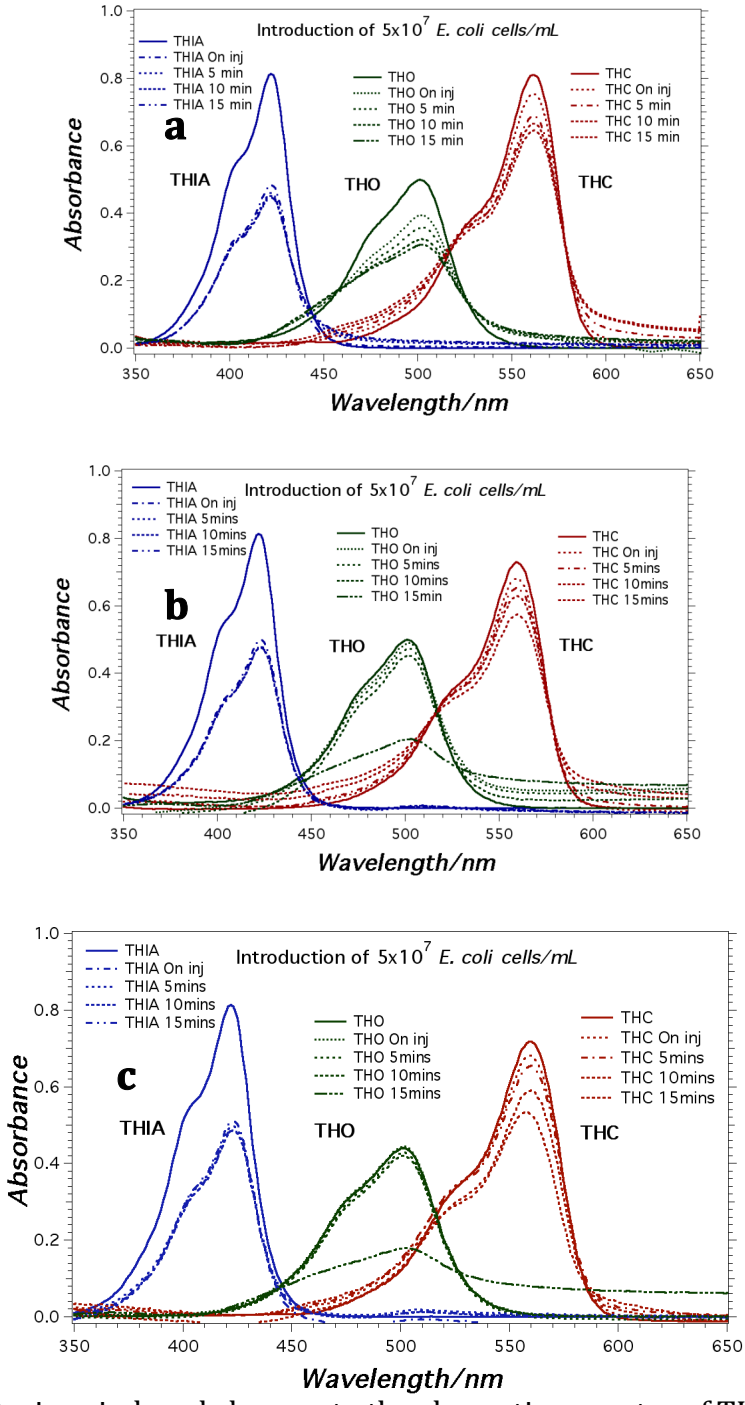

Figure 1. Bacterium-induced changes to the absorption spectra of THIA, THO & THC (6 μM) in the presence and absence of *E. coli* 5x10^7 cells mL^{-1} (a) run 1, (b) run 2 and (c) run 3, in 2 mM Tris buffer at pH 8.5 (λ_{ex} = 420 nm, λ_{em} = 475 nm).

Table 2. Changes in absorption spectra with the addition of *E. coli* cells.

Dyes	Runs	$A(t_0)$	$A(t_{0n\ inj})$	$A(t_{15min})$	$\lambda(t_0)$	$\lambda(t_{0n\ inj})$	$\lambda(t_{15min})$
THIA	1	0.814	0.484	0.448	422	422	422
	2	0.814	0.499	0.477	422	423	423
	3	0.814	0.512	0.460	422	423	423
THO	1	0.810	0.755	0.606	562	562	562
	2	0.768	0.681	0.531	559	560	560
	3	0.729	0.681	0.574	559	560	560
THC	1	0.499	0.393	0.307	501	501	501
	2	0.499	0.369	0.114	501	502	502
	3	0.440	0.437	0.100	501	502	502

a. The absorption measurements are corrected for any offset from the baseline.

1.2.1.2. Absorption of cyanine dyes in the presence of E. aerogenes.

The addition of *E. aerogenes* cells to the thiacyanine dye solutions also resulted in perturbation in the absorption spectra (Figure 2); i.e., reduction in the extinction coefficients, shifts in the absorption maxima, and spectral broadening. The changes in the absorption patterns induced by the addition of *E. aerogenes* cells differed form the changes induced by *E. coli*, especially in the case of THIA. The reduction of the absorption peak of THIA was gradual and accompanied by spectral broadening (Figure 2).

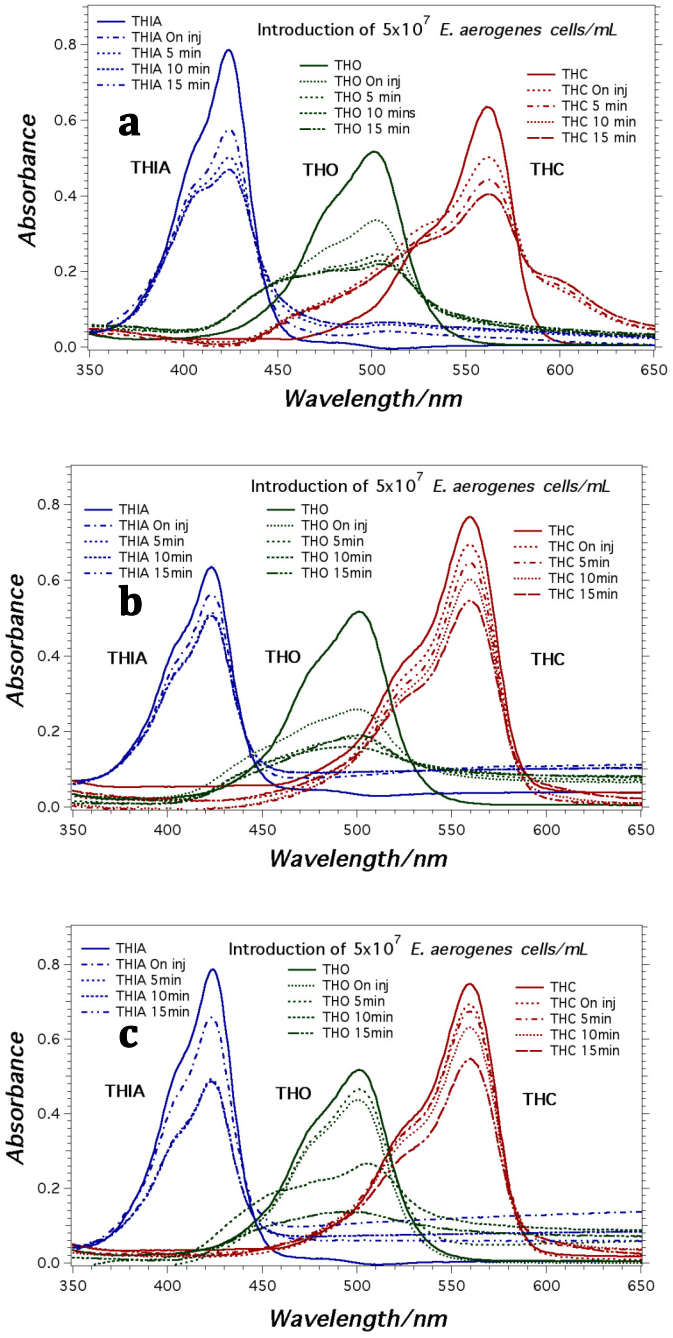

Figure 2. Bacterium-induced changes to the absorption spectra of THIA, THO & THC (6 μM) in the presence and absence of *E. aerogenes* 5x10^7 cells mL^{-1} (a) run 1, (b) run 2 and (c) run 3, in 2mM Tris buffer at pH 8.5 (λ_{ex} = 420 nm, λ_{em} = 475 nm).

Table 3. Changes in absorption spectra with the addition of *E. aerogenes* cells.

Dyes	Runs	$A(t_0)$	$A(t_{0n\ inj})$	$A(t_{15min})$	$\lambda(t_0)$	$\lambda(t_{0n\ inj})$	$\lambda(t_{15min})$
THIA	1	0.787	0.575	0.469	424	425	424
	2	0.633	0.542	0.469	424	424	424
	3	0.633	0.513	0.469	424	424	424
THO	1	0.518	0.336	0.219	501	503	506
	2	0.518	0.259	0.150	501	502	502
	3	0.518	0.465	0.138	501	502	507
THC	1	0.633	0.501	0.404	562	561	561
	2	0.767	0.694	0.544	560	560	560
	3	0.76	0.693	0.547	560	560	560

The absorption measurements are corrected for any offset from the baseline.

1.2.1.3. Absorption of cyanine dyes in the presence of *B. subtilis*.

The addition of Gram-positive cells to the thiacyanine dye solution causes similar pertubation in the absorption spectra (Figure 3). The most distinct feature that set apart *B. subtilis* from the two Gram-negative species was 37% decrease in the absorption of THC (Table 4), while *E. coli* and *E. aerogenes* it was 84% and 60%, respectively (Tables 2-3).

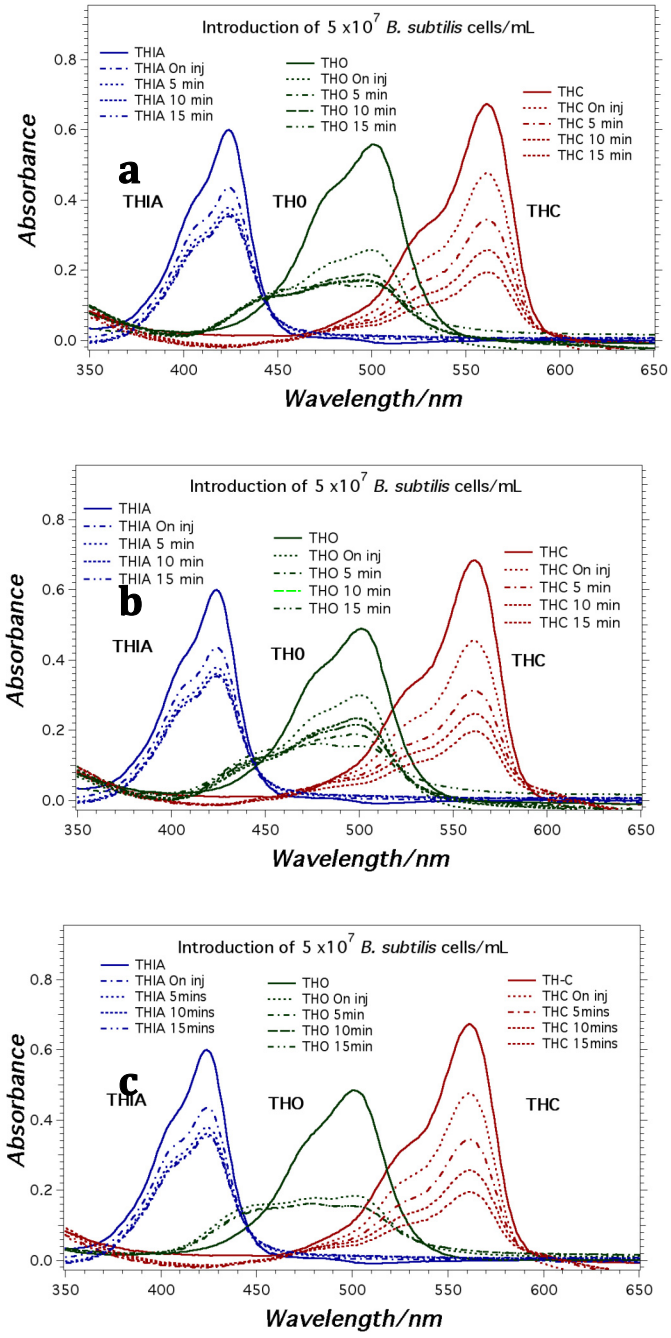

Figure 3. Bacterium-induced changes to the absorption spectra of THIA, THO & THC (6 μM) in the presence and absence of *B. subtilis* 5x10^7 cells mL^{-1} (a) run 1, (b) run 2 and (c) run 3, in 2mM Tris buffer at pH 8.5 (λ_{ex} = 420 nm, λ_{em} = 475 nm).

Table 4. Changes in absorption spectra with the addition of *B. subtilis* cells.

Dyes	Runs	$A(t_0)$	$A(t_{0n\ inj})$	$A(t_{15min})$	$\lambda(t_0)$	$\lambda(t_{0n\ inj})$	$\lambda(t_{15min})$
THIA	1	0.600	0.535	0.454	424	425	425
	2	0.600	0.544	0.486	423	423	424
	3	0.600	0.513	0.475	424	424	424
THO	1	0.485	0.183	0.155	501	503	498
	2	0.485	0.183	0.155	501	502	502
	3	0.486	0.183	0.155	501	501	501
THC	1	0.816	0.348	0.314	554	553	554
	2	0.816	0.348	0.314	554	553	554
	3	0.816	0.348	0.314	554	553	554

The absorption measurements are corrected for any offset from the baseline.

1.2.1.4. Absorption of cyanine dyes in the presence of *B. sphaericus*.

The addition of *B. sphaericus* cells to a thiacyanine dye solution resulted in significant perturbation in the spectra of both THIA and THO but not of THC, as seen in Figure 4 (a-c). The absorbance of THIA was reduced by 30% after 15 minutes while the absorption spectra for THO were reduced by approximately 95% or more after 15 minutes and were reduced by 30% for THC over the same 15-minute period.

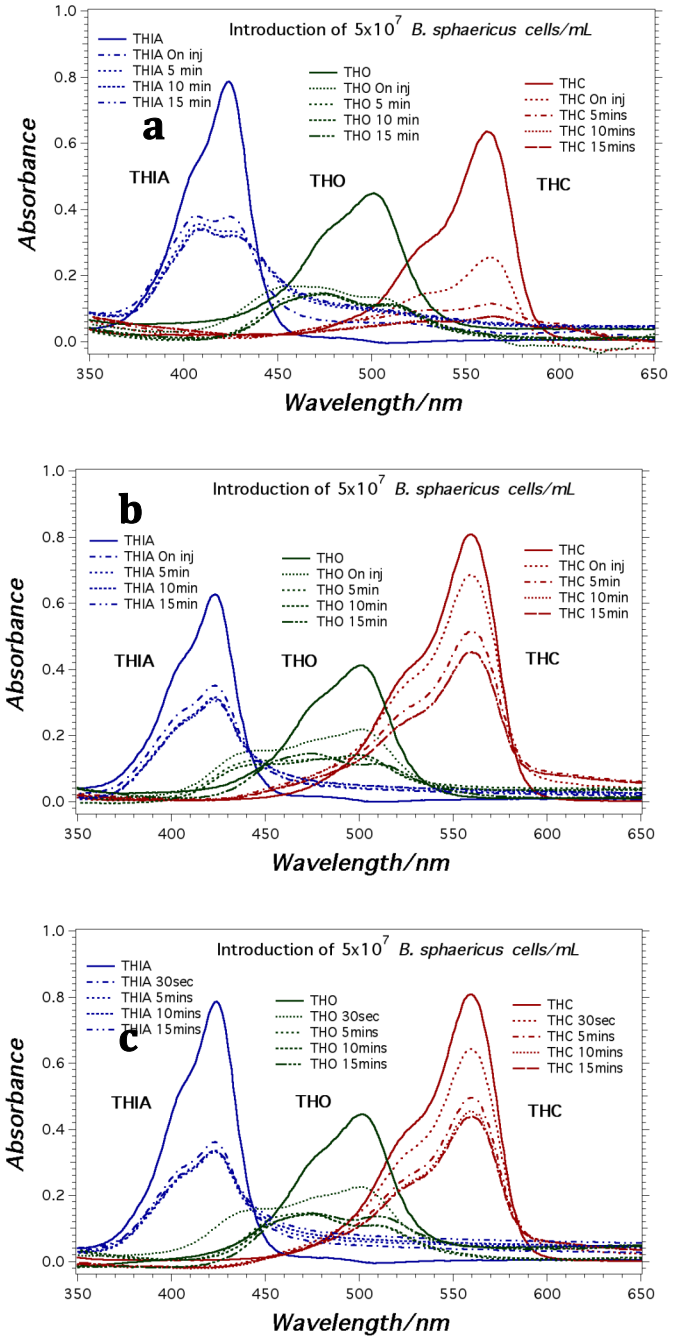

Figure 4. Bacterium-induced changes to the absorption spectra of THIA, THO & THC (6 μM) in the presence and absence of *B. sphaericus* 5x10^7 cells mL^{-1} (a) run 1, (b) run 2 and (c) run 3, in 2mM Tris buffer at pH 8.5 (λ_{ex} = 420 nm, λ_{em} = 475 nm).

Table 5. Changes in absorption spectra with the addition of *B. sphaericus* cells.

Dyes	Runs	$A(t_0)$	$A(t_{0n\ inj})$	$A(t_{15min})$	$\lambda(t_0)$	$\lambda(t_{0n\ inj})$	$\lambda(t_{15min})$
THIA	1	0.787	0.379	0.338	424	406	410
	2	0.656	0.362	0.306	423	423	423
	3	0.655	0.361	0.301	423	423	423
THO	1	0.365	0.315	0.135	501	503	476
	2	0.366	0.165	0.142	502	467	475
	3	0.366	0.164	0.142	501	503	476
THC	1	0.635	0.315	0.135	561	563	565
	2	0.809	0.647	0.413	559	560	560
	3	0.809	0.624	0.436	559	560	560

The absorption measurements are corrected for any offset from the baseline.

1.2.1.5. Absorption of cyanine dyes in the presence of *B. globigii* endospores.

B. globigii endospores induced the dramatic effect in the reduction of the absorption of the three cyanine dyes. *B. globigii* endospores displayed significant uptake of the dyes, as seen in (Figure 5). The dye solution was almost completely taken up by the addition of *B. globigii* endospores at a density of $5x10^7$ cell mL^{-1}. The extinction coefficient of THIA was reduced by approximately 80% after 15 minutes while the absorption spectra for THO were reduced by approximately 60% after 15 minutes and were reduced by less than 60% for THC over the same 15-minute period.

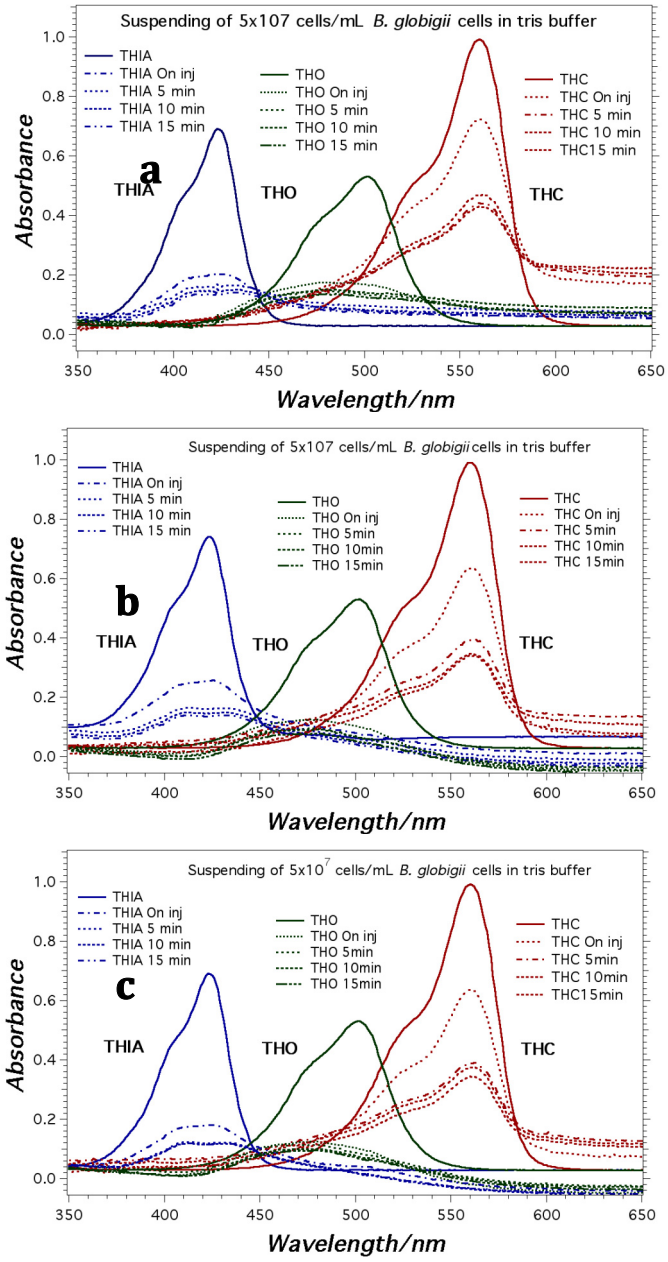

Figure 5. Bacterium-induced changes to the absorption spectra of THIA, THO & THC (6 μM) in the presence and absence of *B. globigii* endospores $5x10^7$ cells mL^{-1} (a) run 1, (b) run 2 and (c) run 3, in 2mM tris buffer at pH 8.5 (λ_{ex} = 420 nm, λ_{em} = 475 nm).

Table 6. Changes in absorption spectra with the addition of *B. globigii* endospores.

Dyes	Runs	$A(t_0)$	$A(t_{0n\ inj})$	$A(t_{15min})$	$\lambda(t_0)$	$\lambda(t_{0n\ inj})$	$\lambda(t_{15min})$
THIA	1	0.673	0.319	0.195	422	422	423
	2	0.741	0.256	0.139	423	425	415
	3	0.690	0.210	0.143	423	423	423
THO	1	0.515	0.357	0.185	501	504	462
	2	0.531	0.175	0.136	502	485	485
	3	0.530	0.124	0.072	502	481	481
THC	1	0.991	0.722	0.480	560	560	563
	2	0.991	0.722	0.428	560	561	562
	3	0.989	0.636	0.340	560	561	562

The absorption measurements are corrected for any offset from the baseline.

1.2.1.6. Absorption of cyanine dyes in the presence of B. thuringiensis endospores.

The main feature that distinguishes *B. thuringiensis* endospores inform B. globigii endospores is the absorption of THIA and THO which were 77% compared to 45% and 75% compared to 60%, respectively (Figure 5-6). The dye solution was almost completely taken up by the addition of *B. thuringiensis* endospores at a density of $5x10^7$ cell mL^{-1}.

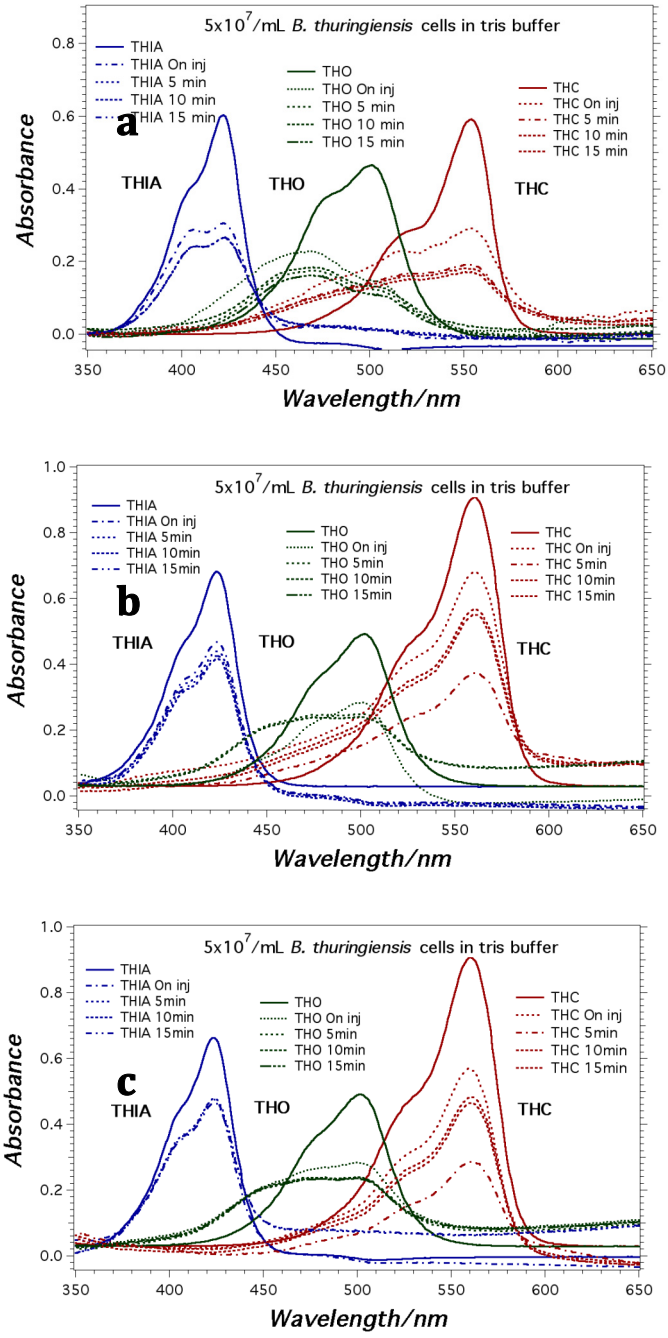

Figure 6. Bacterium-induced changes to the absorption spectra of THIA, THO & THC (6 μM) in the presence of *B. thuringiensis* endospores $5x10^7$ cells mL^{-1} (a) run 1, (b) run 2 and (c) run 3, in 2mM tris buffer at pH 8.5 (λ_{ex} = 420 nm, λ_{em} = 475 nm).

Table 7. Changes in absorption spectra with the addition of *B. thuringiensis* endospores.

Dyes	Runs	$A(t_0)$	$A(t_{0n\ inj})$	$A(t_{15min})$	$\lambda(t_0)$	$\lambda(t_{0n\ inj})$	$\lambda(t_{15min})$
THIA	1	0.733	0.475	0.464	423	424	424
	2	0.681	0.467	0.424	423	424	425
	3	0.673	0.304	0.267	422	423	423
THO	1	0.515	0.308	0.208	501	467	474
	2	0.489	0.284	0.239	503	501	499
	3	0.515	0.227	0.162	501	470	468
THC	1	0.910	0.569	0.284	560	560	561
	2	0.907	0.680	0.33	560	561	560
	3	0.592	0.290	0.171	554	554	551

*The absorption measurements are corrected for any offset from the baseline.

1.2.1.7. Comparison of bacterium-induced changes in the absorption properties of thiacyanine.

The Vegetative bacterial cells: *E. coli*, *E. aerogenes*, *B. sphaericus* and *B. subtilis*, induced different absorption patterns when in the absorption of the three single dyes. The two Gram-negative bacterial cells; *E. coli* and *E. aerogenes*, had similar absorption for THO of 43% and 44% respectively. However, the absorption for THIA were different with 16% compared to 56% respectively while the absorption for THC was 84% and 60% respectively.

The Gram-positive bacterial cells, *B. subtilis* and *B. sphaericus*, had had similar absorption for THC with 37% and 30% respectively. The absorption for THIA were different with 59% and 30% respectively while the absorption for THO was 95% and 75% respectively. There did not appear to be any correlation between absorption values between Gram-negative and Gram-positive species.

The *Bacillus* endospores also displayed significantly different absorption patterns from each other. The absorption patterns between *B. globigii* and *B. thuringiensis* were: 77% compared to 45% for THIA, 75% compared to 60% for THO and 58% compared to 66% for THC .

The data from the study were tabulated and summarized (Tables 2–7). The perturbation of the absorption spectra appeared to be species-specific and concentration-dependent, as seen in (Figure 1–Figure 6). Tables were constructed using the values for the changes in the observed absorption spectra for two time points, immediately after injection and 15 minutes post injection (Tables 2–7).

We used the data provided (Tables 2–7) to determine the relative changes to the properties of the absorption spectra. The information was used to generate the relative rates of changes in the absorption properties (Tables 8–10). The rate of the changes in the properties of the absorption spectra was a direct measure of the bacterial cell's ability to remove dye molecules from solution (Tables 8–10). The values for $\Delta A(t)$ were determined by measuring the level of absorption before and after the addition of bacterial cells at the wavelength corresponding to the absorption maximum. The decrease in the level of absorption was reported as $\Delta A(t)A(t)^{-1}$.

Table 8. Change in absorption and wavelength shifts as a function of time.

Bacterial species	Dyes	ΔA ($t_{0n\ inj}$)	ΔA ($t_{15\ min}$)	$\Delta\lambda$ ($t_{0n\ inj}$)	$\Delta\lambda$ ($t_{15\ min}$)
E. coli	THIA	0.330	0.367	0	0
	THIA	0.315	0.337	-1	-1
	THIA	0.303	0.354	-1	-1
E. coli	THO	0.056	0.205	0	0
	THO	0.087	0.237	-1	-1
	THO	0.049	0.155	-1	-1
E. coli	THC	0.106	0.192	0	0
	THC	0.131	0.385	-1	-1
	THC	0.003	0.340	-1	-1
E. aerogenes	THIA	0.212	0.318	-1	0
	THIA	0.091	0.164	0	0
	THIA	0.120	0.164	0	0
E. aerogenes	THO	0.182	0.299	-2	-5
	THO	0.259	0.368	-1	-1
	THO	0.052	0.380	-1	-6
E. aerogenes	THC	0.132	0.229	1	1
	THC	0.073	0.224	0	0
	THC	0.073	0.221	0	0

a. ΔA given in units of absorption units

b. $\Delta\lambda$ given in units of nm

Table 9. Change in absorption wavelength shift as a function of time after introduction of bacterial cells.

Bacterial species	Dyes	ΔA ($t_{On\ inj}$)	ΔA ($t_{15\ min}$)	$\Delta\lambda$ ($t_{On\ inj}$)	$\Delta\lambda$ ($t_{15\ min}$)
B. subtilis	THIA	0.066	0.147	-1	-1
	THIA	0.056	0.115	0	-1
	THIA	0.087	0.125	0	0
B. subtilis	THO	0.302	0.330	-2	3
	THO	0.302	0.330	1	1
	THO	0.303	0.331	0	0
B. subtilis	THC	0.469	0.502	1	0
	THC	0.469	0.502	1	0
	THC	0.469	0.502	1	0
B. sphaericus	THIA	0.409	0.450	18	14
	THIA	0.294	0.350	0	0
	THIA	0.294	0.354	0	0
B. sphaericus	THO	0.050	0.230	-2	25
	THO	0.201	0.223	35	27
	THO	0.201	0.223	-2	25
B. sphaericus	THC	0.320	0.500	-2	-4
	THC	0.162	0.396	-1	-1
	THC	0.185	0.373	-1	-1

a. ΔA given in units of absorption units

b. $\Delta\lambda$ given in units of nm

Table 10. Changes in absorption and wavelength shift as a function of time from introduction of bacterial cells.

Bacterial species	Dyes	ΔA ($t_{0n\ inj}$)	ΔA ($t_{15\ min}$)	$\Delta\lambda$ ($t_{0n\ inj}$)	$\Delta\lambda$ ($t_{15\ min}$)
B. globigii	THIA	0.354	0.478	0	-1
endospores	THIA	0.484	0.602	-2	8
	THIA	0.480	0.547	0	0
B. globigii	THO	0.159	0.330	-3	39
endospores	THO	0.356	0.395	17	17
	THO	0.405	0.457	21	21
B. globigii	THC	0.269	0.510	0	-3
endospores	THC	0.269	0.562	-1	-2
	THC	0.353	0.649	-1	-2
B. thuringiensis	THIA	0.258	0.269	-1	-1
endospores	THIA	0.215	0.258	-1	-2
	THIA	0.369	0.406	-1	-1
B. thuringiensis	THO	0.207	0.307	34	27
endospores	THO	0.205	0.250	2	4
	THO	0.288	0.353	31	33
B. thuringiensis	THC	0.341	0.626	0	-1
endospores	THC	0.228	0.535	-1	0
	THC	0.301	0.421	0	3

a. ΔA given in units of Absorption units
b. $\Delta\lambda$ given in units of nm

The data were tabulated in Tables 8–10 and used to determine the relative changes for each run. The rate of absorption was calculated for immediately after introduction of the bacterial cells to the dye solution with the time for analysis approximated to be 30 seconds and 900 seconds for 15 minutes after introducing the bacterial cells to the dye solution. The time used for samples immediately introduced was 30 seconds and was based on a 60-second scan time for the samples with approximately 30 seconds before scanning the wavelength of interest. The

second time point used was 15 minutes after introduction of cells or 900 seconds (Table 11).

Table 11. Rates for the change in absorption as a function of time from the introduction of bacterial cells.

Bacterial species	Dyes	$\Gamma_{0n\ injection}$	$\Gamma_{15\ min}$
E. coli	THIA	1.05E-02 ± 4.6E-04	3.92E-04 ± 1.7E-05
	THO	2.12E-03 ± 6.7E-04	2.21E-04 ± 4.6E-05
	THC	2.66E-03 ± 2.3E-03	3.39E-04 ± 1.1E-04
E. aerogenes	THIA	4.70E-03 ± 2.1E-04	2.39E-04 ± 9.9E-05
	THO	5.48E-03 ± 3.5E-04	3.88E-04 ± 4.7E-05
	THC	3.10E-03 ± 1.1E-04	2.49E-04 ± 4.6E-06
B. subtilis	THIA	2.32E-03 ± 5.3E-04	1.43E-04 ± 1.8E-05
	THO	1.01E-02 ± 2.1E-05	3.68E-04 ± 7.03E-07
	THC	1.56E-02 ± 0E-00	5.58E-04 ± 1.9E-08
B. sphaericus	THIA	1.11E-02 ± 2.2E-03	4.27E-04 ± 6.3E-05
	THO	5.03E-03 ± 2.9E-03	2.51E-04 ± 4.4E-06
	THC	7.41E-03 ± 2.9E-03	4.70E-04 ± 7.5E-05
B. globigii endospores	THIA	1.46E-02 ± 2.5E-03	6.03E-04 ± 6.9E-05
	THO	1.02E-02 ± 4.4E-03	4.38E-04 ± 7.1E-05
	THC	9.90E-03 ± 1.6E-03	6.38E-04 ± 7.8E-05
B. thuringiensis endospores	THIA	9.35E-03 ± 2.7E-03	3.46E-04 ± 9.2E-05
	THO	7.78E-03 ± 1.6E-03	3.37E-04 ± 5.8E-05
	THC	9.67E-03 ± 1.9E-03	5.86E-04 ± 1.1E-04

a. Γ - The rate of absorbance per time is presented in units of s^{-1}
b. The errors listed are the standard deviation of the changes in the absorbance value.

The rates of dye absorption had larger error bars for the early time points; however, there are smaller errors for the 15-minute time points. This is because we sampled immediately after injection, trying to capture very rapid kinetics,

and our instruments were not ideal for capturing such rapid kinetics. The longer kinetics are ideal for our data collection system and are much more accurate.

1.2.2. Absorption spectra of mixtures of cyanine dyes.

We examined the question of whether mixed-dye solutions could provide additional unique species-specific signature for each bacterial species. Interaction of bacteria with mixtures of dyes will reveal features that result from cooperative or comperative dye-cell interactertion processes.

An equimolar dye solution was prepared to have a final concentration of 6 μM of each of the three thiacyanine dyes: THIA, THO and THC. Despite the spectral overlap, the obsorption peaks of the three dyes are well separated from one another and apparent in the spectra of the mix-dye solution.

The use of the mixed-dye solution demonstrated the possibility of using a single solution, with a combination of three dyes, to rapidly analyze bacterial samples. The corrected mixed-dye absorption spectra showed that the uptake of dye molecules by the bacterial cells started immediately after introduction of the cells to the dye solution, as seen with the individual dyes. The corrected mixed-dye spectra (Figure 7–Figure 12) displayed unique absorption patterns for each of the four vegetative bacteria tested.

We monitored the changes of the absorption of the mixed-dye spectra at three wavelengths that corresponded to the absorption maximum of each dye

before the addition of bacterial cells. The spectra after the addition of cells were recorded at four different time points to establish time-dependence.

1.2.2.1. Absorption of a mixture of cyanine dyes in the presence of *E. coli*.

The mixed-dye solution (Figure 7) displayed a different absorption pattern compared to the collective spectra from the individual dye solution (Figure 1). For the mixed solution of THIA, THO and THC, the decrease in the absorption in the region of the spectrum where THIA absorbs, was noticeably smaller than the decrease in the absorption observed for THIA solutions without the two other dyes (Figure 1 versus Figure 7).

While we do not know the reason for this finding, it does suggest that the dyes may have common binding sites and there is competition for these sites among the dye molecules. The unique bacterium-induced absorption pattern that resulted from measuring the light absorption after 15 minutes' incubation in the dye solution allowed us to determine a three-digit code for *E. coli* cells. The three-digit code represents the relative absorption changes at wavelengths corresponded to the three spectral maxima of the dye solutions. We used the three maxima of the mixed solution, rather than the absorption maxima from the individual dye solutions, as there were minor shifts in the wavelengths of maximum absorption when the dyes were mixed versus having individual free dyes, due to spectral overlaps.

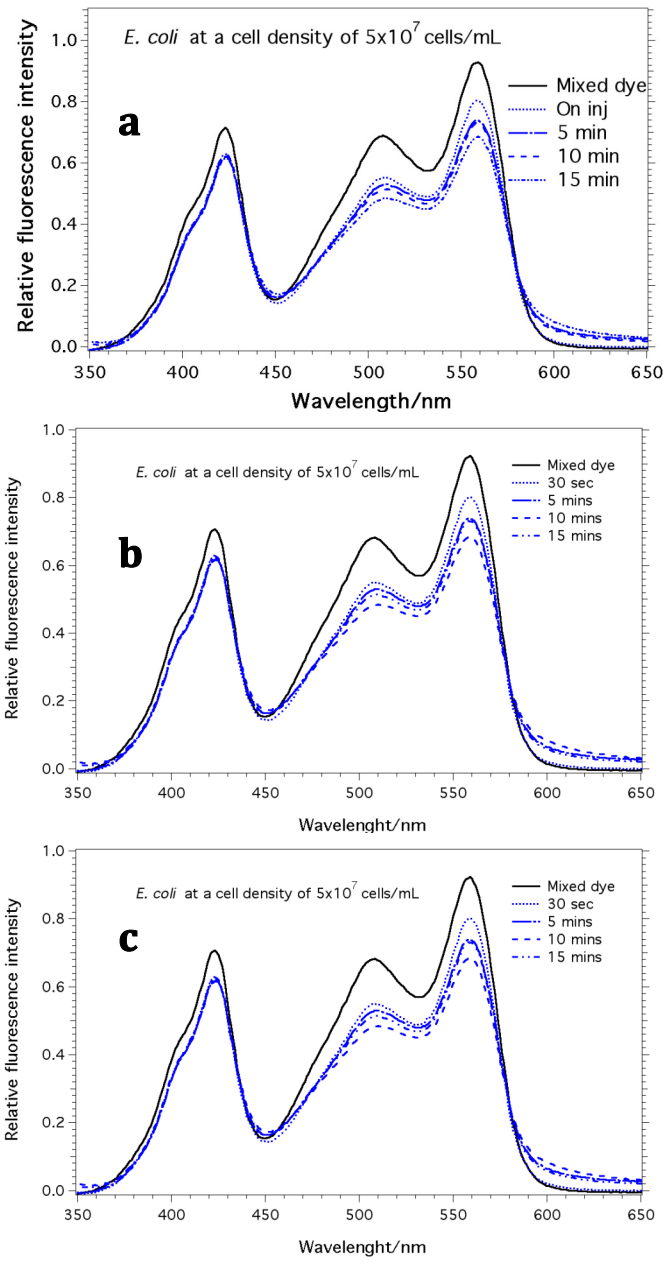

Figure 7. Bacterium-induced changes to the properties of the mixed-dye absorption spectra of a 6 µM mixed-dye solution in the presence and absence of *E. coli cells* (a) run 1 (b), run 2 and (c) run 3, at a cell density of $5x10^7$ cells mL^{-1}.

1.2.2.2. Absorption of mixture of cyanine dyes in the presence of *E. aerogenes*.

For the mixed-dye solution, the spectral perturbation, induced by *E. aerogenes*, differed from the spectral changes we observed for *E. coli*. The *E. aerogenes*-induced decrease in the absorption of THIA, for the mixed dye and single dye solution was identical (Figure 2 and Figure 8) while the absorption of THO and THC varied. The decrease in the absorption in the real region of the spectrum, corresponding to THC, was considerably more pronounced for the mixed-dye than for the single-dye solution (Figure 2 and Figure 8). This improved pertubation of the THC spectra, when in a mixture with the other two dyes, suggested coooerative interaction with the bacterial cells. This suggest that cooperative interaction with bacterial cells when THIA and/or THO are present, the binding of THC improves. The unique bacterium-induced absorption pattern, which resulted from measuring the light absorption after 15 minutes of incubation in the dye solution, allowed us to determine a three-digit code for *E. aerogenes* cells.

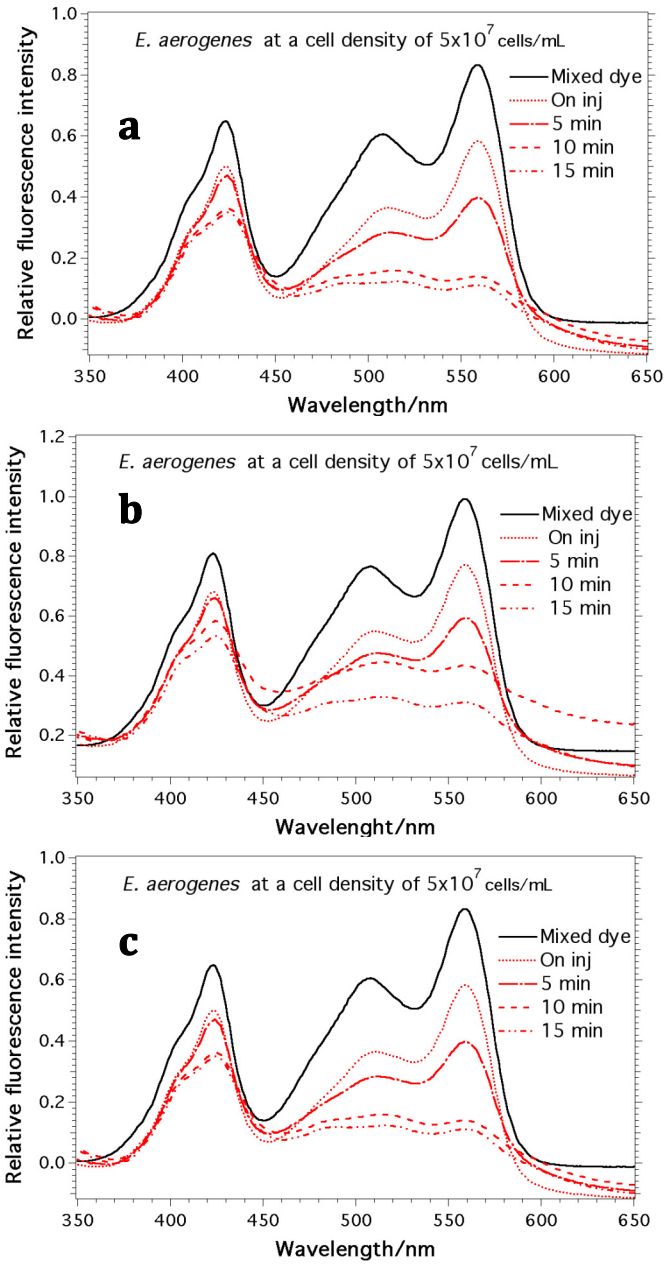

Figure 8. Bacterium-induced changes to the properties of the mixed-dye absorption spectra of a 6 µM mixed-dye solution in the presence and absence of *E. aerogenes* cells (a) run 1, (b) run 2 and (c) run 3, at a cell density of $5x10^7$ cells mL^{-1}.

1.2.2.3. Absorption of mixture of cyanine dyes in the presence of *B. subtilis*.

The mixed-dye solution displayed a different absorption pattern compared to the individual dye solution. The absorption of THIA decreased while the absorption of THO and THC increased. The unique bacterium-induced absorption pattern that resulted from measuring light absorption after 15 minutes' incubation in the due solution, allowed us to determine a three-digit code for *B. subtilis* cells. The three-digit code was obtained by measuring the level of absorption at three different wavelengths that corresponded to the wavelengths of maximum absorption for the three main peaks in the dye solutions. We used the three main peaks for characterizing the dye uptake by the bacteria in a mixed-dye solution (Figure 9).

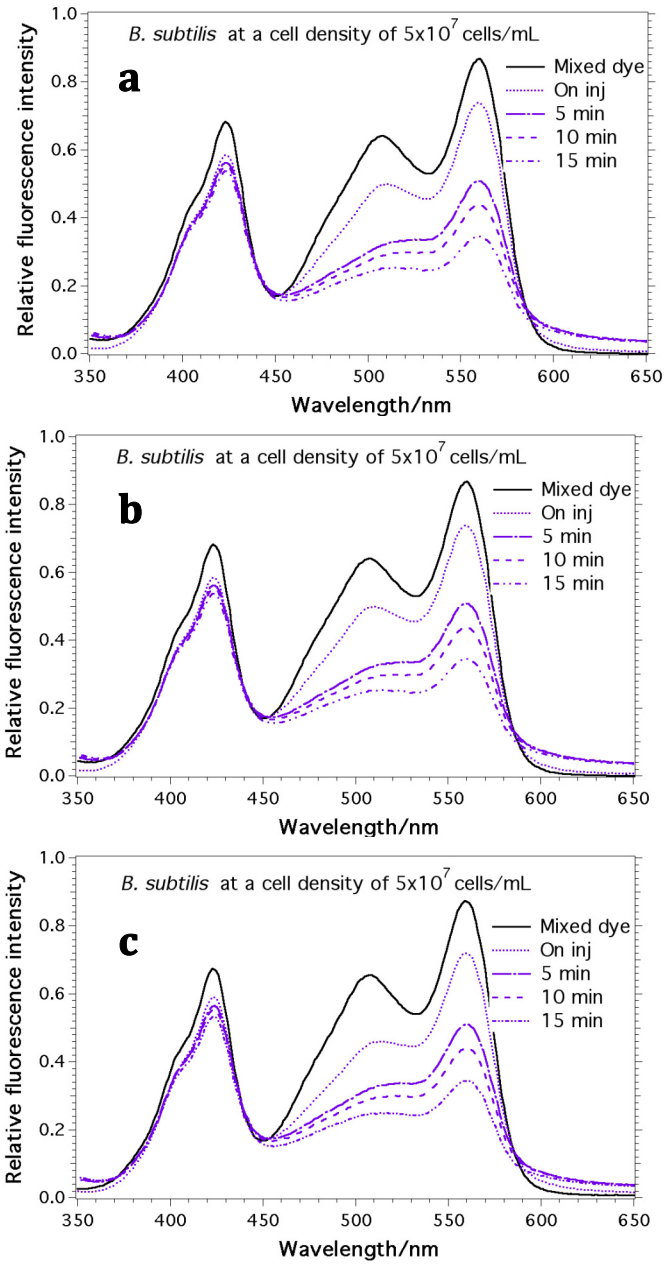

Figure 9. Bacterium-induced changes to the properties of the mixed-dye absorption spectra of a 6 µM mixed-dye solution in the presence and absence of *B. subtilis* cells (a) run 1, (b) run 2 and (c) run 3, at a cell density of $5x10^7$ cells mL^{-1}.

1.2.2.4. Absorption of mixture of cyanine dyes in the presence of *B. sphaericus.*

The mixed-dye solution displayed a different absorption pattern compared to the individual dye solution. The absorption of THIA molecules increased while the absorption of THO decreased and the absorption of THC increased. The unique bacterium-induced absorption pattern that resulted from measuring light absorption after 15 minutes' incubation in the dye solution, allowed us to determine a three-digit code for *B. sphaericus* cells. The three-digit code was obtained by measuring the level of absorption at three different wavelengths that corresponded to the wavelengths of maximum absorption for the three main peaks in the dye solutions. Like the previous examples, we used the three main peaks to evaluate the rate of dye uptake (Figure 10).

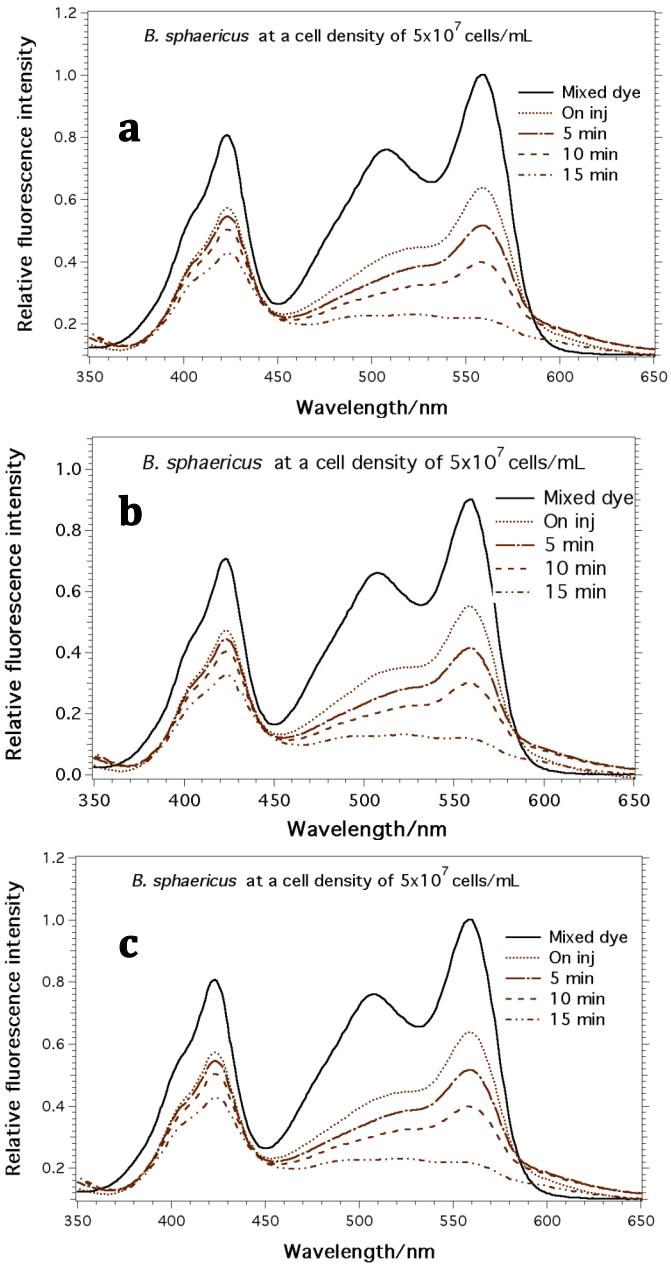

Figure 10. Bacterium-induced changes to the properties of the mixed-dye absorption spectra of a 6 μM mixed-dye solution in the presence and absence of *B. sphaericus cells* (a) run 1, (b) run 2 and (c) run 3, at a cell density of $5x10^7$ cells mL^{-1}.

1.2.2.5. Absorption of mixture of cyanine dyes in the presence of bacterial endospores.

The mixed-dye solution displayed different endospore-induced changes in the absorption spectra. The absorption of the three dye species was strong for the endospore solution compared to vegetative bacterial cells. The three dyes in the mixture were absorbed well by both endospores evaluated. One feature of the endospore absorption spectra was that the dyes seem to have less competition for binding sites compared to vegetative cells. This may be primarily due to the vastly different structure of the bacterial cell wall compared to the spore coat. The two *Bacillus* endospore species used in this study were *Bacillus globigii* and *Bacillus thuringiensis*. These two *Bacillus* species are believed to have similar cell-wall structures; however, we attempted to use absorption spectroscopy to distinguish the two.

The three-digit code was obtained by measuring the level of absorption at three different wavelengths that corresponded to the wavelengths of maximum absorption for the three main peaks in the dye solutions. We used the three main peaks rather than simply the absorption maximum from the individual dye solution, as there were minor shifts in the wavelengths of maximum emission when the dyes were mixed versus individual free dyes. The bacterium-induced changes in the properties of the absorption spectra of the mixed-dye solution with *B. globigii* resulted in increased dye absorption for all three species. The bacterium-induced changes in the properties of the absorption spectra of the mixed-dye solution with

B. thuringiensis also resulted in increased dye absorption for all three dyes; however, the absorption was not as significant as in the case of *B. globigii*. The bacterium-induced changes in the properties of the absorption spectra can be seen below in (Figure 11-Figure 12).

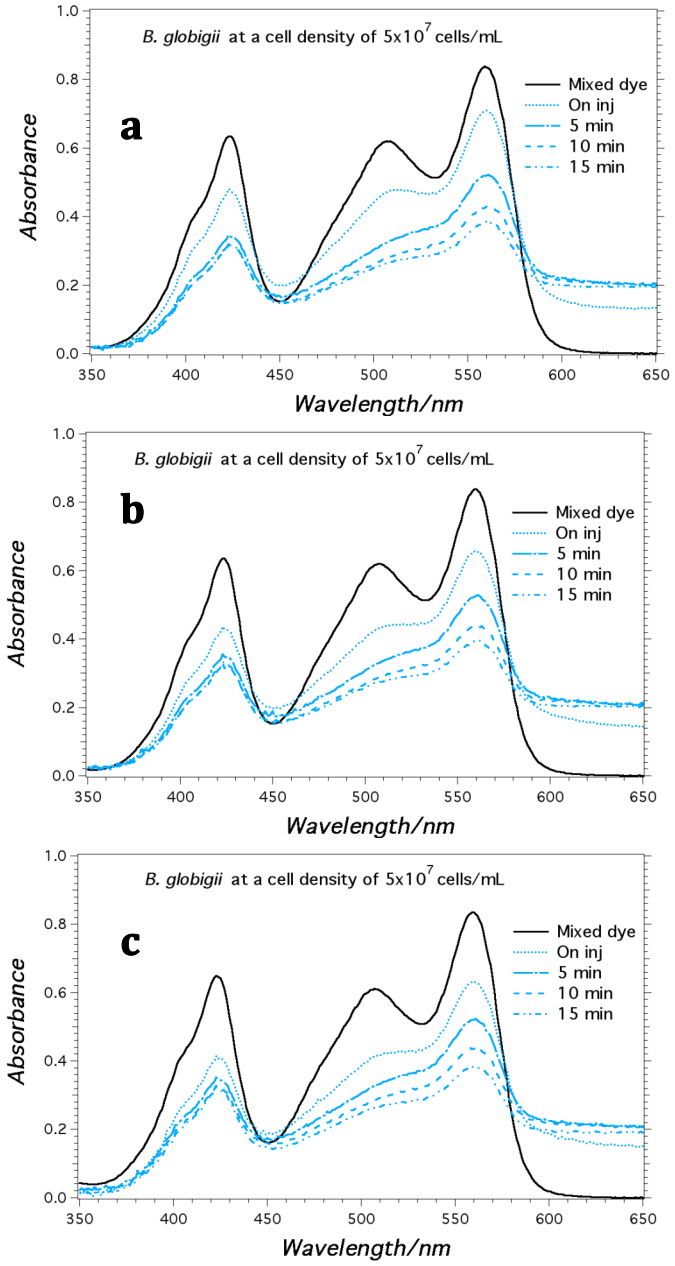

Figure 11. Bacterium-induced changes to the properties of the mixed-dye absorption spectra of a 6 µM mixed-dye solution in the presence and absence of *B. globigii* endospores (a) run 1, (b) run 2 and (c) run 3, at a cell density of $5x10^7$ cells mL^{-1}.

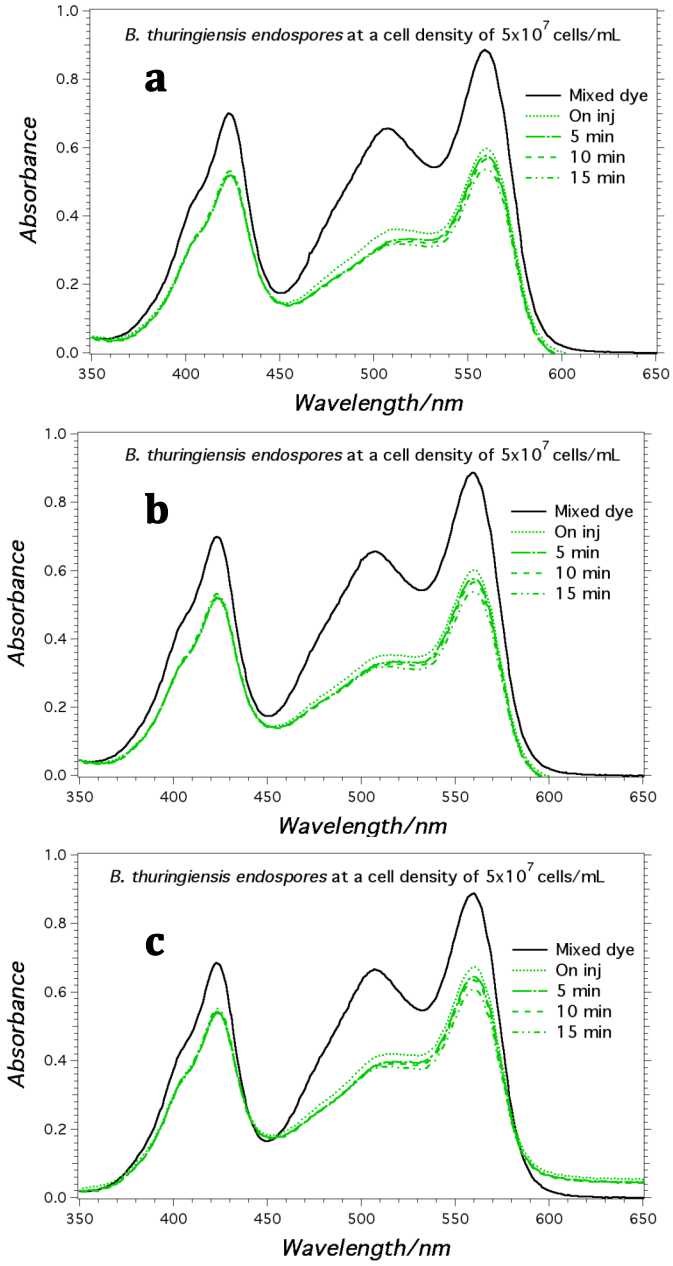

Figure 12. Bacterium-induced changes to the properties of the mixed-dye absorption spectra of a 6 µM mixed-dye solution in the presence and absence of *B. thuringiensis* endospores (a) run 1, (b) run 2 and (c) run 3, at a cell density of $5x10^7$ cells mL^{-1}.

1.2.2.6. Mixed-dye versus single-dye solution.

The bacterium-induced changes in the mixed-dye absorption spectra displayed unique patterns for each of the four vegetative bacterial species evaluated in this study. In addition, there was significant distinction between the two *Bacillus* endospores evaluated in this study. Comparison of the three-digit codes extracted from the series of mixed-dye absorption spectra of both the vegetative and endospore species revealed that these species in this relatively small population gave unique codes for each (Table 12).

Table 12. Relative changes in absorption properties of dye by bacterial species.

		Relative change in Absorbance of dye by bacterial species					
Samples	Dye	*E. coli*	*E. aerogenes*	*B. subtilis*	*B. sphaericus*	*B. globigii*	*B. thuringiensis*
Individual dye	THIA	0.16±0.02	0.56±0.01	0.59±0.03	0.30±0.01	0.77±0.05	0.45±0.13
	THO	0.43±0.02	0.44±0.01	0.41±0.09	0.95±0.02	0.75±0.11	0.60±0.09
	THC	0.84±0.06	0.60±0.20	0.37±0.12	0.30±0.01	0.58±0.07	0.66±0.06
Mixture of dyes	THIA	0.19±0.02	0.56±0.01	0.19±0.01	0.56±0.02	0.50±0.11	0.25±0.02
	THO	0.61±0.02	0.82±0.02	0.61±0.02	0.82±0.13	0.58±0.00	0.56±0.10
	THC	0.59±0.08	0.87±0.01	0.59±0.02	0.87±0.02	0.53±0.01	0.41±0.12

1.2.3. Fluorescence spectra of cyanine dyes.

The addition of bacterial cells to the thiacyanine dye solutions results in an increase in the intensity of the peak of maximum emission at 475 nm, 531 nm and 577, respectively, for THIA, THO and THC. The addition of bacterial cells to the thiacyanine dye solutions, in some cases, in the appearance of red-shifted emission

bands.

The photo-physical properties of the dyes, including the molar extinction coefficient of the chromophores at the excitation wavelength, are affected by the microenvironment of the dye. Decrease in the absorption spectra suggested a decrease in the molar extinction coefficient of each of the chromophores upon cell uptake (Figure 1–Figure 6). The bacterial uptake, however, caused an enhancement in the corresponding emission intensity for THIA and THO. Because the decrease in the extinction coefficient which was accompanied by an increase in the emission intensity, we ascribed the phenomena to an increase in the fluorescence quantum yield of the molecule. Fluorescence enhancement was observed for all dyes; THIA; THO and THO, with THIA having the most significant levels of enhancement (Figure 13–Figure 30).

The fluorescence intensity was reported as relative fluorescence intensity for all emission spectra. To obtain the relative fluorescence intensity, we divide the fluorescence emission, measured in counts per second (CPS) by a reference beam, which monitors the excitation light source. Expressing this quantity as a ratio corrects for any random fluctuations in the excitation beam. The emission spectra of some of the dye-bacteria pairs offer less unique characteristics than the absorption spectra; however, there were some differences in shape and emission intensity that could be correlated to species-specific interactions. These features could potentially be used to distinguish among bacterial species.

1.2.3.1. Fluorescence spectra of THIA in the presence of bacterial cells.

The emission intensity and general shape of the emission curves were both changed with the addition of bacteria compared to the dye-only solution. Significant fluorescence enhancement was observed for bacterial species in THIA, THO and THC solutions. THIA and THO displayed emission enhancement that was over an order of magnitude while THC did not display emission enhancement on the time scale on which the emission was measured. The relative fluorescence intensities are reported, as they are the ratio of the signal and the reference beam. The reference beam is used to monitor the excitation lamp. The emission spectra for the four vegetative bacterial cells and two *Bacillus* endospores used in this study are presented below in (Figure 13–Figure 30).

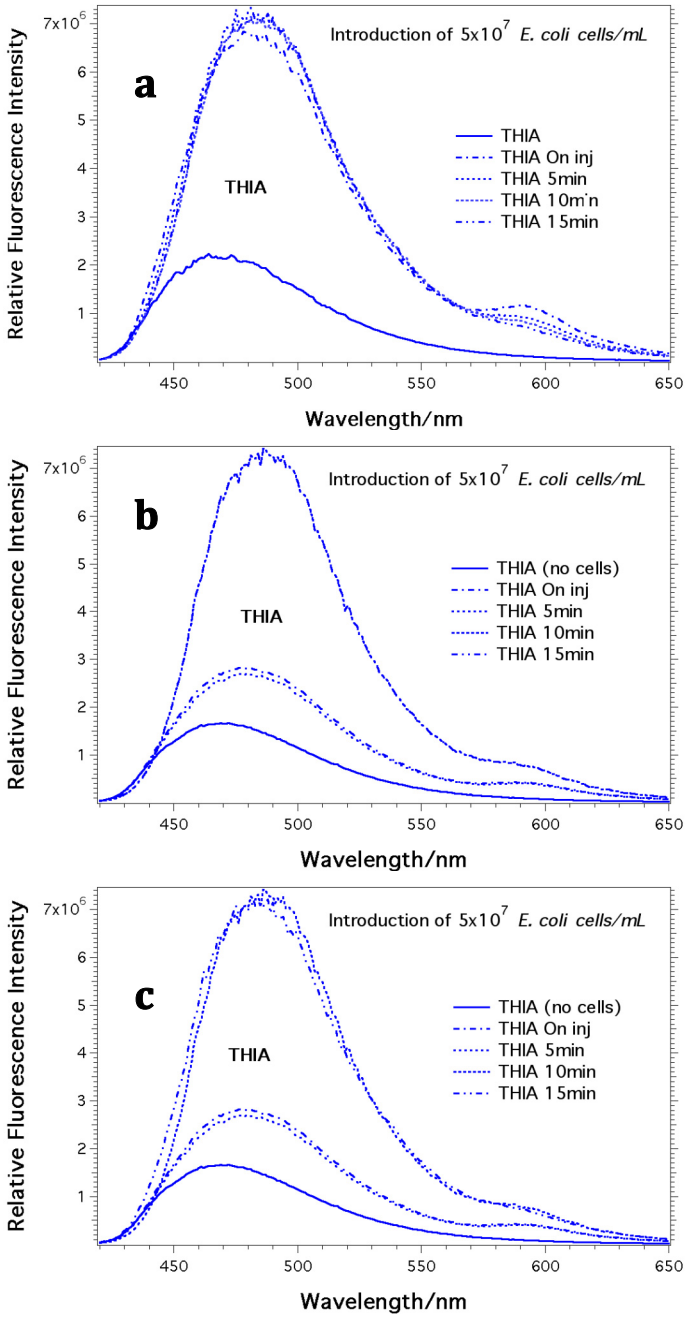

Figure 13. Bacterium-induced changes in the properties of the emission spectra for a 6 μM THIA with *E. coli* cells (a) run 1, (b) run 2 and (c) run 3, at a cell density of $5x10^7$ cells mL^{-1}.

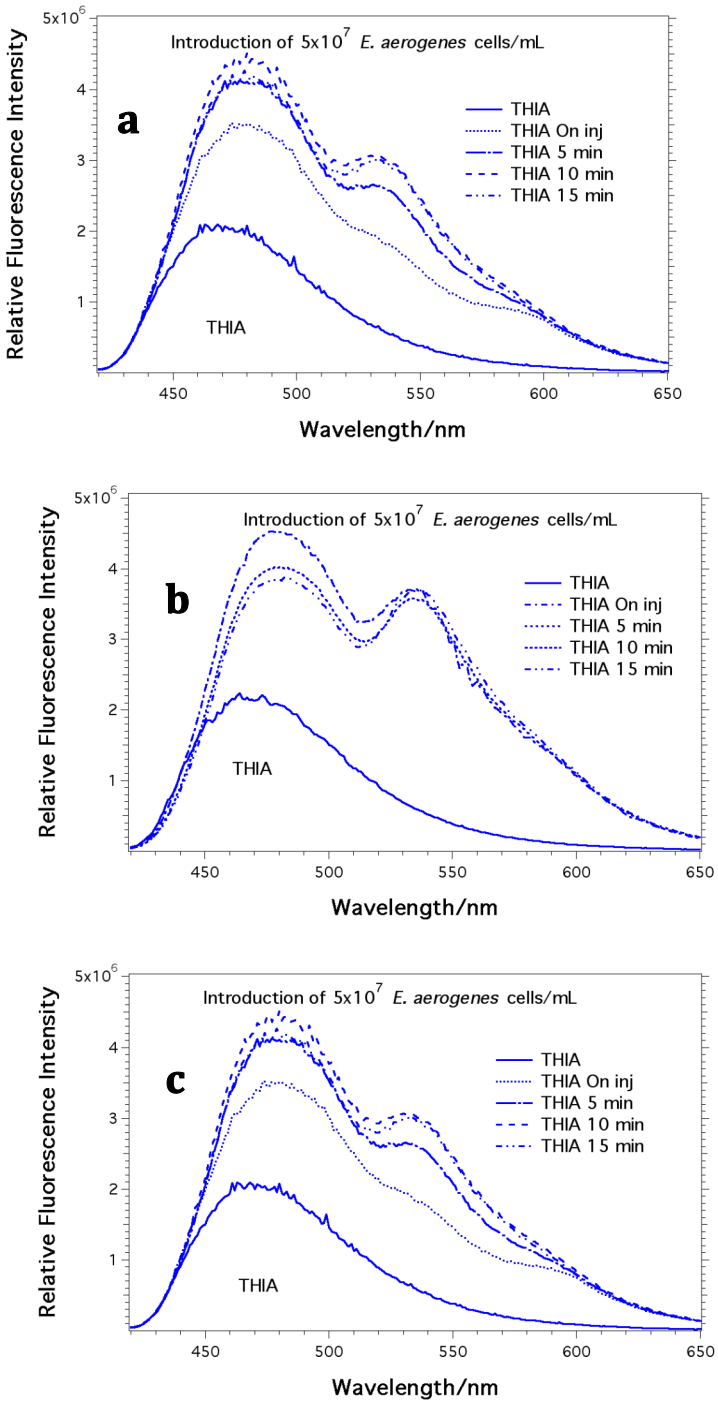

Figure 14. Bacterium-induced changes in the properties of the emission spectra for a 6 µM THIA with *E. aerogenes* cells (a) run 1, (b) run 2 and (c) run 3, at a cell density of $5x10^7$ cells mL^{-1}.

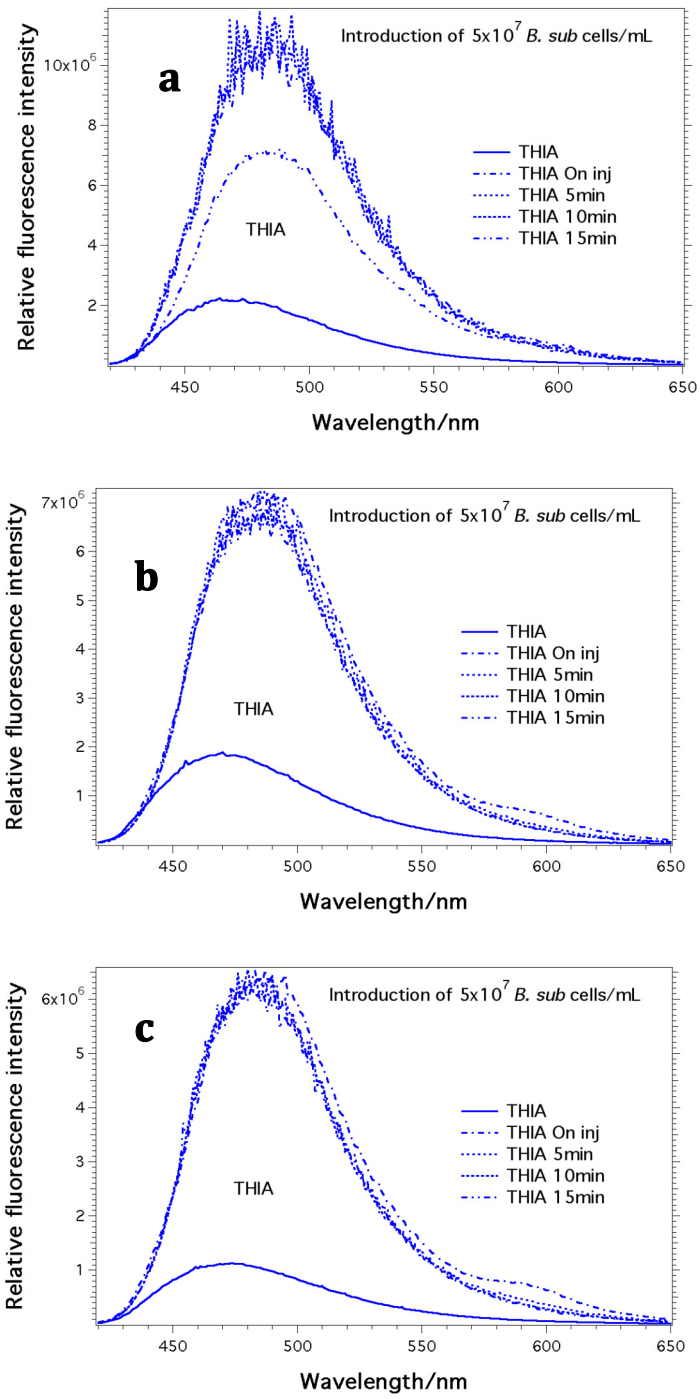

Figure 15. Bacterium-induced changes in the properties of the emission spectra for a 6 μM THIA with *B. subtilis* cells (a) run 1, (b) run 2 and (c) run 3, at a cell density of $5x10^7$ cells mL^{-1}.

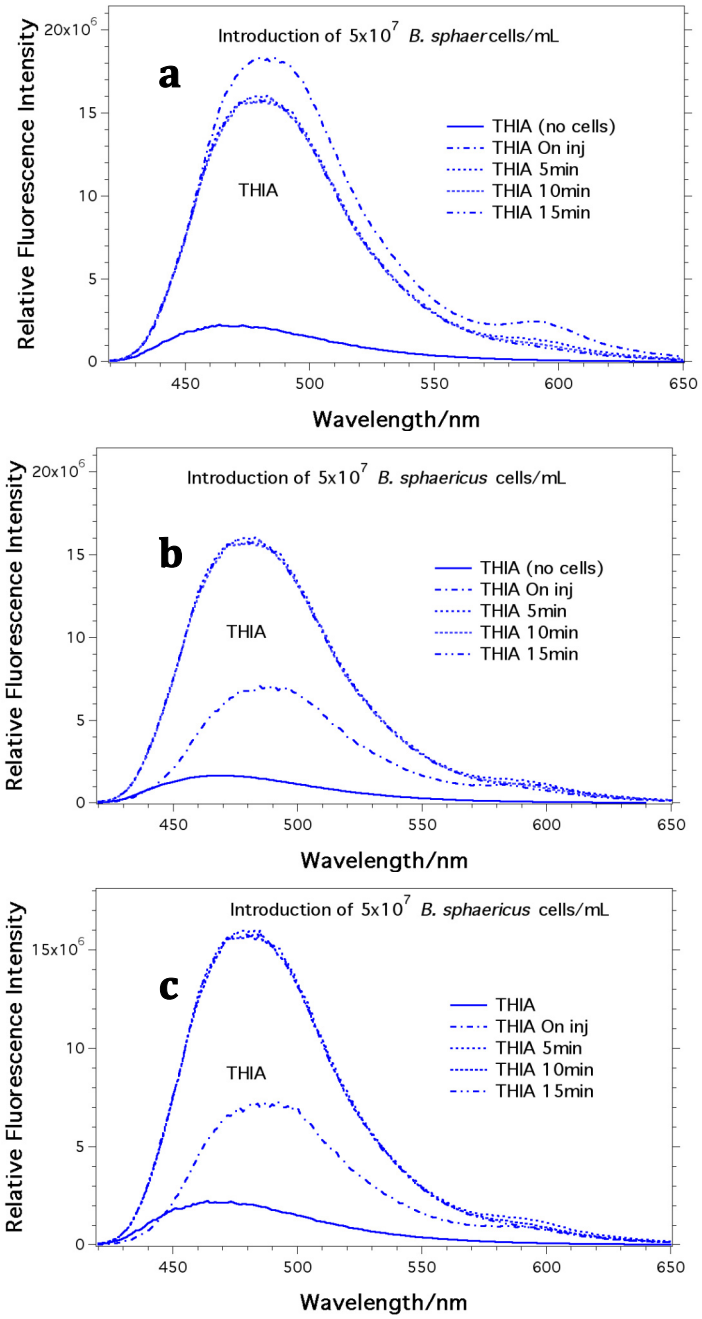

Figure 16. Bacterium-induced changes in the properties of the emission spectra for a 6 µM THIA with *B. sphaericus* cells (a) run 1, (b) run 2 and (c) run 3, at a cell density of $5x10^7$ cells mL^{-1}.

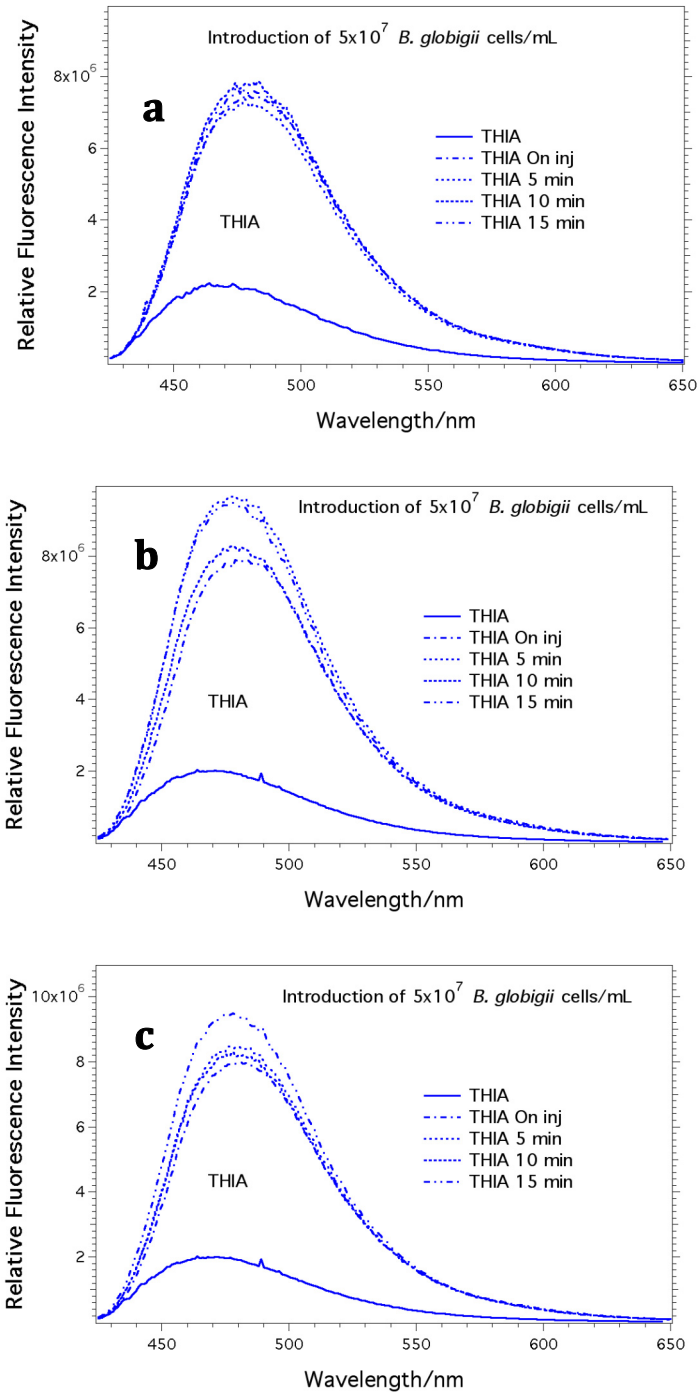

Figure 17. Bacterium-induced changes in the properties of the emission spectra for a 6 μM THIA with *B. globigii* endospores (a) run 1, (b) run 2 and (c) run 3, at a cell density of $5x10^7$ cells mL^{-1}.

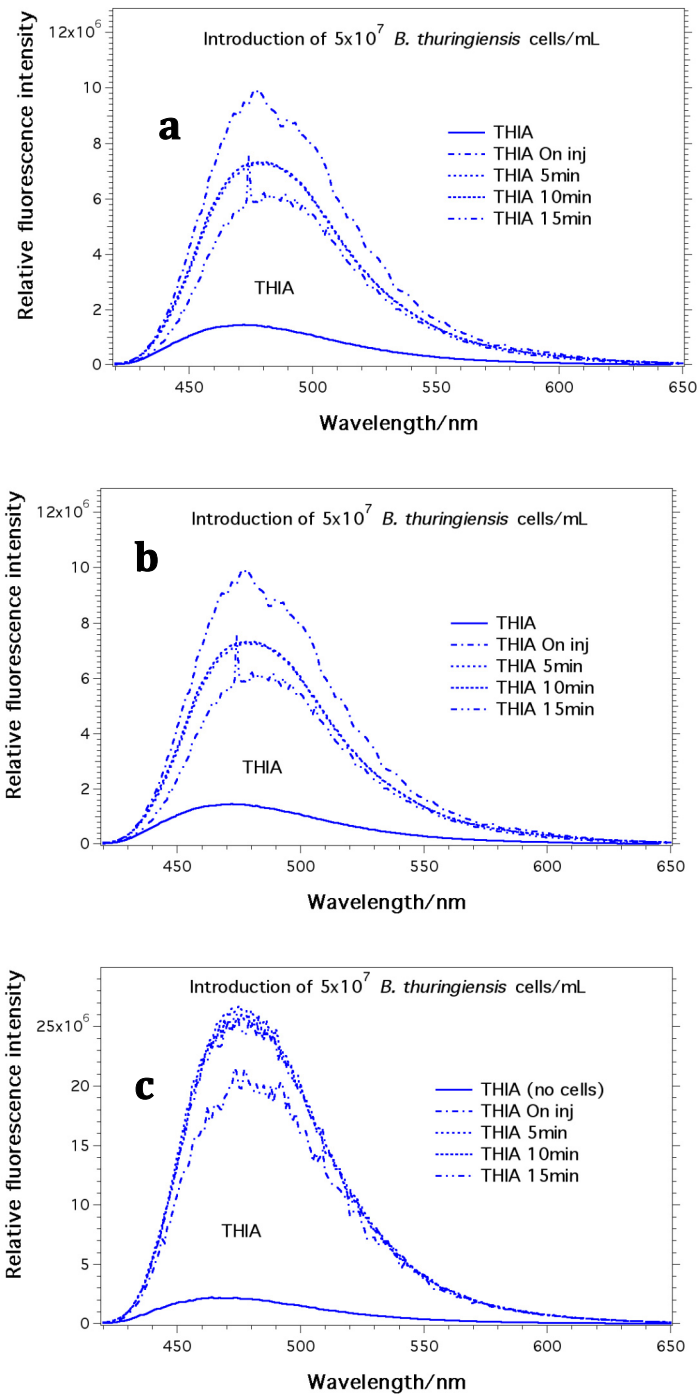

Figure 18. Bacterium-induced changes in the properties of the emission spectra for a 6 μM THIA with *B. thuringiensis* endospores (a) run 1, (b) run 2 and (c) run 3, at a cell density of $5x10^7$ cells mL^{-1}.

1.2.3.2. Fluorescence spectra of THO in the presence of bacterial cells.

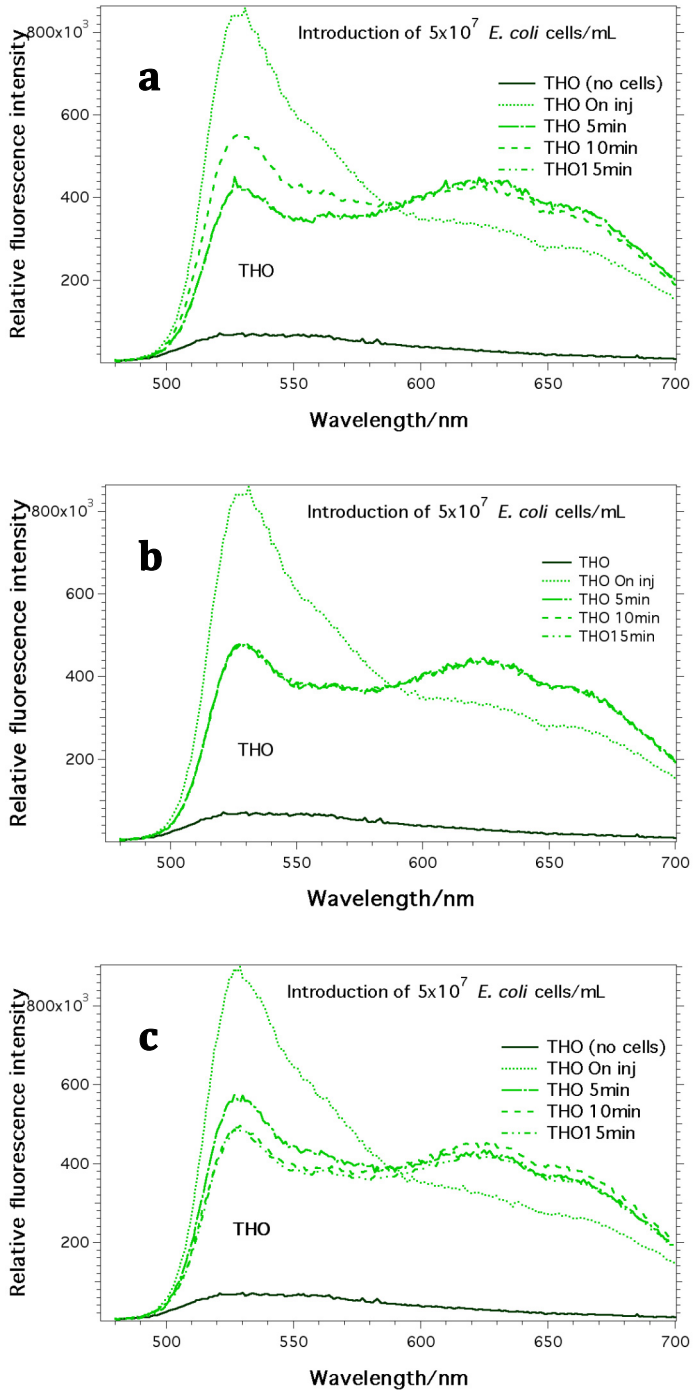

Figure 19. Time-dependent emission spectra of 6 µM THO with *E. coli* cells (a) run 1, (b) run 2 and (c) run 3, at a cell density of $5x10^7$ cells mL^{-1}.

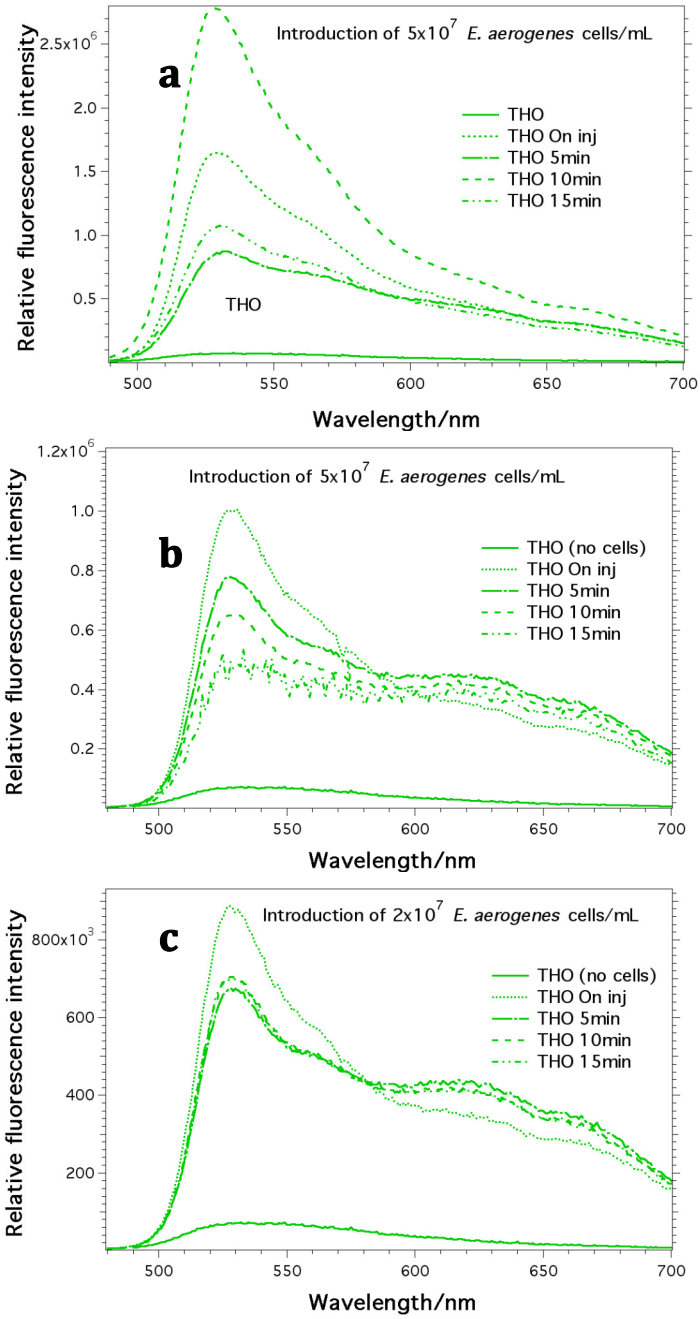

Figure 20. Time-dependent emission spectra of 6 μM THO with *E. aerogenes* cells (a) run 1, (b) run 2 and (c) run 3, at a cell density of $5x10^7$ cells mL^{-1}.

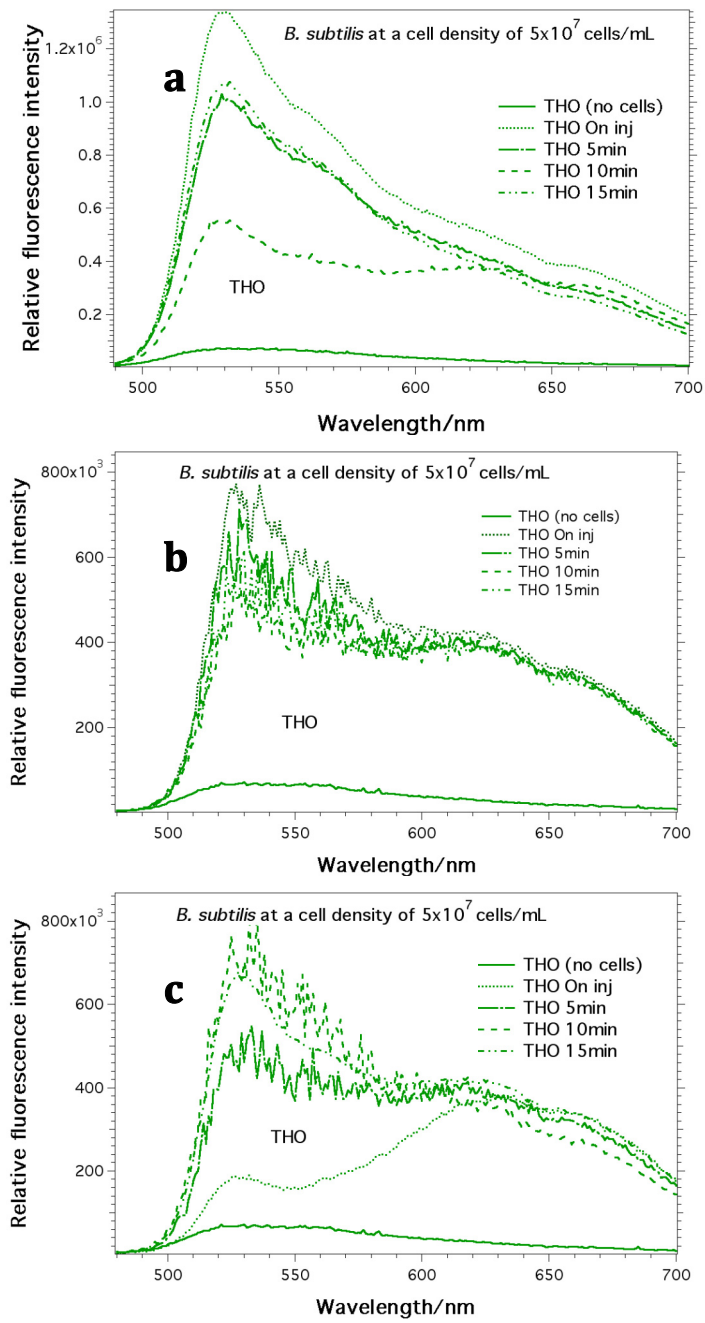

Figure 21. Time-dependent emission spectra of 6 μM THO with *B. subtilis* cells (a) run 1, (b) run 2 and (c) run 3, at a cell density of $5x10^7$ cells mL^{-1}.

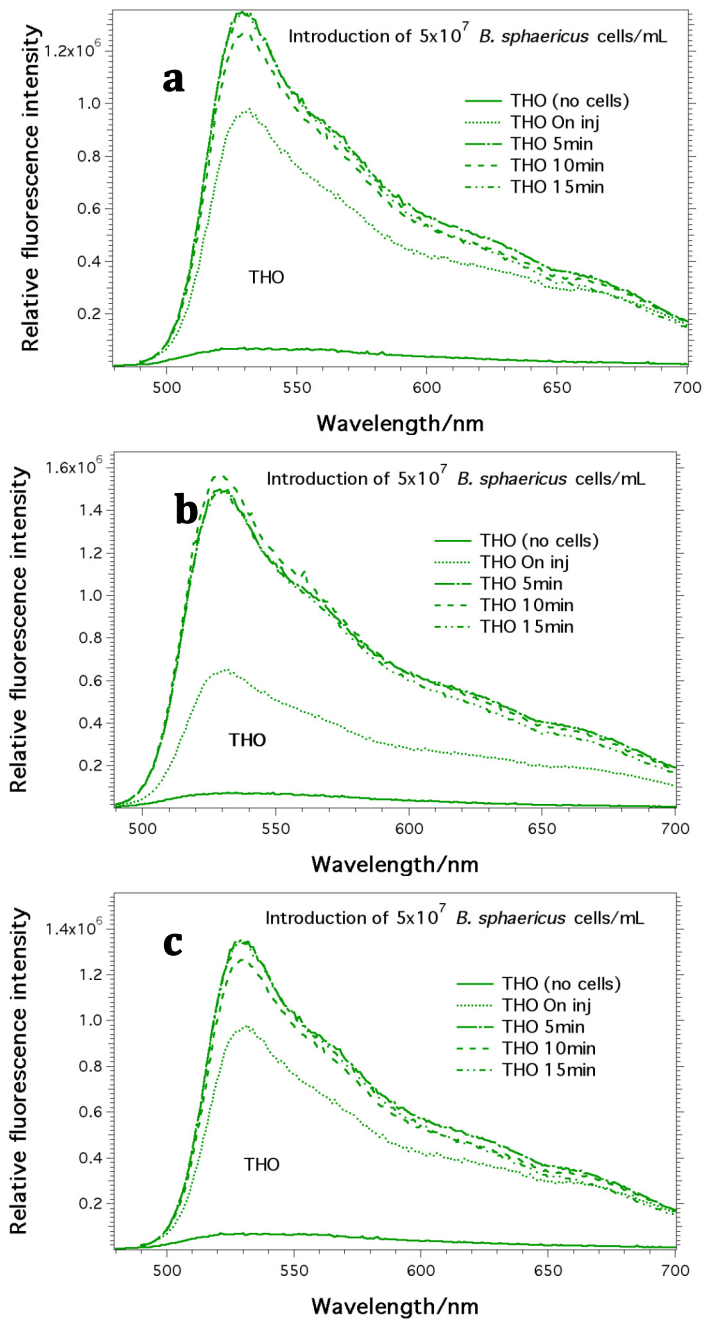

Figure 22. Time-dependent emission spectra of 6 µM THO with *B. sphaericus* (a) run 1, (b) run 2 and (c) run 3, at a cell density of $5x10^7$ cells mL^{-1}.

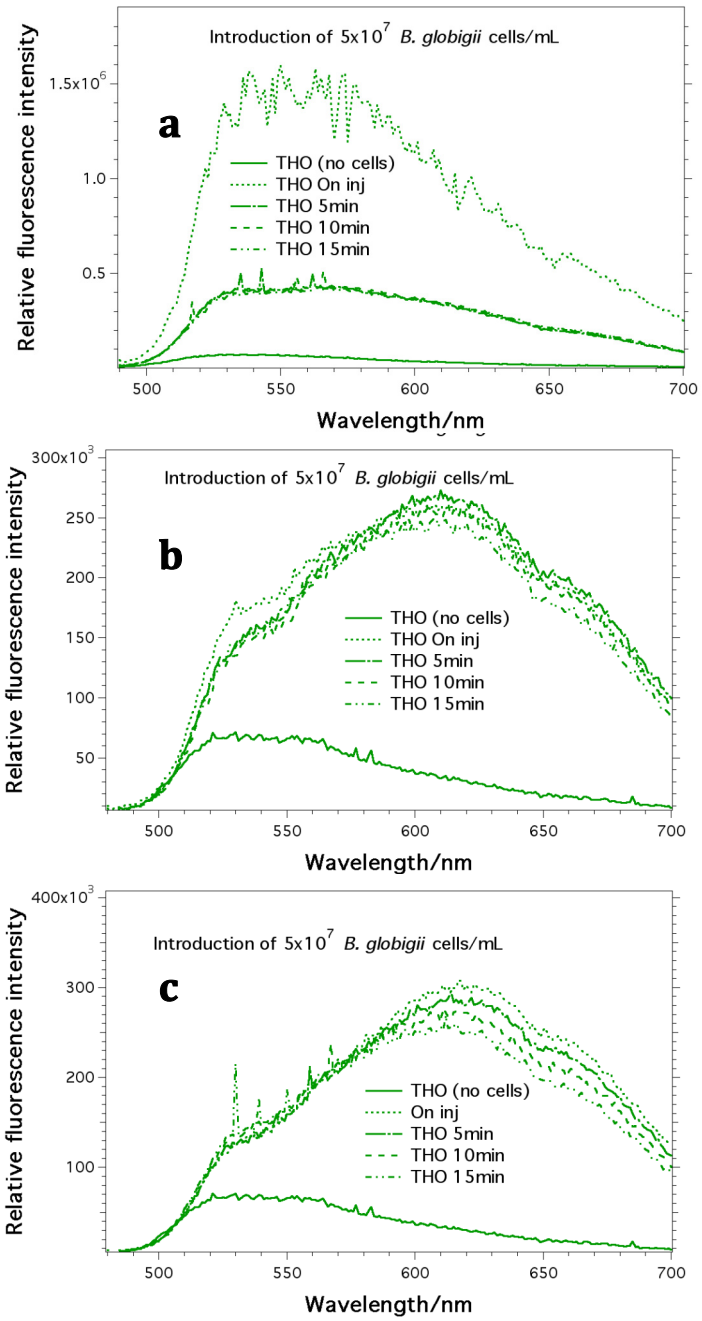

Figure 23. Time-dependent emission spectra of 6 µM THO with *B. globigii* endospores (a) run 1, (b) run 2 and (c) run 3, at a cell density of $5x10^7$ cells mL^{-1}.

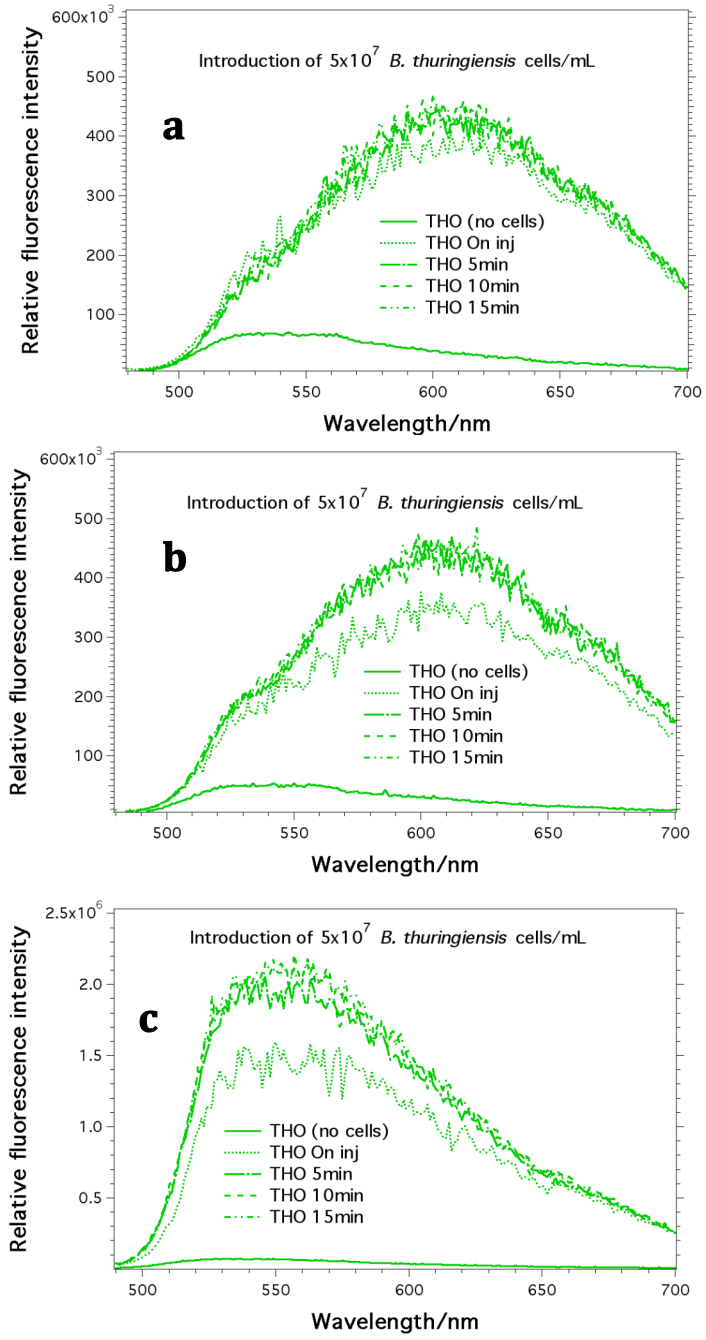

Figure 24. Time-dependent emission spectra of 6 μM THO with *B. thuringiensis* (a) run 1, (b) run 2 and (c) run 3, at a cell density of $5x10^7$ cells mL^{-1}.

1.2.3.2. Fluorescence spectra of THC in the presence of bacterial cells.

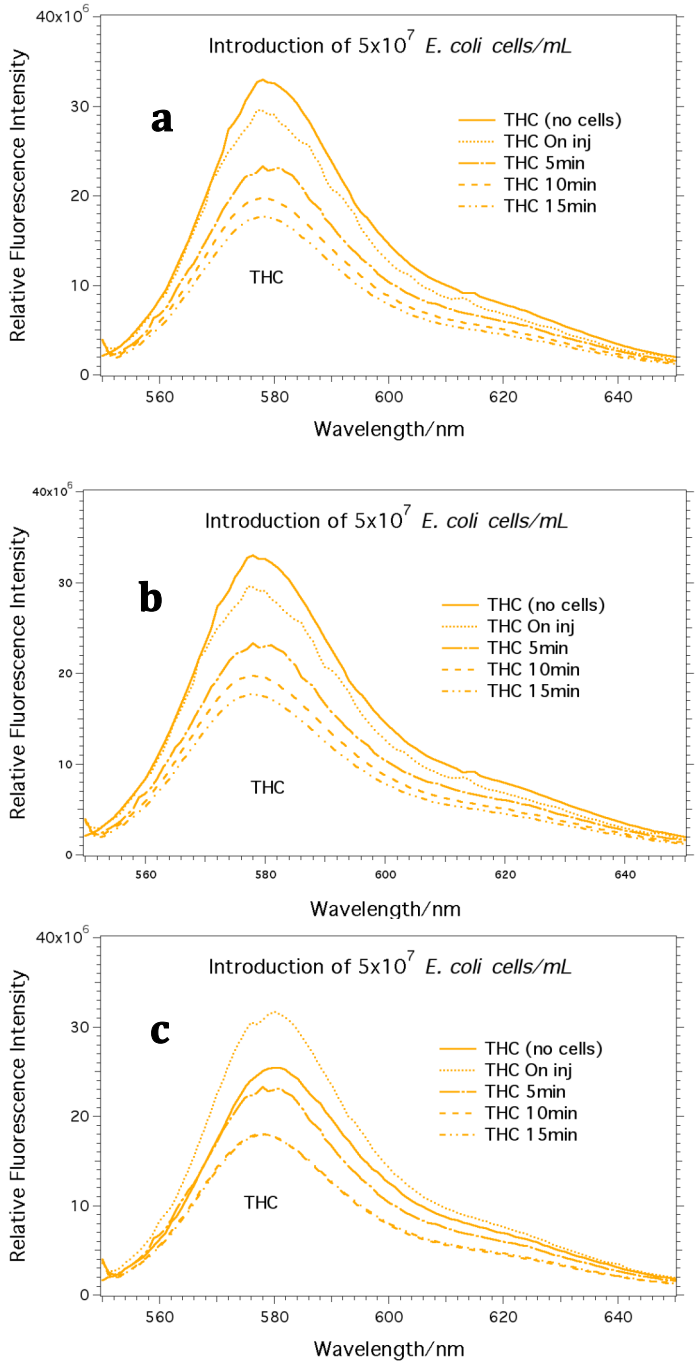

Figure 25. Time-dependent emission spectra of 6 µM THO with *E. coli* cells (a) run 1, (b) run 2 and (c) run 3, at a cell density of $5x10^7$ cells mL^{-1}.

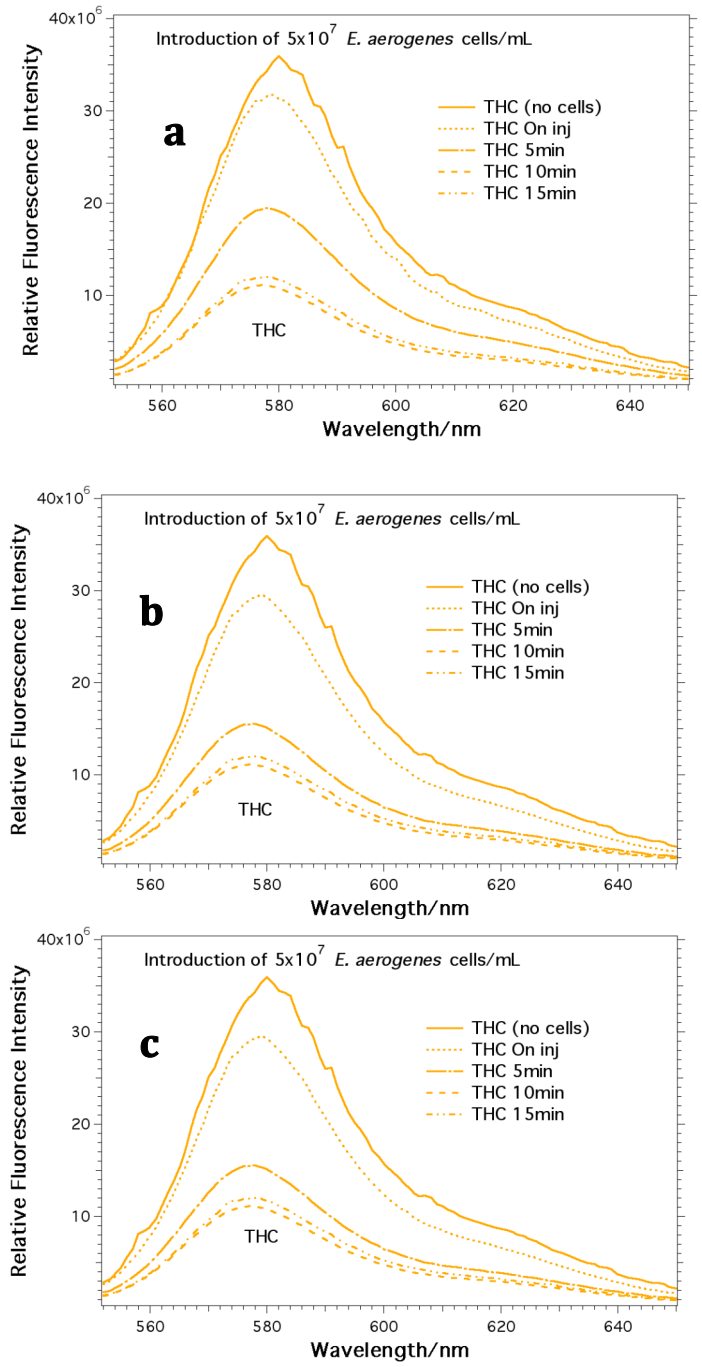

Figure 26. Time-dependent emission spectra of 6 μM THO with *E. aerogenes* cells (a) run 1, (b) run 2 and (c) run 3, at a cell density of $5x10^7$ cells mL^{-1}.

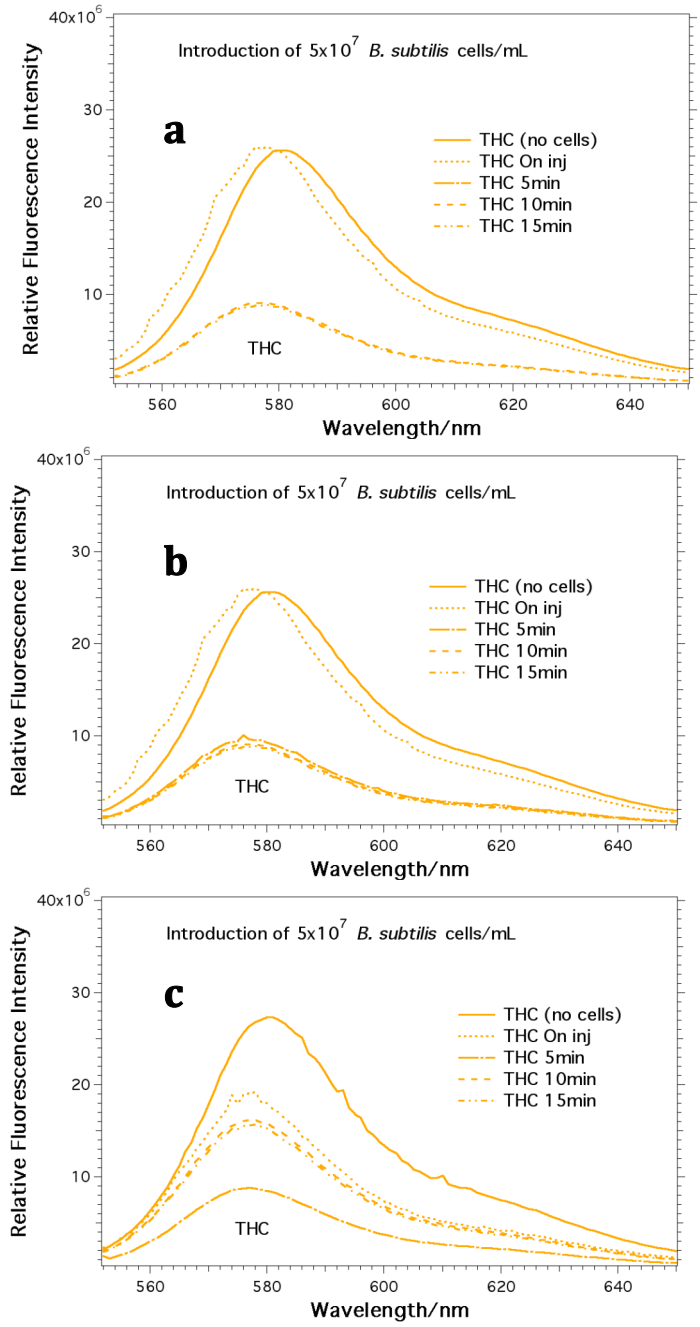

Figure 27. Time-dependent emission spectra of 6 μM THO with *B. subtilis* cells (a) run 1, (b) run 2 and (c) run 3, at a cell density of $5x10^7$ cells mL^{-1}.

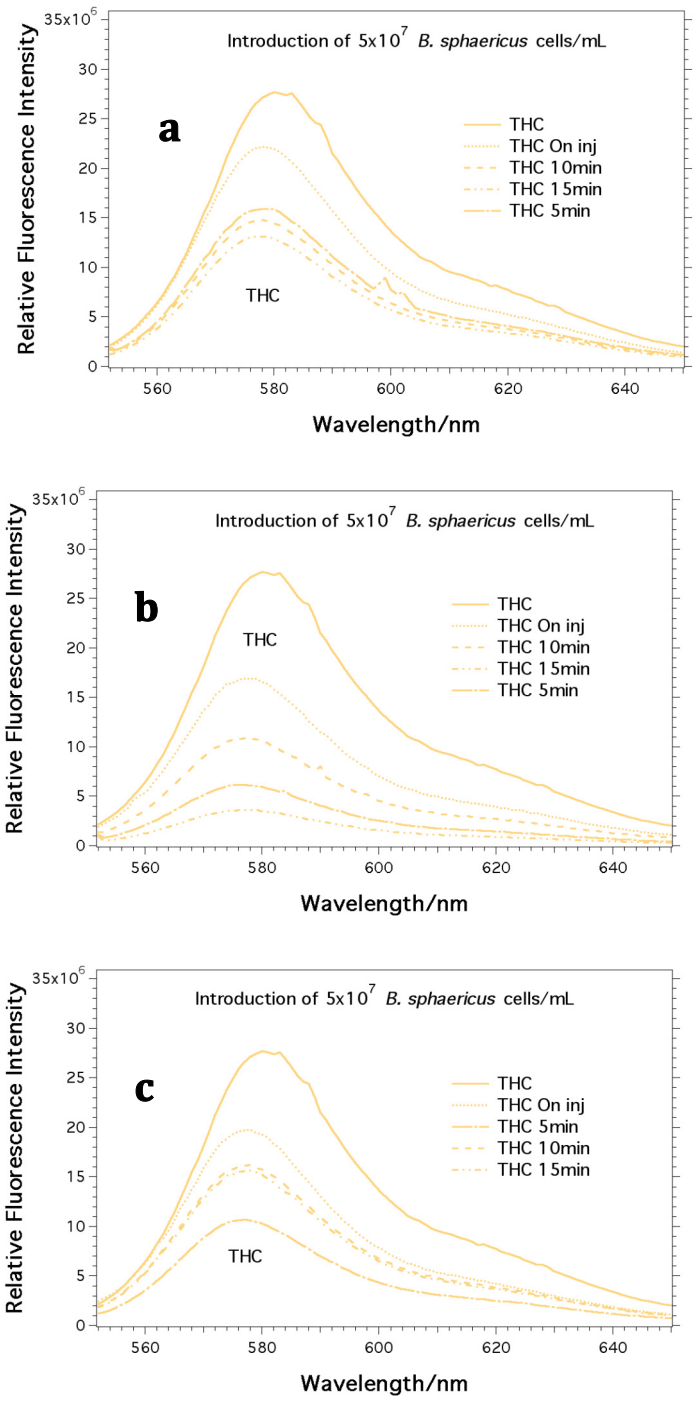

Figure 28. Time-dependent emission spectra of 6 µM THO with *B. sphaericus* (a) run 1, (b) run 2 and (c) run 3, at a cell density of $5x10^7$ cells mL^{-1}.

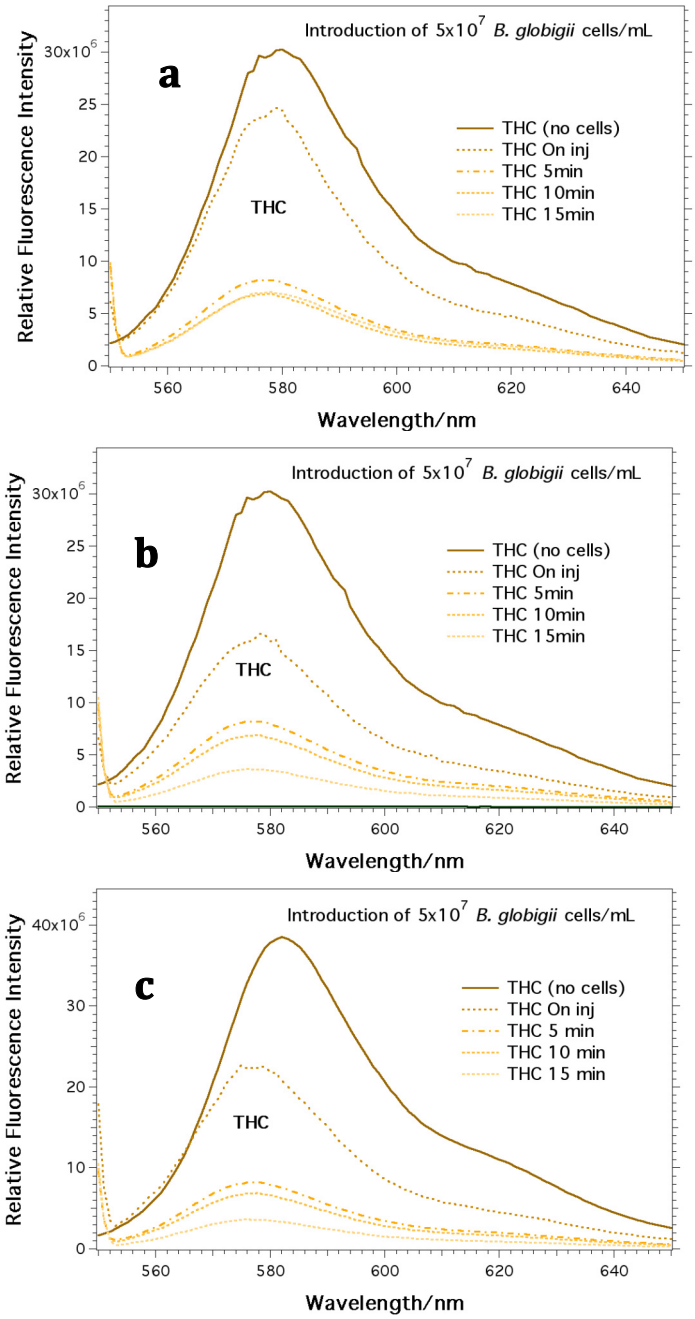

Figure 29. Time-dependent emission spectra of 6 µM THO with *B. globigii* endospores (a) run 1, (b) run 2 and (c) run 3, at a cell density of $5x10^7$ cells mL^{-1}.

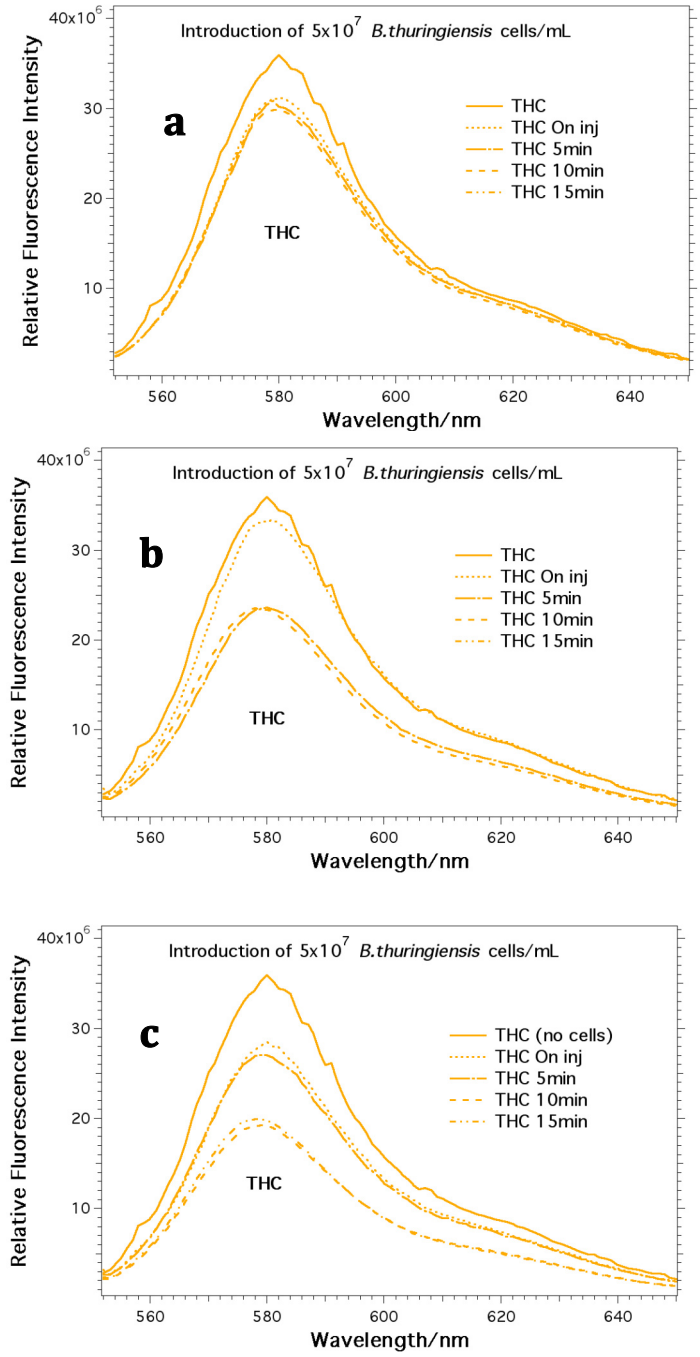

Figure 30. Time-dependent emission spectra of 6 μM THO with *B. thuringiensis* endospores (a) run 1, (b) run 2 and (c) run 3, at a cell density of $5x10^7$ cells mL^{-1}.

1.2.3.3. Comparison between the fluorescence properties of the cyanine dyes in the presence of bacterial cells.

Comparison of the emission spectra from each bacteria revealed that there was increased emission enhancement in two of the three cases (Figure 13–Figure 30), though the magnitude of that enhancement varied. The introduction of bacterial samples to THIA and THO resulted in significant emission enhancement. The level of emission enhancement was time-dependent; that is, it had some dependence on how long after the introduction of bacterial cells the measurements were made. THC, however, did not display emission enhancement. This may be because THC has a rapid emission enhancement but also has an equally rapid decay. The emission takes about 2 minutes to measure, so it is conceivable that the enhancement and decay occur during this time. The level of emission enhancement for each thiacyanine dye was recorded in Tables 13–18.

Table 13. Emission intensity of thiacyanine dyes with the addition of *E. coli* cells.

Dyes	Runs	I (t_0)	I ($t_{On\ inj}$)	I (t_{15min})	λ(t_0)	λ($t_{On\ inj}$)	λ(t_{15min})
THIA	1	1.60E+06	7.40E+06	2.80E+06	469	486	479
	2	1.70E+06	7.50E+06	2.80E+06	471	482	480
	3	1.70E+06	7.60E+06	2.80E+06	474	482	480
THO	1	7.10E+04	8.60E+05	4.80E+05	530	531	529
	2	7.00E+04	8.60E+05	4.50E+05	530	531	527
	3	7.10E+04	8.60E+05	4.80E+05	530	531	528
THC	1	2.80E+07	1.70E+07	1.30E+07	580	578	578
	2	3.30E+07	3.00E+07	1.80E+07	578	577	578
	3	3.30E+07	2.90E+07	1.80E+07	578	578	578

Table 14. Emission intensity of thiacyanine dyes with the addition of *E. aerogenes* cells.

Dyes	Runs	I (t_0)	I ($t_{On\ inj}$)	I (t_{15min})	λ(t_0)	λ($t_{On\ inj}$)	λ(t_{15min})
THIA	1	2.20E+06	4.50E+06	3.90E+06	473	479	482
	2	2.20E+06	3.50E+06	4.30E+06	468	479	479
	3	2.20E+06	4.00E+06	4.00E+06	473	479	482
THO	1	7.20E+04	4.00E+05	4.70E+05	531	600	600
	2	7.10E+04	3.80E+05	4.80E+05	530	608	557
	3	7.00E+04	1.60E+06	2.20E+06	530	563	580
THC	1	3.60E+07	2.90E+07	1.20E+07	580	580	580
	2	3.60E+07	2.90E+07	1.20E+07	580	580	580
	3	3.60E+07	2.90E+07	1.20E+07	580	580	580

Table 15. Emission intensity of thiacyanine dyes with the addition of *B. subtilis* cells.

Dyes	Runs	I (t_0)	I ($t_{0n\ inj}$)	I (t_{15min})	λ(t_0)	λ($t_{0n\ inj}$)	λ(t_{15min})
THIA	1	2.20E+06	7.50E+06	7.70E+06	473	478	474
	2	2.20E+06	7.50E+06	7.60E+06	473	478	479
	3	2.20E+06	7.80E+06	9.40E+06	471	482	474
THO	1	7.31E+04	1.60E+05	5.20E+05	535	550	543
	2	7.10E+04	2.70E+05	2.70E+05	530	608	610
	3	7.20E+04	3.10E+05	2.90E+05	530	617	616
THC	1	3.90E+07	2.20E+07	3.60E+06	582	578	576
	2	3.00E+07	1.70E+07	3.60E+06	580	578	576
	3	3.00E+07	2.50E+07	6.90E+06	580	579	578

Table 16. Emission intensity of thiacyanine dyes with the addition of *B. sphaericus* cells.

Dyes	Runs	I (t_0)	I ($t_{On\ inj}$)	I (t_{15min})	λ(t_0)	λ($t_{On\ inj}$)	λ(t_{15min})
THIA	1	2.20E+06	1.60E+07	2.20E+07	473	478	478
	2	2.20E+06	1.80E+07	1.60E+07	473	480	479
	3	2.20E+06	2.14E+07	1.60E+07	474	487	478
THO	1	7.10E+04	9.70E+05	1.30E+06	530	530	529
	2	7.10E+04	1.00E+06	1.30E+06	530	529	530
	3	7.00E+04	5.80E+05	1.40E+06	530	530	528
THC	1	2.80E+07	2.20E+07	1.60E+07	580	578	577
	2	2.80E+07	1.70E+07	3.60E+06	580	578	576
	3	2.80E+07	2.00E+07	1.60E+07	580	578	578

Table 17. Emission intensity of thiacyanine dyes with the addition of *B. globigii* endospores.

Dyes	Runs	I (t_0)	I ($t_{On\ inj}$)	I (t_{15min})	λ(t_0)	λ($t_{On\ inj}$)	λ(t_{15min})
THIA	1	2.00E+06	9.50E+06	7.90E+06	471	478	478
	2	2.10E+06	8.00E+06	7.50E+06	470	478	478
	3	2.00E+06	9.20E+06	7.80E+06	471	478	478
THO	1	7.20E+04	2.70E+05	2.40E+05	530	609	609
	2	7.10E+04	3.10E+05	2.60E+05	530	616	615
	3	7.10E+04	3.00E+05	2.50E+05	530	615	615
THC	1	3.60E+07	2.50E+07	7.10E+06	580	579	578
	2	3.60E+07	1.70E+07	3.60E+06	580	579	577
	3	3.60E+07	2.20E+07	3.60E+06	580	579	577

Table 18. Emission intensity of thiacyanine dyes with the addition of *B. thuringiensis* endospores.

Dyes	Runs	I (t_0)	I ($t_{On\ inj}$)	I (t_{15min})	λ(t_0)	λ($t_{On\ inj}$)	λ(t_{15min})
THIA	1	1.50E+06	1.00E+07	5.90E+06	472	477	478
	2	1.50E+06	1.00E+07	5.90E+06	469	477	478
	3	1.50E+06	2.14E+07	2.60E+07	472	477	478
THO	1	6.90E+04	4.00E+05	4.70E+05	531	600	600
	2	6.90E+04	3.80E+05	4.80E+05	530	608	557
	3	7.00E+04	1.60E+06	2.20E+06	530	563	580
THC	1	3.60E+07	3.10E+07	3.00E+07	580	580	580
	2	3.60E+07	3.30E+07	2.30E+07	580	580	580
	3	3.60E+07	2.90E+07	2.00E+07	580	580	580

Table 19. Changes in emission intensity of thiacyanine dyes due to the addition of bacterial species.

Bacterial species	Dyes	$\Delta I\ (t_{0n\ inj})$	$\Delta I\ (t_{15\ min})$	$\Delta\lambda\ (t_{0n\ inj})$	$\Delta\lambda\ (t_{15min})$
E. coli	THIA	5.80E+06	1.20E+06	17	10
	THIA	5.80E+06	1.10E+06	11	9
	THIA	5.90E+06	1.10E+06	8	6
E. coli	THO	7.89E+05	4.09E+05	1	-1
	THO	7.90E+05	3.80E+05	1	-3
	THO	7.89E+05	4.09E+05	1	-2
E. coli	THC	-1.10E+07	-1.50E+07	-2	-2
	THC	-3.00E+06	-1.50E+07	-1	0
	THC	-4.00E+06	-1.50E+07	0	0
E. aerogenes	THIA	2.30E+06	1.70E+06	6	9
	THIA	1.30E+06	2.10E+06	11	11
	THIA	1.80E+06	1.80E+06	6	9
E. aerogenes	THO	3.28E+05	3.98E+05	69	69
	THO	3.09E+05	4.09E+05	78	27
	THO	1.53E+06	2.13E+06	33	50
E. aerogenes	THC	-7.00E+06	-2.40E+07	0	0
	THC	-7.00E+06	-2.40E+07	0	0
	THC	-7.00E+06	-2.40E+07	0	0

Table 20. Changes in emission intensity of thiacyanine dyes due to the addition of bacterial species.

Bacterial species	Dyes	ΔI ($t_{On\ inj}$)	ΔI ($t_{15\ min}$)	$\Delta\lambda$ ($t_{On\ inj}$)	$\Delta\lambda$ ($t_{15\ min}$)
B. subtilis	THIA	5.30E+06	5.50E+06	5	1
	THIA	5.30E+06	5.40E+06	5	6
	THIA	5.60E+06	7.20E+06	11	3
B. subtilis	THO	8.69E+04	4.47E+05	15	8
	THO	1.99E+05	1.99E+05	78	80
	THO	2.38E+05	2.18E+05	87	86
B. subtilis	THC	-1.70E+07	-3.54E+07	-4	-6
	THC	-1.30E+07	-2.64E+07	-2	-4
	THC	-5.00E+06	-2.31E+07	-1	-2
B. sphaericus	THIA	1.38E+07	1.98E+07	5	5
	THIA	1.58E+07	1.38E+07	7	6
	THIA	1.92E+07	1.38E+07	13	4
B. sphaericus	THO	1.38E+07	1.98E+07	5	5
	THO	1.58E+07	1.38E+07	7	6
	THO	1.92E+07	1.38E+07	13	4
B. sphaericus	THC	1.38E+07	1.98E+07	5	5
	THC	1.58E+07	1.38E+07	7	6
	THC	1.92E+07	1.38E+07	13	4

Table 21. Changes in emission intensity of thiacyanine dyes due to the addition of bacterial species.

Bacterial species	Dyes	$\Delta I\ (t_{0n\ inj})$	$\Delta I\ (t_{15\ min})$	$\Delta\lambda\ (t_{0n\ inj})$	$\Delta\lambda\ (t_{15\ min})$
B. globigii endospores	THIA	7.50E+06	5.90E+06	7	7
	THIA	5.90E+06	5.40E+06	8	8
	THIA	7.20E+06	5.80E+06	7	7
B. globigii endospores	THO	1.98E+05	1.68E+05	79	79
	THO	2.39E+05	1.89E+05	86	85
	THO	2.29E+05	1.79E+05	85	85
B. globigii endospores	THC	-1.10E+07	-2.89E+07	-1	-2
	THC	-1.90E+07	-3.24E+07	-1	-3
	THC	-1.40E+07	-3.24E+07	-1	-3
B. thuringiensis endospores	THIA	8.50E+06	4.40E+06	5	6
	THIA	8.50E+06	4.40E+06	8	9
	THIA	1.99E+07	2.45E+07	5	6
B. thuringiensis endospores	THO	3.31E+05	4.01E+05	69	69
	THO	3.11E+05	4.11E+05	78	27
	THO	1.53E+06	2.13E+06	33	50
B. thuringiensis endospores	THC	5.00E+06	-6.00E+06	0	0
	THC	-3.00E+06	-1.30E+07	0	0
	THC	-7.00E+06	-1.60E+07	0	0

Table 22. Rates of change in the emission from thiacyanine dyes with the addition of bacterial species.

Bacterial species	Dyes	$\vartheta_{0n\ injection}$ [a]	$\vartheta_{15\ min}$ [a]
E. coli	THIA	1.94E+05 ± 1.92E+03	1.26E+03 ± 6.4E+01
	THO	2.63E+04± 1.92E+01	4.44E+02 ± 1.9E+01
	THC	-2.00E+05 ± 1.45E+05	-1.67E+04 ± 0E+00
E. aerogenes	THIA	6.00E+04± 1.67E+04	2.07E+03 ± 2.3E+02
	THO	2.41E+04 ± 2.33E+04	1.09E+03 ± 1.1E+03
	THC	-2.33E+05 ± 0E+00	-2.67E+04 ± 3.5E-04
B. subtilis	THIA	1.80E+05 ± 5.8E+03	6.70E+03 ± 1.1E+03
	THO	5.82E+03 ± 2.6E+03	3.20E+02 ± 1.92E+03
	THC	-3.89E+05 ± 2.0E+05	-3.14E+04 ± 1.5E+03
B. sphaericus	THIA	5.42E+05 ± 9.1E+04	1.76E+04 ± 7.1E+03
	THO	2.60E+04 ± 9.1E+04	1.40E+03 ± 0E+00
	THC	-2.78E+05 ± 9.0E+04	-1.79E+04 ± 3.9E+03
B. globigii endospores	THIA	2.29E+05 ± 2.8E+04	6.33E+03 ± 2.9E+02
	THO	7.40E+03 ± 7.1E+02	2.0E+02 ± 1.2E+01
	THC	-4.89E+05 ± 1.4E+05	-3.5E+04 ± 2.3E+03
B. thuringiensis endospores	THIA	4.10E+05 ± 2.2E+05	1.23E+04 ± 1.3E+03
	THO	2.41E+04 ± 1.92E+03	1.1E+03 ± 1.1E+03
	THC	-1.70E+05 ± 6.7E+04	-1.30+04 ± 5.7E+03

a. The unit for ϑ is relative intensity s^{-1}

The changes in the emission intensity was determined by calculating the difference in the emission intensity of the dye solution without bacterial cells and the emission intensity of the dye solution with bacterial cells. Calculations were made for the emission intensity immediately after injection (which is approximated to be 30 seconds post inject) and the emission intensity 15 minutes post injection using the Equation 4.

$$\Delta I = I(t_0) - I(t)$$ Equation 4.

Where I is the emission intensity and t is the time after injection.

The rate of emission was calucalted by dividing ΔI by the time the emission was recorded (Equation 4). The rates of emission from the three thiacyanine dyes had larger error bars. This could be attributed to the fact that the emission is not linearly proportional to the concentration and can be affected by many variables. Significant errors will be displayed if the dye and bacterial cells are not at equilibrium at the time the experiments are conducted.

The steady-state emission spectra were useful because they provided, at least for some species, unique emission patterns. For example, the addition of *E. aerogenes* to THIA gave a unique emission pattern. However, in several cases, the emission spectra did not prove to be a good method for distinguishing bacterial cells. The addition of bacterial species to a THO solution did result in perturbation in the emission spectra; however, it would be difficult to distinguish among different bacterial cells by merely examining the emission enhancement. This was because the majority of the emission spectra give similar emission patterns, irrespective of the bacterial species added to the dye solution. THC did not prove to be a particularly useful dye to use in emission studies. We were not able to record any emission enhancement using THC and any of the six bacterial species examined.

1.2.4. Absorption and fluorescence properties of THIA.

Among the thiacyanine dyes used in this thesis, THIA had the largest extinction coefficient and the strongest emission enhancement. For this reason, THIA was used as a model dye with the findings extended to other thiacyanine dyes. To elucidate the reasons for the observed changes in the spectra of the cyanine dyes induced by bacterial cells, we investigated the photophysical properties of THIA. Like the other members of the thiacyanine family of dyes, THIA exhibits a strong affinity for bacterial cells, protein and DNA.[56, 87] THIA is a symmetric cationic organic molecule with two aromatic ring groups connected by a vinyl group having

a delocalized resonance structure (Scheme 3). This structure allows rotation around the central carbon in the vinyl group that separates either side of this symmetric molecule. The rotation, however, is impeded by the extended π-conjugation.

THIA exhibits absorption maximum at approximately 420 nm and displays fluorescence maximum at approximately 475 nm, as seen in (Figure 1–Figure 6) and (Figure 6–Figure 12). Aggregates of THIA have been shown to emit light at 594 nm and 601 nm.[88] The absorption and fluorescence spectra of THIA have similar shapes for a broad range of protic solvents (Figure 31).

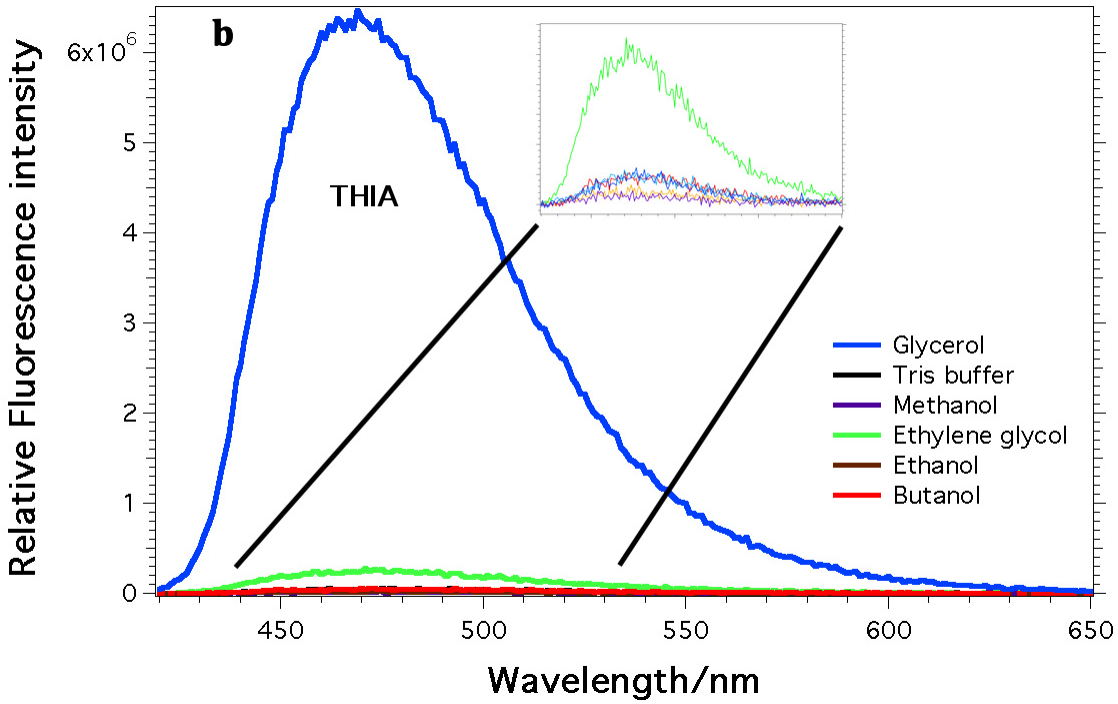

Figure 31. Absorption and fluorescence spectra of THIA (6 μM) for various protic solvents: (a) absorption spectra and (b) fluorescence spectra (λ_{ex} = 420 nm). The curves correspond to different media: **Blue –** Glycerol; **Black –** Tris buffer (2 mM aqueous Tris

buffer, pH = 8.5); **Violet –** Methanol; Light **Green –** Ethylene glycol; **Brown –** Ethanol; and **Red –** Butanol. The emission spectrum for glycerol was reduced 10x for clarity.

1.2.4.1. Bacterium-induced changes in the photophysical properties of THIA.

The introduction of bacterial cells into a thiacyanine dye solution results in three distinct phenomena taking place: a reduction in the extinction coefficient, an increase in the emission intensity and the appearance of a red-shifted emission band.

Indeed, we see correlations between the extent of changes in dye absorption and the bacterial cell density (data no shown). Increasing the bacterial cell density results in a decrease in the dye's extinction coefficient. It was observed that the introduction of bacterial cells to a thiacyanine dye solution, after a brief delay of approximately 200 ms, results in a 1-2 orders-of-magnitude increase in the fluorescent quantum yield of the dye (Figure 33).

The appearance of an emission peak at 600 nm was observed approximately 10 minutes after the introduction of bacterial cells for some bacteria species. This peak was ascribed to ground-state aggregation. To support the assertion that the new peak was related to ground-state aggregation, the absorption spectrum at 420 nm was monitored over a 15-minute time course after the addition of *E. coli* cells to THIA dye solutions. We observed a steady decrease in the absorption of THIA at 420 nm, which was proportional to increases in the emission intensity of the peak at 600 nm. The peak at 600 nm is consistent with findings elsewhere and was ascribed to

aggregate formation of THIA. We believe ground-state aggregation is responsible for the peak at 600 nm because of the broadening of the absorption peak.[89] *E. coli* cells exhibited the most pronounced peak at 600 nm of the six bacterial species examined. This may be due to the volume of dye molecules that were taken up into the cell relative to the other bacterial species. We saw from the absorption spectra that the vast majority of dye molecules taken up from solution by the bacterial species saturate within the first two minutes. The time required for saturation is species-dependent; however, most samples saturate within 15 minutes. This is supported by the fact that there are few if any changes between the absorption spectrum at 10 minutes after introduction of cells to the dye solution and the spectrum at 15 minutes after introduction of cells for all four thiacyanine dyes, as seen in (Figure 12–Figure 17). The absorption spectra of the endospores, as seen in (Figure 16-Figure 17), were similar to the absorption spectra of the vegetative bacteria.

An emission spectrum taken after the interaction of THIA with *E. coli* cells shows that the decrease in absorption correlated with the increases in the appearance of a red-shifted peak, which appears at approximately 600 nm. Others have previously ascribed the 600-nm peak to dye aggregation.[88] Measurements were made of the absorption kinetics at 600 nm over a 20-minute time course with *E. coli* cells being introduced at approximately one minute. Introduction of bacterial species to a 6-μM solution of THIA resulted in a gradual reduction in the absorption spectrum that continued at a slower rate for the next 19 minutes, as seen in (Figure

32). The kinetics emission spectrum of THIA, recorded after the introduction of *E. coli* cells in the absence of stirring (Figure 33), confirmed the inverse relationship between the decreasing absorption at 420 nm and the increasing emission peak at 600 nm.

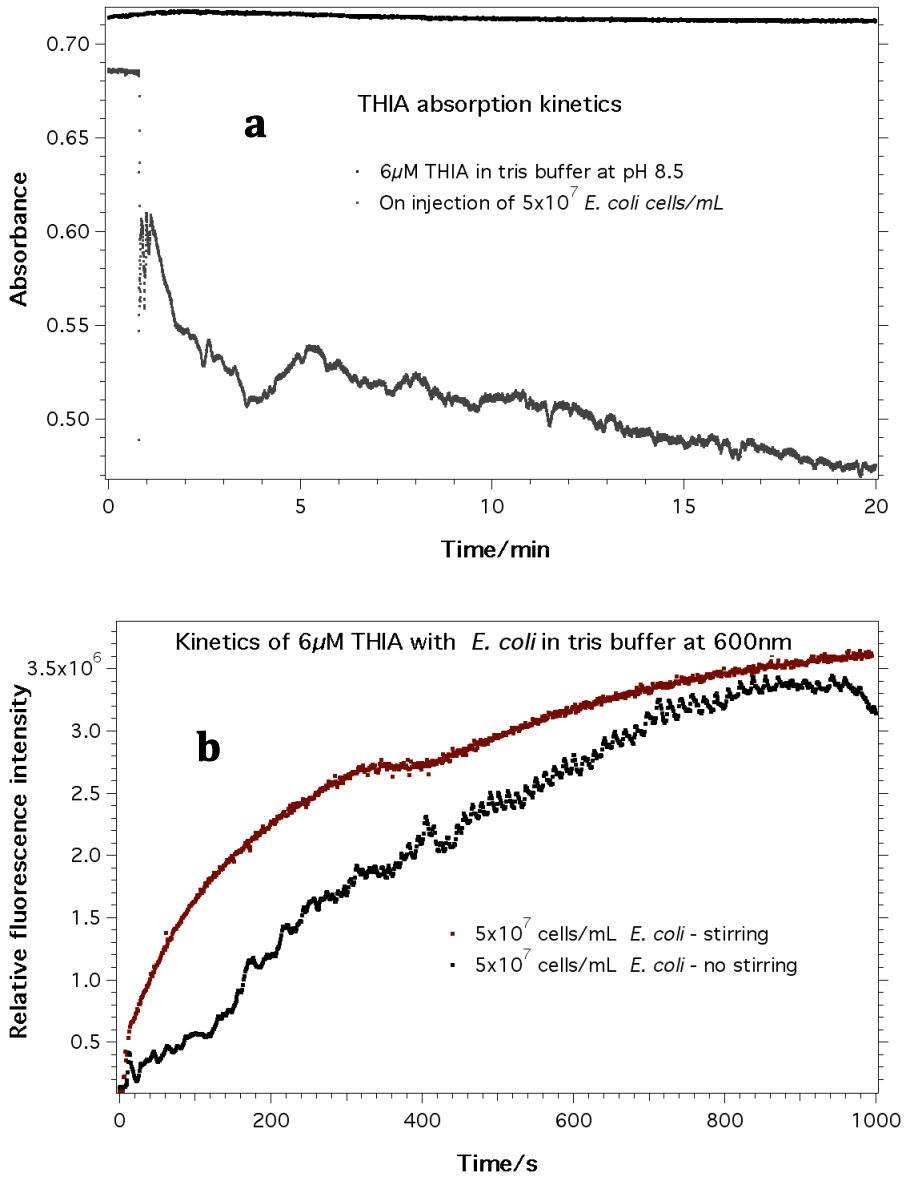

Figure 32. The steady-state absorption spectra of THIA at 420 nm: (a) before and after the introduction of $5x10^7$ *E. coli* cells mL^{-1}; (b) the kinetics of the absorption spectra of THIA over a 20-minute time course with and without $5x10^7$ *E. coli* cells mL^{-1}.

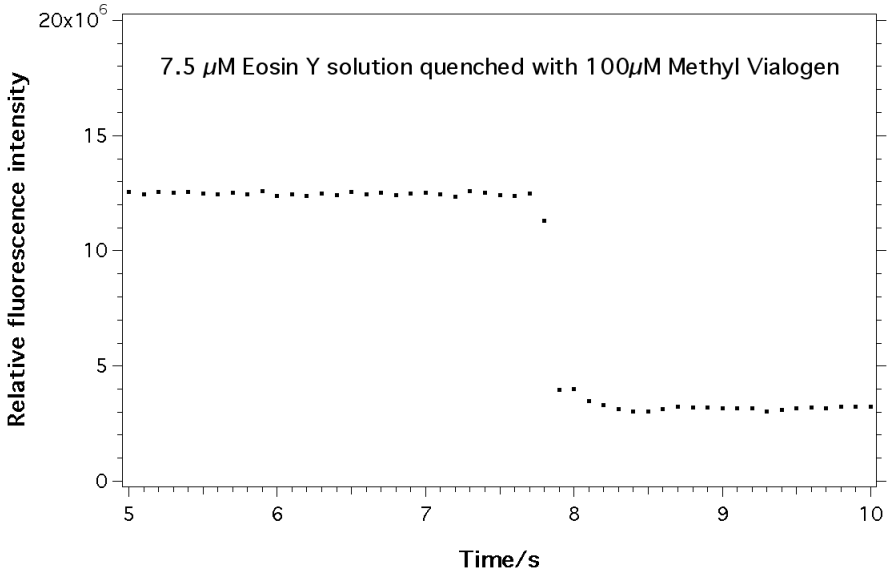

Figure 33. Dynamics of the quenching of the fluorescence of a 7.5 μM eosin Y (EY) solution with 100 μM methyl vialogen (MV) at similar conditions as the measurements of the absorption spectra (without stirring).

1.2.4.2. Surfactant modulation of the fluorescence spectra of THIA.

Initially, we performed our analysis without adding surfactants to the dye solution. This resulted in less emission enhancement and more dye aggregation, as can be seen in Figure 33. The addition of the surfactants TWEEN 20 and TWEEN 40 modulated the emission enhancement of the thiacyanine dyes with and without bacterial species. The addition of the weak surfactants TWEEN 20 or TWEEN 40 to the dye solution weakly enhanced the emission of the dye. TWEEN 20 enhances the fluorescence signal recorded for the dye relative to the emission enhancement due

to the introduction of bacterial cells.[90] An increase in the fluorescence intensity of THIA was observed with the increase in the TWEEN 20 concentration (Figure 34).

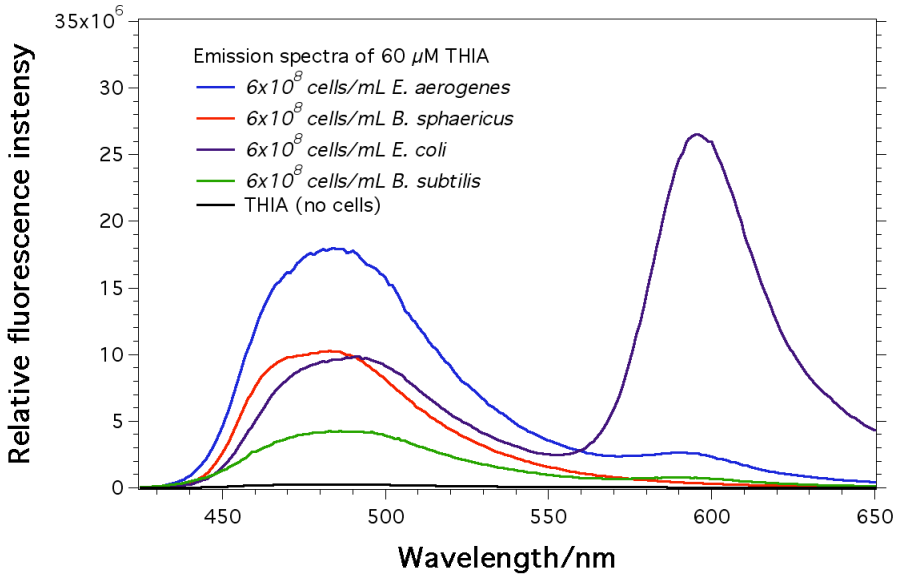

Figure 33. Emission spectra of THIA (475 nM) in Tris buffer (no TWEEN added) with $6x10^8$ cells mL^{-1} of bacterial cells: Black – no cells; Green – *B. subtilis*; Red – *B. sphaericus*; Violet – *E. coli*; and Blue – *E. aerogenes*. (λ_{ex} = 420 nm, 2 mM Tris aqueous buffer, pH = 8.5).

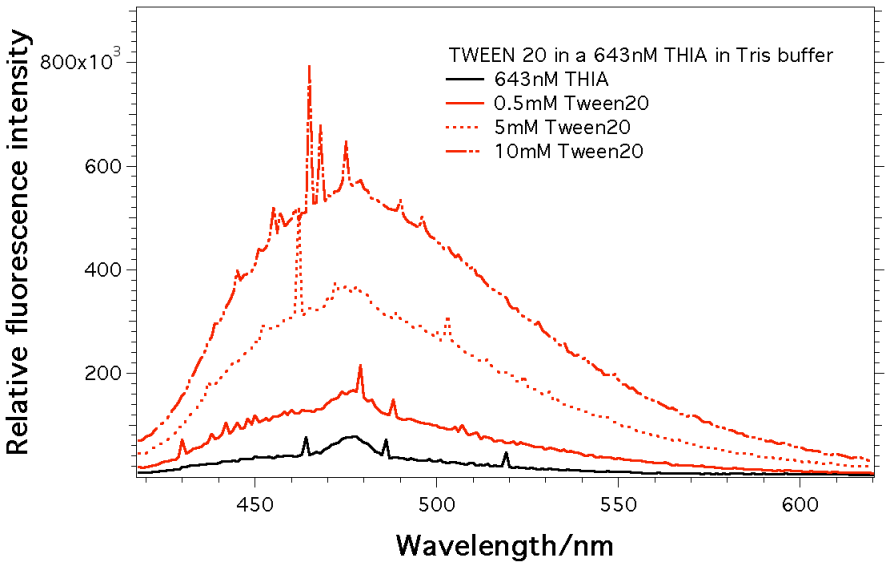

Figure 34. Emission spectra of THIA (475 nM) in the presence of various concentrations of TWEEN 20: black – no TWEEN 20; green – 0.5 mM TWEEN; blue – 5 mM TWEEN; red – 10 mM TWEEN. (λ_{ex} = 420 nm, 2 mM Tris aqueous buffer, pH = 8.5).

1.2.4.3. Solvent dependence of the fluorescence properties of THIA.

The spectral data from (Figure 1–Figure 12 and Figure 34), suggest that the bacterium-induced fluorescence enhancement is a corollary of an increase in the emission quantum yield of the dye, Φ_f. After the addition of bacteria, we observed an increase in the emission intensity while the absorption at the excitation wavelength decreased at a factor of two or less (Figure 1–Figure 12). These findings illustrate that the increase in the fluorescence intensity cannot simply be attributed to changes in the amount of light being absorbed or in the number of dye molecules in the excitation volume.

The molecular structure of the thiacyanine dyes as seen in (Scheme 4) elucidates the sensitivity of their fluorescence quantum yield to any restrictions from their micro-environment. THIA has a symmetric molecular structure, in which extended π-conjugation, spanning over the bonds connecting the two ring systems, supports its planar conformation.[91]

Chromophores with molecular structures like THIA and many other thiacyanine dyes exist in either a planar conformation or in one or more twisted conformations. In their ground state, such chromophores exist preferably in a planar conformation.[60, 61, 69-71, 92] The twisted conformation is energetically preferred for the excited state due to the weakened π-bonding and to the steric hindrance between the aromatic rings.[60, 71] The radiative deactivation (i.e., fluorescence) of the excited-state dye molecules occurs solely from its planar excited-state conformation (to the planar ground state).[60, 70] Photo-excitation (leading to $\pi^* \leftarrow \pi$ transition) decreases the bonding character of the π-conjugation, and the twisted conformer becomes preferred for the excited state due to the steric repelling interactions. The narrow energy gap between the ground and excited states of the twisted conformer provides efficient pathways for internal conversion (Scheme 4). The weakened π-bonding character of the photo-excited THIA increases the propensity for rotation around the two bonds connecting the ring systems. Rotational motions around these two bonds provide pathways for an efficient non-radiative decay through the twisted conformer (Scheme 5).[71]

An increase in the rigidity of the dye molecular microenvironment due, for example, to binding of the dye molecule to a biological macromolecule such as a protein or to DNA has been shown to reduce such rotational motions and to suppress the exploration of the conformational space (within the lifetime of the excited state of THIA).[57, 73, 93, 94] The decrease in the likelihood of excited-state conformers leading to non-radiative deactivation, a corollary of the increase in the rigidity of the molecule, results in an increase in the fluorescence quantum yield of the cyanine dye (Scheme 5).[91]

To examine the validity of the proposed mechanism of emission enhancement, which we gathered from previous reports for THIA and other cyanine dyes, we examined the solvent dependence of the THIA fluorescence. The absorption spectra of THIA are similar for a broad range of protic solvents. THIA exhibits absorption maximum at about 420 nm and displays fluorescence maximum at 475 nm, as seen in (Figure 1-Figure 30). The absorption and emission measurements of THIA, in a series of solvents, indicated that the restriction of the dye molecule was due to an increased restriction of the dye's micro-environment that. The solvent dependence of the fluorescence quantum yield of THIA for protic solvents was investigated at different viscosities (η).

The fluorescence quantum yield of THIA increased over an order of magnitude when the dye was placed in solvents more viscous than water; i.e., for viscous solvents with moderate polarity, glycerol and ethylene glycol, the quantum

yields of THIA were Φ_f = 0.014 and Φ_f = 5.9×10^{-3}, respectively (Table 19). The coefficient of correlation between Φ_f and η was close to unity, as seen in (Figure 35). The correlation coefficient or the residual, R, reflects the interdependence of the two quantities. A strong correlation of the two quantities results in a value of *R* close to 1 or -1. A lack of correlation between the two quantities will give a value close to zero. The plot of solvent viscosity versus fluorescence quantum yield gave strong correlations using a 4th-order polynomial fit. The fit had an R^2 value of 0.98. It should be noted that while a polynomial fit was used to correlate the data, a number of different correlations could have been used and would have been just as appropriate, considering that the function fits the data within a pre-defined tolerance.

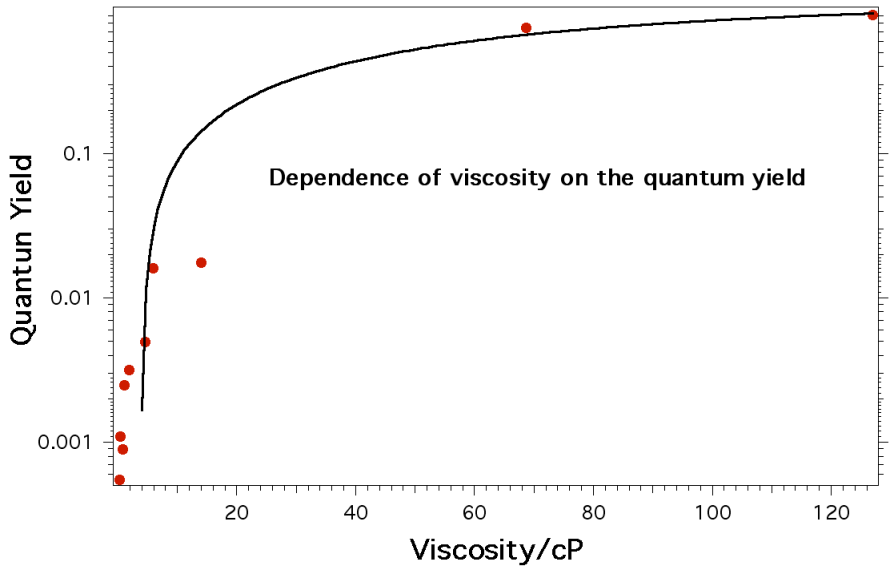

Figure 35. Polynomial correlation of solution viscosity with the emission quantum yield of THIA. The data used for the correlation were acquired by introducing a 600-nM THIA dye solution into samples of varying viscosity, R^2 = 0.98.

Table 23. Fluorescence quantum yield of THIA for protic solvents with different polarities and viscosities.

Protic solvents	Φ_f **x** 10^3	η_o [(b)]/cP
100% Glycerol	127	905.4
99% Glycerol/water	68.7	741
70% Glycerol/water	14.0	17.5
50% Glycerol/water	4.5	4.98
40% Glycerol/water	1.84	3.15
Ethylene glycol	5.94	16.1
Methanol	0.276	0.55
Ethanol	0.443	1.1
Butanol	1.07	2.5
Water	0.857	0.89

(b) Dynamic viscosity

Time-resolved fluorescence measurements confirmed our findings from the steady-state spectroscopic studies. The fluorescence lifetime of THIA, *t* (i.e., the lifetime of its lowest excited state), was close to 1 ns for glycerol media, and for all other solvents we tested, *t* was shorter than 200 ps (that is, the detection limit of our time-correlated single-photon-counting spectrometer). These findings suggested that the restriction of the THIA molecules by increased rigidity of the molecules' microenvironment or by binding to a substrate could be the mechanism that drives the increase in the fluorescence quantum yield, Φ_f, and causes the observed emission enhancement (Scheme 4.). However, it should be pointed out that the cell wall is a micro-porous structure that is made up of 60% polysaccharides by mass.

The remaining mass can be attributed to water, proteins and phosphates. Therefore, the viscosity should not be significantly higher than water and certainly

not to the level to see the observed changes in emission intensity. This leads us to believe that the fluorescence enhancement is a result of the dye binding to an anionic or poly-anionic molecule such as a protein or DNA.

Scheme 5. Modified Jablonski diagram representing the electronic transitions during the photoactivation and the excited-state deactivation by photon emission or rotational relaxation.

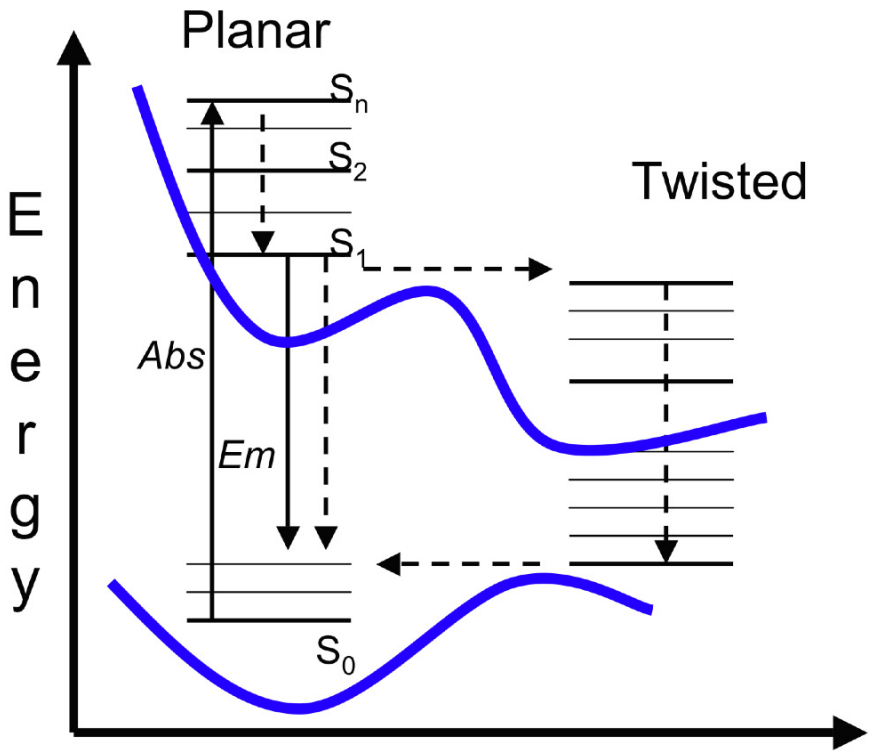

1.3. Conclusions

Absorption spectroscopy of the three thiacyanine dyes; THIA, THO and THC, was investigated with and without the introduction of bacterial cells. The bacterium-induced changes in the absorption spectra of the three dyes were analyzed in the study. Combining the bacterium-induced changes from the three dyes gave a three-digit code for each bacterial species. For rapid analysis, a mixture of the three dyes was used to analyze bacterium-induced changes in the absorption spectra. The mixed-dye spectra display a unique absorption pattern for each bacterial species being investigated. These characteristic absorption patterns were evaluated by monitoring three positions on the curve and using the absorption from these three positions to for a three-digit code for identification of these bacterial species in solution.

The emission enhancement was observed for two of the three thiacyanine dyes used in this study. The changes in emission intensity along with the rate of emission, as a function of time, were determined. The rate of emission enhancement was informative about the identity of the bacterial specie.

The simultaneous decrease in dye absorption with increase in emission intensity led us to ascribe the emission enhancement to changes in the quantum yield of the dye. These observations were supported using high-viscosity solvents to restrict the molecular motions of the dye molecules in solution. The interaction of these bacterial species with three dyes resulted in orders-of-magnitude increases in the fluorescence emission of the dyes. The changes in the absorption spectra of the

thiacyanine dyes with the addition of each bacterial species were distinct and valuable in trying to distinguish among the various bacterial species.

Modulation to the emission enhancement of THIA and the other thiacyanine dyes was achieved by addition of TWEEN surfactants to the dye solution. Addition of surfactants to the dye solution with any addition of cells results in increases to the fluorescence intensity; however, the addition of bacterial cells magnifies these phenomena.

The findings from these studies of the interaction of cyanine dyes with bacteria set guidelines for experiments using this technique.

1.4. Experimental

1.4.1. Materials

E. coli TOP 10 and *E. aerogenes, B. subtilis* and *B. sphaericus* strains were used for all experiments. Propidium iodide and SYTO 9 were obtained from Invitrogen. LB broth, LB Agar, 3,3'-diethylthiacyanine iodide, 3,3'-diethylthiacarbocyanine iodide (THIA-CARB) (Sigma), Thiazole orange, Stain all and alcohols (methanol, ethanol, 1-propanol, 1-butanol, ethylene glycol and glycerol: all spectroscopic grade) were purchased from Sigma-Aldrich. Tris (hydroxylmethyl) aminomethane was obtained from Acros Organics. Sodium hydroxide was purchased from Fisher Scientific. For all aqueous solutions, we used Milli-Q water (from an in-house purification system). *B. subtilis*, *B. sphaericus* and *E. aerogenes* were purchased from Carolina Biologicals. *E. coli* (TOP 10) was purchased from Invitrogen. The United States Army supplied endospores from *B. globigii* and *B. thuringiensis*.

1.4.2. Methods

1.4.2.1. Bacterial sample preparation

The bacterial cultures for two Gram-positive species, *Bacillus subtilis* and *Bacillus sphaericus*, and two Gram-negative species, *Escherichia coli* and *Enterobacter aerogenes* were prepared on solid Luria Bertani (LB) agar media. Colonies from these cultures were transferred to liquid media and allowed to grow overnight, up

to 24 hours. The solid LB agar with bacterial culture was stored at -4 ^{o}C in a refrigerator. Prior to use in the experiment, the liquid cultures were centrifuged, pellet, washed twice and re-suspended in 2 mM Tris buffer solution. Stock solutions were prepared by suspending spores in 2 mM Tris buffer, then stored at 4 ^{o}C and used completely within 24 hours (to prevent contamination). Cells were cultured overnight at 37 ^{o}C in liquid media with shaking at 200 rpms in LB Broth cultures. Prior to analysis, the cell media were changed from LB Broth to Tris buffer at pH 8.5 (2 mM) by centrifuging the bacteria to a pellet, decanting the LB Broth and re-suspending the cells in Tris buffer. To ensure that all bacteria used in our experiments were in their growth phase, we constructed growth curves for the bacterial strains being investigated. The curves revealed that bacteria in liquid cultures, grown 18–24 hours, are within their growth phases. All bacterial strains were maintained at room temperature.

1.4.2.2. Endospore preparation

B. globigii and *B. thuringiensis* endospores were removed from storage (4 oC in a refrigerator) and 4 mg were weighed out and placed in a 1-mL plastic centrifuge vial. We made a suspension by delivering 1 ml of a 2-mM Tris buffer solution (pH 8.5) to the endospores. The sample was vortexed and stored at room temperature until used.

1.4.2.3. Preparing a stock solution of thiacyanine dyes.

A stock solution of each dye (600 μM) was prepared by dissolving solid dye in a 75% ethanol/25% water solution. Solutions were prepared for bacterial analyses by diluting the dye stock solution by 10x, 100x and 1000x in 2mM Tris buffer (pH 8.5). This procedure was followed for all dyes used in this study.

Reference

1. Cheng, J. C.; Huang, C. L.; Lin, C. C.; Chen, C. C.; Chang, Y. C.; Chang, S. S.; Tseng, C. P., Rapid detection and identification of clinically important bacteria by high-resolution melting analysis after broad-range ribosomal RNA real-time PCR. *Clin Chem* **2006,** 52, (11), 1997-2004.

2. Klevens, R. E., J; Richards, C; Horan, T; Gaynes, R; Pollack, D; Cardo, D;, Estimating Health Care-Associated Infections and Death in U.S. Hospitals, 2002. *Public Health Reports, National Center for Infectious Disease, CDC* **2007,** 122.

3. Klevens, R. M.; Morrison, M. A.; Nadle, J.; Petit, S.; Gershman, K.; Ray, S.; Harrison, L. H.; Lynfield, R.; Dumyati, G.; Townes, J. M.; Craig, A. S.; Zell, E. R.; Fosheim, G. E.; McDougal, L. K.; Carey, R. B.; Fridkin, S. K.; Investigators, A. M.; , Invasive methicillin-resistant Staphylococcus aureus infections in the United States. *Jama-Journal of the American Medical Association* **2007,** 298, (15), 1763-1771.

4. Clark CD, J. K., Jones JL, et al. , Incidence of hand infections and their bacterial flora. *Presented at the American Academy of Orthopaedic Surgeons 74th Annual Meeting. Feb. 14-18, 2007. San Diego.* **2007**.

5. Bond, P. L.; Erhart, R.; Wagner, M.; Keller, J.; Blackall, L. L., Identification of some of the major groups of bacteria in efficient and nonefficient biological phosphorus removal activated sludge systems. *Applied and Environmental Microbiology* **1999,** 65, (9), 4077-4084.

6. Sakata, H.; Comparative study on bacterial eradication rate and clinical efficacy of CDTR, CFPN, and FRPM for treatment of children with otitis media and lower respiratory tract infection due to Streptococcus pneumoniae and Haemophilus influenzae; *Jpn J Antibiot* **2001,** 54 Suppl B, 96.

7. Tambic, A.; Methicillin-resistant Staphylococcus aureus (MRSA), a predictor of the end of the antibiotic era--diagnosis, epidemiology, therapy and dissemination prevention; *Lijec Vjesn* **1997,** 119, (5-6), 166-71.

8. Thorell, E. A.; Jackson, M. A.; Harrison, C.; Selvarangan, R., Methicillin-resistant Staphylococcus aureus (MRSA) in healthy children: Risk factor (RF) analysis and pulsed field gel electrophoresis (PFGE) of colonizing and invasive strains. *Pediatric Research* **2006,** 60, (4), 498-498.

9. Fogarty, C. M.; Greenberg, R. N.; Dunbar, L.; Player, R.; Marrie, T. J.; Kojak, C. M.; Morgan, N.; Williams, R. R., Effectiveness of levofloxacin for adult community-acquired pneumonia caused by macrolide-resistant Streptococcus pneumoniae:

integrated results from four open-label, multicenter, phase III clinical trials. *Clin Ther* **2001,** 23, (3), 425-39.

10. Hadley, J. A., The Microbiology and Management of Acute and Chronic Rhinosinusitis. *Curr Infect Dis Rep* **2001,** 3, (3), 209-216.

11. Kashani, H.; Dahlin, C.; Alse'n, B., Influence of different prophylactic antibiotic regimens on implant survival rate: a retrospective clinical study. *Clin Implant Dent Relat Res* **2005,** 7, (1), 32-5.

12. Kruger, A. J.; Raptis, S.; Fitridge, R. A., Management practices of Australian surgeons in the treatment of venous ulcers. *ANZ J Surg* **2003,** 73, (9), 687-91.

13. Madridejos-Mora, R.; Amado-Guirado, E.; Perez-Rodriguez, M. T., Effectiveness of the combination of feedback and educational recommendations for improving drug prescription in general practice. *Med Care* **2004,** 42, (7), 643-8.

14. Manfredi, R., [Antibiotic resistance and community-acquired infections]. *Recenti Prog Med* **2002,** 93, (3), 149-56.

15. Rossi, C.; Sternon, J., [Flouroquinolones of the third and fourth generations]. *J Pharm Belg* **2001,** 56, (6), 137-48.

16. Rossi, C.; Sternon, J., [Third and fourth generation fluoroquinolones]. *Rev Med Brux* **2001,** 22, (5), 443-56.

17. Rutschmann, O. T.; Domino, M. E., Antibiotics for upper respiratory tract infections in ambulatory practice in the United States, 1997-1999: does physician specialty matter? *J Am Board Fam Pract* **2004,** 17, (3), 196-200.

18. Sternon, J.; Glupczynski, Y., [Overprescribing of antibiotics outside the hospital]. *Rev Med Brux* **1999,** 20, (1), 43-7.

19. Alberts, B., From the National Academies. *Cell Biol Educ* **2002,** 1, (4), 109-10.

20. Kaplan, M. L.; Kaplan, L., The Gram Stain and Differential Staining. *J Bacteriol* **1933,** 25, (3), 309-21.

21. Baddiley, J., Teichoic acids in cell walls and membranes of bacteria. *Essays Biochem* **1972,** 8, 35-77.

22. Beveridge, T. J.; Graham, L. L., Surface layers of bacteria. *Microbiol Rev* **1991,** 55, (4), 684-705.

23. Todar, K.; , Todar's Online Textbook of Bacteriology. **2008**.

24. Nakae, T., Permeability properties of the outer membrane of gram-negative bacteria--a discover of porin. *Kitasato Arch Exp Med* **1984,** 57, (1), 1-20.

25. Nikaido, H.; Nakae, T., The outer membrane of Gram-negative bacteria. *Adv Microb Physiol* **1979,** 20, 163-250.

26. Raetz, C. R. H.; Whitfield, C., Lipopolysaccharide endotoxins. *Annual Review of Biochemistry* **2002,** 71, 635-700.

27. Smit, J.; Nikaido, H., Outer membrane of gram-negative bacteria. XVIII. Electron microscopic studies on porin insertion sites and growth of cell surface of Salmonella typhimurium. *J Bacteriol* **1978,** 135, (2), 687-702.

28. Tono, H.; Kornberg, A., Biochemical studies of bacterial sporulation. IV. Inorganic pyrophosphatase of vegetative cells and spores of Bacillus megaterium. *J Bacteriol* **1967,** 93, (6), 1819-24.

29. Dubos, R. J.; Hotchkiss, R. D., The Production of Bactericidal Substances by Aerobic Sporulating Bacilli. *J Exp Med* **1941,** 73, (5), 629-640.

30. Kubitschek, H. E., Growth during the bacterial cell cycle: analysis of cell size distribution. *Biophys J* **1969,** 9, (6), 792-809.

31. Pooley, H. M., Layered distribution, according to age, within the cell wall of bacillus subtilis. *J Bacteriol* **1976,** 125, (3), 1139-47.

32. Forbes, B. A.; Sahm, D. F.; Weissfeld, A. S.; Bailey, W. R. Bailey & Scott's diagnostic microbiology.

33. Gillespie, S. H.; Hawkey, P. M., *Principles and practice of clinical bacteriology*. 2nd ed.; John Wiley & Sons: Chichester, West Sussex, England ; Hoboken, NJ, 2006; p viii, 605 p.

34. Henriques, A. O.; Moran, C. P., Jr. , Structure, assembly, and function of the spore surface layers. *Annu Rev Microbiol* **2007,** 61, 555-88.

35. Klotz, L. C., Overproduction of proteins in recombinant organisms. *Ann N Y Acad Sci* **1983,** 413, 1-11.

36. Nicholson, W. L.; Fajardo-Cavazos, P.; Rebeil, R.; Slieman, T. A.; Riesenman, P. J.; Law, J. F.; Xue, Y., Bacterial endospores and their significance in stress resistance. *Antonie Van Leeuwenhoek* **2002,** 81, (1-4), 27-32.

37. Peck, M. W., Biology and genomic analysis of Clostridium botulinum. *Adv Microb Physiol* **2009,** 55, 183-265, 320.

38. Dixon, T. C.; Fadl, A. A.; Koehler, T. M.; Swanson, J. A.; Hanna, P. C., Early Bacillus anthracis-macrophage interactions: intracellular survival survival and escape. *Cell Microbiol* **2000,** 2, (6), 453-63.

39. Iandolo, J. J.; Ordal, Z. J., Germination System for Endospores of Sarcina Ureae. *J Bacteriol* **1964,** 87, 235-6.

40. Kobayashi, N.; Bauer, T. W.; Sakai, H.; Togawa, D.; Lieberman, I. H.; Fujishiro, T.; Procop, G. W., The use of newly developed real-time PCR for the rapid identification of bacteria in culture-negative osteomyelitis. *Joint Bone Spine* **2006,** 73, (6), 745-7.

41. Kotilainen, P.; Jalava, J.; Meurman, O.; Lehtonen, O. P.; Rintala, E.; Seppala, O. P.; Eerola, E.; Nikkari, S., Diagnosis of meningococcal meningitis by broad-range bacterial PCR with cerebrospinal fluid. *Journal of Clinical Microbiology* **1998,** 36, (8), 2205-2209.

42. Rudi, K.; Kleiberg, G. H.; Heiberg, R.; Rosnes, J. T., Rapid identification and classification of bacteria by 16S rDNA restriction fragment melting curve analyses (RFMCA). *Food Microbiology* **2007,** 24, (5), 474-481.

43. Jonasson, J.; Monstein, H. J., Classification, identification and subtyping of bacteria based on pyrosequencing and signature matching of 16s rDNA fragments - Commentary. *Apmis* **2007,** 115, (5), 678-679.

44. Struthers, J. K.; Westran, R. P. Clinical bacteriology.

45. Denis, O.; Deplano, A.; De Beenhouwer, H.; Hallin, M.; Huysmans, G.; Garrino, M. G.; Glupczynski, Y.; Malaviolle, X.; Vergison, A.; Struelens, M. J., Polyclonal emergence and importation of community-acquired methicillin-resistant Staphylococcus aureus strains harbouring Panton-Valentine leucocidin genes in Belgium. *Journal of Antimicrobial Chemotherapy* **2005,** 56, (6), 1103-1106.

46. Berney, M.; Hammes, F.; Bosshard, F.; Weilenmann, H. U.; Egli, T., Assessment and interpretation of bacterial viability by using the LIVE/DEAD BacLight Kit in combination with flow cytometry. *Appl Environ Microbiol* **2007,** 73, (10), 3283-90.

47. Deka, C.; Steinkamp, J. A., Time-resolved fluorescence-decay measurement and analysis on single cells by flow cytometry. *Applied Optics* **1996,** 35, (22), 4481-4489.

48. Eray, M.; Matto, M.; Kaartinen, M.; Andersson, L.; Pelkonen, J., Flow cytometric analysis of apoptotic subpopulations with a combination of annexin V-FITC, propidium iodide, and SYTO 17. *Cytometry* **2001,** 43, (2), 134-42.

49. Hofmann, O.; Murray, K.; Wilkinson, A. S.; Cox, T.; Manz, A., Laser induced disruption of bacterial spores on a microchip. *Lab on a Chip* **2005,** 5, (4), 374-377.

50. van Baar, B. L. M., Characterisation of bacteria by matrix-assisted laser desorption/ionisation and electrospray mass spectrometry. *Fems Microbiology Reviews* **2000,** 24, (2), 193-219.

51. Anaya, C.; Church, N.; Lewis, J. P., Detection and identification of bacterial cell surface proteins by fluorescent labeling. *Proteomics* **2007,** 7, (2), 215-9.

52. Bierne, H.; Mazmanian, S. K.; Trost, M.; Pucciarelli, M. G.; Liu, G.; Dehoux, P.; Jansch, L.; Garcia-del Portillo, F.; Schneewind, O.; Cossart, P., Inactivation of the srtA gene in Listeria monocytogenes inhibits anchoring of surface proteins and affects virulence. *Mol Microbiol* **2002,** 43, (4), 869-81.

53. Dworzanski, J. P.; Snyder, A. P., Classification and identification of bacteria using mass spectrometry-based proteomics. *Expert Review of Proteomics* **2005,** 2, (6), 863-878.

54. Goodacre, R.; Heald, J. K.; Kell, D. B., Characterisation of intact microorganisms using electrospray ionisation mass spectrometry. *Fems Microbiology Letters* **1999,** 176, (1), 17-24.

55. Hari-Dass, R.; Shah, C.; Meyer, D. J.; Raynes, J. G., Serum amyloid A protein binds to outer membrane protein A of gram-negative bacteria. *J Biol Chem* **2005,** 280, (19), 18562-7.

56. Pragl, B.; Koschak, A.; Trieb, M.; Obermair, G.; Kaufmann, W. A.; Gerster, U.; Blanc, E.; Hahn, C.; Prinz, H.; Schutz, G.; Darbon, H.; Gruber, H. J.; Knaus, H. G., Synthesis, characterization, and application of cy-dye- and alexa-dye-labeled hongotoxin(1) analogues. The first high affinity fluorescence probes for voltage-gated K+ channels. *Bioconjug Chem* **2002,** 13, (3), 416-25.

57. Friedlander, C. Die Mikrokokken der Pneumonie. Fortschr.

58. Gram, H. C., Über die isolirte Färbung der Schizomyceten in Schnitt- und Trockenpräparaten. . *Fortschritte der Medizin* **1884,** 2, (186).

59. Romero, S.; Schell, R. F.; Pennell, D. R., Rapid Method for the Differentiation of Gram-Positive and Gram-Negative Bacteria on Membrane Filters. *Journal of Clinical Microbiology* **1988,** 26, (7), 1378-1382.

60. Stahl, C.; Olsen, E., Gram-negative staining of gram-positive intestinal bacteria with particular reference to examinations of faeces in infants. *Acta Paediatr* **1950,** 39, (6), 372-80.

61. Bronk, B. V.; Reinisch, L., Variability of Steady-State Bacterial Fluorescence with Respect to Growth-Conditions. *Applied Spectroscopy* **1993,** 47, (4), 436-440.

62. Marlon Thomas, E. Z., Valentine Vullev A method and device for real-time fluorescence detection of bacterial pathogens. *Provisional patent* **2007**.

63. Elizabeth Zeilins, M. T. G. s. a., Valentine Vullev, Bacterium-Induced Fluorescence-Enhancement Kinetics: Breaking 100-Year Old Traditions of Staining Bioanalyses. *Undergraduate Research Journal, University of California-Riverside* **June 2008,** II.

64. Busso, D.; Stierle, M.; Thierry, J. C.; Moras, D., Automated recombinant protein expression screening in Escherichia coli. *Methods Mol Biol* **2008,** 426, 175-86.

65. Kang, C. I.; Kim, S. H.; Park, W. B.; Lee, K. D.; Kim, H. B.; Oh, M. D.; Kim, E. C.; Choe, K. W., Bloodstream infections caused by Enterobacter species: predictors of 30-day mortality rate and impact of broad-spectrum cephalosporin resistance on outcome. *Clin Infect Dis* **2004,** 39, (6), 812-8.

66. Ballou, B.; Fisher, G. W.; Waggoner, A. S.; Farkas, D. L.; Reiland, J. M.; Jaffe, R.; Mujumdar, R. B.; Mujumdar, S. R.; Hakala, T. R., Tumor labeling in vivo using cyanine-conjugated monoclonal antibodies. *Cancer Immunol Immunother* **1995,** 41, (4), 257-63.

67. Antelmann, H.; Scharf, C.; Hecker, M., Phosphate starvation-inducible proteins of Bacillus subtilis: proteomics and transcriptional analysis. *J Bacteriol* **2000,** 182, (16), 4478-90.

68. Meador-Parton, J.; Popham, D. L., Structural analysis of Bacillus subtilis spore peptidoglycan during sporulation. *J Bacteriol* **2000,** 182, (16), 4491-9.

69. Hansen, M. E.; Wangari, R.; Hansen, E. B.; Mijakovic, I.; Jensen, P. R., Engineering of Bacillus subtilis 168 for increased nisin resistance. *Appl Environ Microbiol* **2009,** 75, (21), 6688-95.

70. Klein D, U. I., Braun S, Tightly Bound Binary Toxin in the Cell Wall of Bacillus sphaericus. *Applied and Environmental Microbiology* **2002,** 68, (7), 3300-3307.

71. de Boer, A. S.; Diderichsen, B., On the safety of Bacillus subtilis and B. amyloliquefaciens: a review. *Appl Microbiol Biotechnol* **1991,** 36, (1), 1-4.

72. Zhou, B.; Wirsching, P.; Janda, K. D., Human antibodies against spores of the genus Bacillus: a model study for detection of and protection against anthrax and the bioterrorist threat. *Proc Natl Acad Sci U S A* **2002,** 99, (8), 5241-6.

73. Turnbull, P. C., Anthrax vaccines: past, present and future. *Vaccine* **1991,** 9, (8), 533-9.

74. Gaur, R.; Gupta, P. K.; Banerjea, A. C.; Singh, Y., Effect of nasal immunization with protective antigen of Bacillus anthracis on protective immune response against anthrax toxin. *Vaccine* **2002,** 20, (21-22), 2836-9.

75. Pena, G.; Miranda-Rios, J.; de la Riva, G.; Pardo-Lopez, L.; Soberon, M.; Bravo, A., A Bacillus thuringiensis S-layer protein involved in toxicity against Epilachna varivestis (Coleoptera: Coccinellidae). *Appl Environ Microbiol* **2006,** 72, (1), 353-60.

76. Farrell, S.; Halsall, H. B.; Heineman, W. R., Immunoassay for B. globigii spores as a model for detecting B. anthracis spores in finished water. *Analyst* **2005,** 130, (4), 489-97.

77. Elizabeth Zeilins, M. S. T., Valentine Vullev Bacterium-Induced Fluorescence-Enhancement Kinetics: Breaking 100-Year Old Traditions of Staining Bioanalyses. *Undergraduate Research Journal* **2008,** II.

78. Grabowski, Z. R.; Dobkowski, J., Twisted Intramolecular Charge-Transfer (Tict) Excited-States - Energy and Molecular-Structure. *Pure and Applied Chemistry* **1983,** 55, (2), 245-252.

79. Grabowski, Z. R.; Rotkiewicz, K.; Rettig, W., Structural changes accompanying intramolecular electron transfer: Focus on twisted intramolecular charge-transfer states and structures. *Chemical Reviews* **2003,** 103, (10), 3899-4031.

80. Grabowski, Z. R., Electron-Transfer in Flexible Molecules and Molecular-Ions. *Pure and Applied Chemistry* **1993,** 65, (8), 1751-1756.

81. Grabowski, Z. R., Electron-Transfer and the Structural-Changes in the Excited-State. *Pure and Applied Chemistry* **1992,** 64, (9), 1249-1255.

82. Cooper, M.; Ebner, A.; Briggs, M.; Burrows, M.; Gardner, N.; Richardson, R.; West, R., Cy3B: improving the performance of cyanine dyes. *J Fluoresc* **2004,** 14, (2), 145-50.

83. Haidekker, M. A.; Brady, T. P.; Lichlyter, D.; Theodorakis, E. A., Effects of solvent polarity and solvent viscosity on the fluorescent properties of molecular rotors and related probes. *Bioorg Chem* **2005,** 33, (6), 415-25.

84. Brooker, L. G., Chemistry of the cyanine dyes. *Ann N Y Acad Sci* **1948,** 50, (21-26), 108.

85. Anikovsky M, T. A., Kuzmin V Fluorescent Properties of Some Thia- and Oxacarbbocyanine Dyes in the Presence of DNA.

86. Roth, B. L.; Poot, M.; Yue, S. T.; Millard, P. J., Bacterial viability and antibiotic susceptibility testing with SYTOX green nucleic acid stain. *Appl Environ Microbiol* **1997,** 63, (6), 2421-31.

87. Yan, X.; Habbersett, R. C.; Yoshida, T. M.; Nolan, J. P.; Jett, J. H.; Marrone, B. L., Probing the kinetics of SYTOX Orange stain binding to double-stranded DNA with implications for DNA analysis. *Anal Chem* **2005,** 77, (11), 3554-62.

88. Marie, D.; Vaulot, D.; Partensky, F., Application of the novel nucleic acid dyes YOYO-1, YO-PRO-1, and PicoGreen for flow cytometric analysis of marine prokaryotes. *Appl Environ Microbiol* **1996,** 62, (5), 1649-55.

89. Luque-Ortega, J. R.; Saugar, J. M.; Chiva, C.; Andreu, D.; Rivas, L., Identification of new leishmanicidal peptide lead structures by automated real-time monitoring of changes in intracellular ATP. *Biochem J* **2003,** 375, (Pt 1), 221-30.

90. Lebaron, P.; Parthuisot, N.; Catala, P., Comparison of blue nucleic acid dyes for flow cytometric enumeration of bacteria in aquatic systems. *Appl Environ Microbiol* **1998,** 64, (5), 1725-30.

91. Zaritsky, A.; Kihara, M.; Macnab, R. M., Measurement of membrane potential in Bacillus subtilis: a comparison of lipophilic cations, rubidium ion, and a cyanine dye as probes. *J Membr Biol* **1981,** 63, (3), 215-31.

92. Yamaguchi, A.; Kometani, N.; Yonezawa, Y., Luminescence properties of the mixed J-aggregate of oxacyanine dye and thiacyanine dye. Formation of a persistence-type aggregate. *J Phys Chem B* **2005,** 109, (4), 1408-14.

93. Wouters, F. S.; Bastiaens, P. I., Imaging protein-protein interactions by Fluorescence Resonance Energy Transfer (FRET) microscopy. *Curr Protoc Neurosci* **2006,** Chapter 5, Unit 5 22.

94. Wang, M.; Holmes-Davis, R.; Rafinski, Z.; Jedrzejewska, B.; Choi, K. Y.; Zwick, M.; Bupp, C.; Izmailov, A.; Paczkowski, J.; Warner, B.; Koshinsky, H., Accelerated Photobleaching of a Cyanine Dye in the Presence of a Ternary Target DNA, PNA Probe, Dye Catalytic Complex: A Molecular Diagnostic. *Anal Chem* **2009,** 81, (6), 2043-52.

95. Volkova, K. D.; Kovalska, V. B.; Balanda, A. O.; Vermeij, R. J.; Subramaniam, V.; Slominskii, Y. L.; Yarmoluk, S. M., Cyanine dye-protein interactions: looking for

fluorescent probes for amyloid structures. *J Biochem Biophys Methods* **2007,** 70, (5), 727-33.

96. Armitage B, Cyanine Dye-Nucleic Acid Interactions. *Top Heterocycl Chem* **2008,** 14, 11-29.

97. Biver T, D. B. A., Secco F, Venturini M, Yarmoluk S, *Cyanine Dyes as Intercalating Agents: Kinetic and Thermodynamic Studies on the DNA/Cyan40 and DNA/CCyan2 Systems*. Biophysicsal Journal: 2005.

98. Ahmad, A. I.; Ghasemi, J. B., New unsymmetrical cyanine dyes for real-time thermal cycling. *Anal Bioanal Chem* **2007,** 389, (3), 983-8.

99. Yan, X.; Grace, W. K.; Yoshida, T. M.; Habbersett, R. C.; Velappan, N.; Jett, J. H.; Keller, R. A.; Marrone, B. L., Characteristics of different nucleic acid staining dyes for DNA fragment sizing by flow cytometry. *Anal Chem* **1999,** 71, (24), 5470-80.

100. Lakowicz, J. R.; SpringerLink (Online service), *Principles of fluorescence spectroscopy*. 3rd ed.; Springer: New York, 2006; p xxvi, 954 p.

101. Albani, J. R., *Principles and applications of fluorescence spectroscopy*. Blackwell Science: Oxford ; Ames, Iowa, 2007; p viii, 255 p., [4] p. of plates.

102. Carreon, J. R.; Stewart, K. M.; Mahon, K. P., Jr.; Shin, S.; Kelley, S. O., Cyanine dye conjugates as probes for live cell imaging. *Bioorg Med Chem Lett* **2007,** 17, (18), 5182-5.

103. Harvey, B. J.; Levitus, M., Nucleobase-specific enhancement of Cy3 fluorescence. *J Fluoresc* **2009,** 19, (3), 443-8.

104. Chibisov, A. Z. G. G. H. S. Y. T. A., Photorelaxation Processes in Covalently Linked Indocarbocyanine and Thiacarbocyanine Dyes. *Journal of Physical Chemistry* **1995,** 99, (3), 886-893.

105. Esposito, A.; Wouters, F. S., Fluorescence lifetime imaging microscopy. *Curr Protoc Cell Biol* **2004,** Chapter 4, Unit 4 14.

106. Taatjes, D. J.; Mossman, B. T., *Cell imaging techniques : methods and protocols*. Humana Press: Totowa, N.J., 2006; p xiv, 490 p.

107. Jones, G., 2nd; Yan, D.; Hu, J.; Wan, J.; Xia, B.; Vullev, V. I., Photoinduced electron transfer in arylacridinium conjugates in a solid glass matrix. *J Phys Chem B* **2007,** 111, (24), 6921-9.

108. Potter, C. A. S.; Brown, R. G.; Vollmer, F.; Rettig, W., Role of Twisted Intramolecular Charge-Transfer States in the Decay of 2-(2'-Hydroxyphenyl)Benzothiazole Following Excited-State Intramolecular Proton-Transfer. *Journal of the Chemical Society-Faraday Transactions* **1994,** 90, (1), 59-67.

109. Ballou, B.; Fisher, G. W.; Deng, J. S.; Hakala, T. R.; Srivastava, M.; Farkas, D. L., Cyanine fluorochrome-labeled antibodies in vivo: assessment of tumor imaging using Cy3, Cy5, Cy5.5, and Cy7. *Cancer Detect Prev* **1998,** 22, (3), 251-7.

110. Mandal A, P. M., Principal Component Analysis of the Absorption Spectra of the Dye Thiacyanine in the Presence of the Surfactant AOT: Precise Identification of the Dye–Surfactant Aggregates. *Journal of Colloid and Interface Science* **1997,** 192, (1), 83-93.

111. Hidalgo, J.; Sanchez-Coronilla, A.; Balon, M.; Asuncion Munoz, M.; Carmona, C., Dual emission of temperature-induced betacarboline self-associated hydrogen bond aggregates. *Photochem Photobiol Sci* **2009,** 8, (3), 414-20.

112. Blatchford, J. W.; Gustafson, T. L.; Epstein, A. J.; Vanden Bout, D. A.; Kerimo, J.; Higgins, D. A.; Barbara, P. F.; Fu, D.; Swager, T. M.; MacDiarmid, A. G., Spatially and temporally resolved emission from aggregates in conjugated polymers. *Phys Rev B Condens Matter* **1996,** 54, (6), R3683-R3686.

113. Vogt, G.; Krampert, G.; Niklaus, P.; Nuernberger, P.; Gerber, G., Optimal Control of Photoisomerization. *Physical Review Letters* **2005,** 94, (6), 068305/1-068305/4.

114. Tolmachev, A. C. G. Z. H. G. Y. S. A. Photorelaxation Processes in Covalently Linked Indocarbocyanine and Thiacarbocyanine Dyes.

115. Malicka, J.; Gryczynski, I.; Fang, J.; Lakowicz, J. R., Fluorescence spectral properties of cyanine dye-labeled DNA oligomers on surfaces coated with silver particles. *Anal Biochem* **2003,** 317, (2), 136-46.

116. Patist A., B. S., Penfield K., Aikens P., Shah D., On the Measurement of Critical Micelle Concentrations
of Pure and Technical-Grade Nonionic Surfactants. *Journal of Surfactants and Detergents* **2000,** 3, (1), 53.

Chapter 2

Kinetics of Fluorescence Staining Bacterial Cells with Thiacyanine Dyes

Abstract

In this chapter, we expanded the analysis of bacterium-induced changes in the emission properties of the thiacyanine dyes discussed in chapter one. We explored the dynamics of the observed emission enhancement. We investigated the kinetics of the emission enhancement by recording and analyzing the kinetics of the increase in the fluorescence intensity at the spectral maxima. We hypothesized that the kinetics of staining process contain a wealth of information, which has the potential for expanding the capabilities of bio-analytical assays for bacterial species beyond their Boolean nature. The dynamics of the staining process indeed allowed us to identify unique emission kinetics for each bacterium when introduced to each of the dye solutions. To test our hypothesis, the recorded kinetics curves were fitted to an exponential functions and the obtained time constants were used as a criterion for comparison between the investigated species. We observed that for all conditions we employed, the time constants did not manifest statistically significant dependence on the dye concentration and on the cell density of the analyzed samples. Under certain conditions, however, the time constants recorded for different species showed statistically significant discernibility. Our additional studies demonstrated the importance of pre-treating the samples with a mild

surfactant, TWEEN 40, for obtaining kinetics behavior that differ for the different species investigated. Although we do not have a good mechanistic understanding about the staining process, our kinetics studies provide an important set of preliminary findings that can serve as a fundation for the development of unprecedented dynamic bacterial assays.

2.1. Introduction

This chapter describes an investigation of the kinetics of bacterial staining with thiacyanine dyes THIA and THO. THC also displayed enhancement, however, the enhancement rapidly decays so analysis ca only be performed on the first 10-20 seconds of enhancement (Figure 43). When the staining was conducted in the presence of a surfactant such as TWEEN 40, the kinetic characteristics of the emission-enhancement process (which reflect the dye uptake by the cells) was slower relative to the process without TWEEN 40. Furthermore, in the absence of surfactant, we did not observe statistically significant discernibility between the fluorescence-enhancement kinetics characteristics for the different species we investigated. The addition of TWEEN 40 to the dye and/or bacterial samples prior to staining resulted in time constants that differed for the different bacterial species.

A range of spectroscopic and cytometric techniques utilized in cell biology and microbiology laboratories are dependent on efficient staining of samples with exogenous fluorophores to improve the contrast of samples being tested.[46, 63, 95-107] The generation of high contrast ratios in biological samples is essential for detection and imaging.[64] Therefore, samples are typically fluorescently labeled either with a single stain or with a series of contrasting stains to reveal the heterogeneity in a cell culture.[64, 108] Fluorescence staining relies on the accumulation of the dye molecules within the cells of interest, as well as on changes in the photo-physical properties of the staining agent, such as molar extinction coefficients, fluorescence maxima and

fluorescence quantum yields.[108] One area of staining that has not received much attention is the area of staining dynamics, which describes time-dependent staining of an object. In this chapter, we explore the kinetics of staining for a series of six bacterial species.

2.1.1. Background.

Differential staining techniques such as Gram staining, take under consideration only at the appearance of cells before and after staining, yielding Boolean outcomes. This type of classification results in bacterial species being grouped into one of two groups. Hence, the Boolean character of the low-specificity assays, such as Gram stains, provide information in the analyzed species are a part of either of the large groups. As an alternative, staining assays with high specificity, such as immuno-stains, allow researchers and clinicians to answer the question of whether the species being targeted is present. The Boolean character of the low-specificity assays, such as Gram stains, provides information if the analyzed species are a part of either of large groups. Based on prior experience of the person conducting the analysis and on the types of species expected for the analyzed samples, the morphology of the stained cells may allow further narrowing of the classification.[20, 109] The highly specific assays, on the other hand, demonstrate if the species probed for is or isn't present: i.e., no information can be derived from the assay beyond the fact that one species has been eliminated. The underlying need for

expedient and cost efficient analytical methods that provide information beyond the expected Bolean outcomes, is the motivation for our line of research. We postulate that an understanding of the dynamics of staining and its relation to the bacterial species may indeed provide means for expanding the staining assays beyond their Boolean nature.

2.1.2. Fluorescence staining with cyanine dyes.

Commercially available cyanine dyes have been shown to be efficient fluorophores for staining both prokaryotic and eukaryotic cells.[46, 73, 110] Gaforio et al. reported using a commercially available cyanine dye to analyze bacterial phagocytosis.[111] Haase reported using a cyanine dye for analyzing the cell cycle of budding yeast.[112] Ruth et al. reported using a cyanine dye as a nucleic acid stain for detecting non-viable bacterial cells.[73] Anaya et al. reported using a series of cyanine dyes to selectively stain various bacterial cell surface proteins.[113] Ballou et al. reported using cyanine-conjugated monoclonal antibodies to label tumors *in vivo*.[114] Little is known about the dynamics of the bacterial staining processes by thiacyanine dyes; however, studies have revealed various modes of this process.[62, 69, 115] Here we investigate the dynamics of staining bacterial cells with a series of thiacyanine dyes with primary focus on THIA. We focused on THIA as it exhibited strong emission enhancement when cells where introduced and the emission decay was slow.

2.2. Results and Discussion

2.2.1. Kinetics of bacterium-induced fluorescence enhancement of THIA in the presence of TWEEN

The thiacyanine dyes displayed bacterium-induced perturbation to their emission spectra (Figure 33). The characteristic changes in the absorption and emission spectra exhibited differences for each of the bacterial species tested. Here we expand on this finding by exploring the kinetics of the interactions between the dye and the bacterial cells. We focused our studies on THIA because of the pronounced emission enhancement it exhibited in the presence of bacterial cells.

The dynamics of the fluorescence enhancement (i.e., the emission intensity of THIA at the fluorescence maximum recorded as a function of time) reveal a saturation type of kinetic behavior. Upon injection of bacterial cells into a stirred dye solution, a fast rise in the fluorescence intensity was observed, which in some cases was followed by a further increase in the intensity at considerably slower rate.

Kinetic measurements, which extended over 30 minutes, revealed little changes in the fluorescence intensity after the initial emission enhancement, occurring within the first minute or so. We focused on the dynamics of the initial enhancement. To extract the characteristic time constants, τ, of the staining processes, we fit the recorded data to mono- or a bi-exponential rise function:

$$F(t)_{t\geq t_0} = \Delta F\left(1-\exp\left(-\frac{t-t_0}{\tau}\right)\right)+F_0 \quad \textbf{Equation 5}$$

$$F(t)_{t\geq t_0} = \Delta F\left(1-A\exp\left(-\frac{t-t_0}{\tau_1}\right)-B\exp\left(-\frac{t-t_0}{\tau_2}\right)\right)+F_0 \quad \textbf{Equation 6}$$

Where F is the measured fluorescence intensity at time, t; F_0 is the initial fluorescence intensity of the dye without bacteria; ΔF is the total increase in the fluorescence intensity; and t_0 is the initial time: i.e., time of introducing the cells to the dye solution.

2.2.1.1. Kinetics of staining of *E. coli* with THIA in the presence of TWEEN 40

The introduction of *E. coli* cells into a THIA solution containing THIA and 565 μM TWEEN gave emission enhancement. The fluorescence intensity increased, by nearly an order-of-magnitude, in less than a minute after the injection of bacterial cells (Figure 36-37).

Fitting the data to a bi-exponential function (Equation 6) allowed us to extract the characteristic time constants (Table 29-39). The bi-exponential function produced a better fit than the mono-exponential function. The time constants were independent of the slow-rate bi-exponential component captured the species-specific information. The time constants of the fast component, however, were not discernible among the bacterial species evaluated in this study.

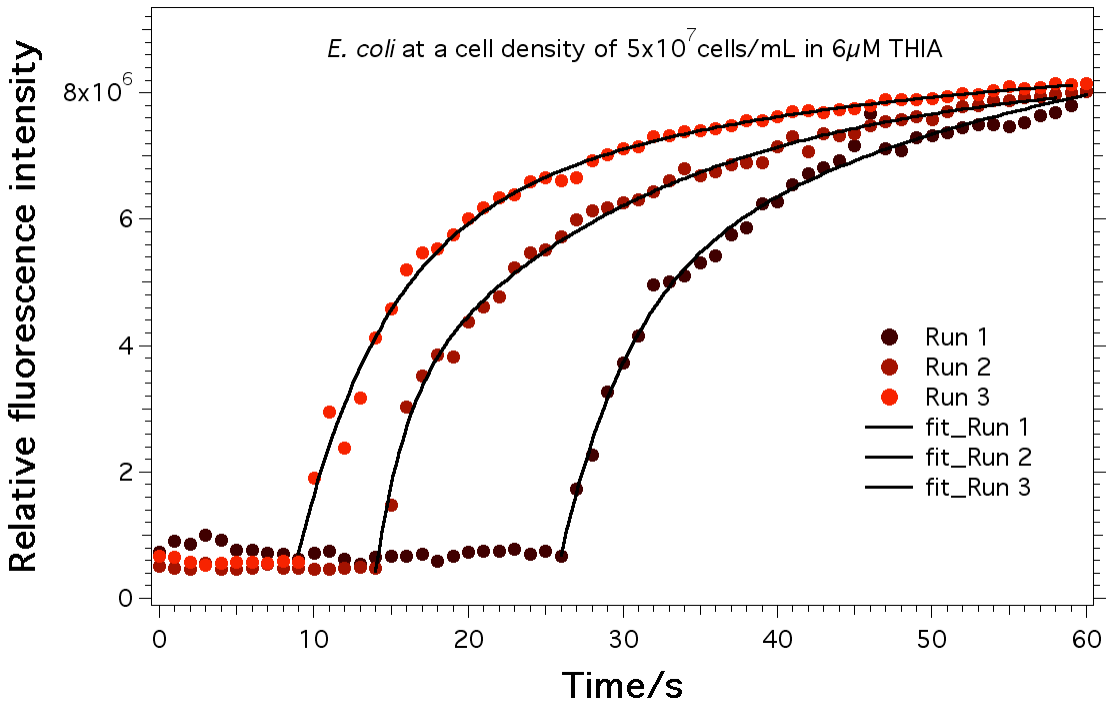

Figure 36. Kinetic curves resulting from the introduction of *E. coli* cells into a 6 μM THIA in Tris buffer with and without cells at a cell density of $5x10^7$ cells mL^{-1}. The red points represent discrete data points averaged over one second.

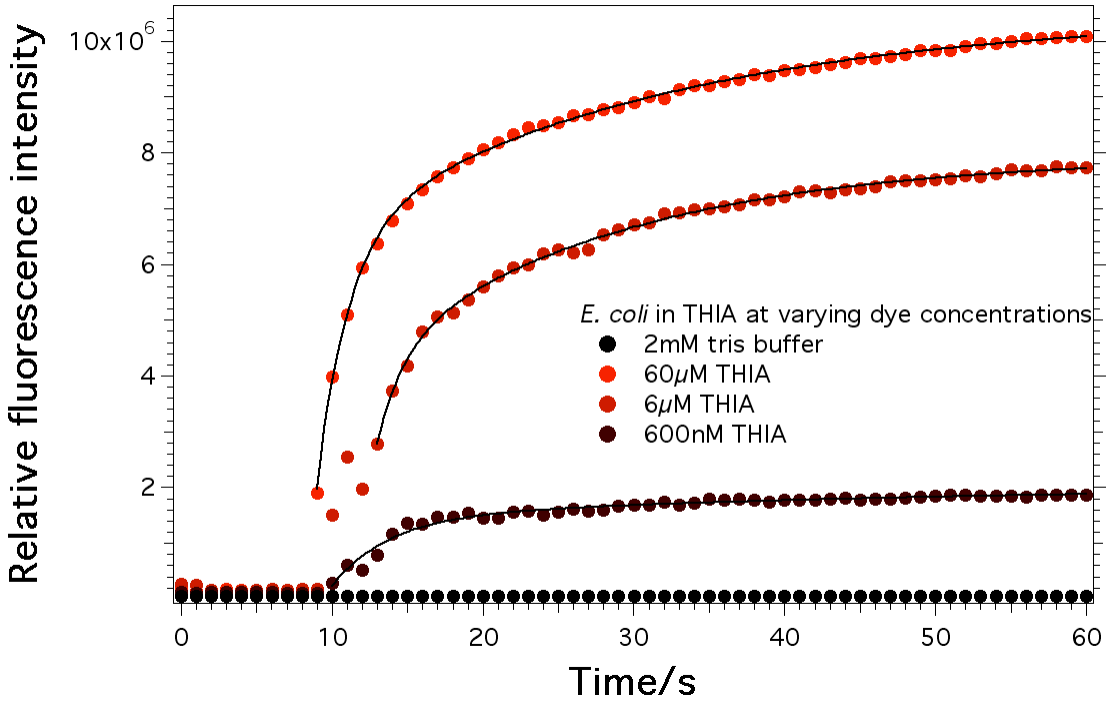

Figure 37. Kinetic curves for THIA with and without *E. coli* (λ_{ex} = 420 nm, λ_{em} = 480 nm; aqueous Tris buffer containing 565 μM TWEEN 40, 2 mM, pH = 8.5) $5x10^8$ cells mL^{-1} *E. coli* in different dye concentrations: **Black** – Tris buffer; Maroon – 600 nM; Dark red – 6 μM; Red – 60 μM.

We evaluated of the time constant dependence on the cell density of the bacterial species and on the dye concentration. Two-factor analysis of the variance (ANOVA) allowed us to estimate the concentration dependence of the kinetics of staining. The two null hypotheses state that the time constants do not depend on (1) on the dye concentration and (2) on the cell density. The probability values or the p-values, of the data, obtained from the ANOVA analysis, indicates the probability for the experiments to yield the analyzed data, should the null hypothesis be correct. However, an arbitrary criterion, usually p = 0.05, is selected

for evaluating the validity of either of the null hypotheses. *E. coli*, the *p-vaules* for the dye-concentration and for the cell-density dependence were $p = 0.07$ and $p = 0.08$, respectively. These *p-values* prevented the rejection of either of the null hypothesis, suggesting for a lack of concentration dependence of the kinetics of staining of *E. coli* with THIA.

2.2.1.2. Kinetics of staining of *E. aerogenes* with THIA in the presence of TWEEN

The kinetics of the emission-enhancement from the introduction of cells of another Gram-negative bacterium, *E. aerogenes*, into a THIA solution manifested a saturation character. The curve had similar characteristics to the kinetic curve of *E. coli*, taking less than two minutes to reach saturation (Figure 38). Visual examination revealed differences in the shapes of the kinetic curves for the two Gram-negative species (Figures 36 and 38), which was reflected in the different values of the time constants obtained for *E. earogenes* and *E. coli* (Tables 31-32).

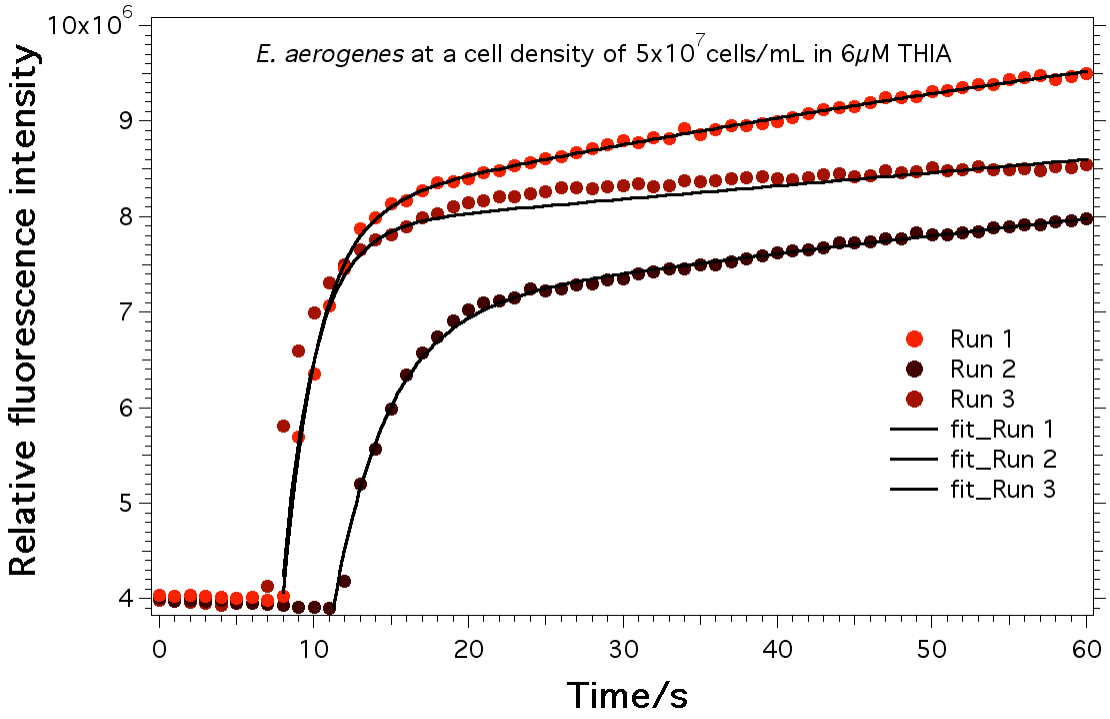

Figure 38. Kinetic curves resulting from the introduction of *E. aerogenes* cells into a 6 μM THIA in Tris buffer with and without cells at a cell density of $5x10^7$ cells mL^{-1}. The red points represent discrete data points collected every tenth of a second while the black curves represent best-fit lines that were extracted by regressing on the experimental data.

Two-factor ANOVA for the time constants of staining of *E. aerogenes* with THIA yielded $p = 0.30$ and $p = 0.53$ for the cell density and for the dye concentration dependence. Obviously, such large p-values indicate that the kinetics is concentration independent.

To compare the discernibility between the kinetics of THIA staining of *E. coli* and *E. aerogenes,* we employed a single-factor ANOVA. The null hypothesis stated that the time constants measured for E. coli and E. aerogenes were identical. ANOVA produced $p = 5x10^{-12}$ (Table 24), which allowed for rejecting the null hypothesis.

Therefore, we concluded that the kinetics of staining of *E. coli* manifested statistically significant difference from the kinetics of staining *E. aerogenes*.

Table 24. ANOVA output for a single-parameter ANOVA analysis analyzing time constants from *E. coli* and *E. aerogenes*.

SUMMARY

Groups	*Count*	*Sum*	*Average*	*Variance*
19.3	26.0	777	29.9	20.5
24.0	26.0	496	19.1	11.5

ANOVA

Source of Variation	*SS*	*df*	*MS*	*F*	*P-value*	*F crit*
Between Groups	1.52E3	1.00	1.52E3	95.0	0.00	4.03
Within Groups	8.01E2	50.0	1.60E1			
Total	2.32E3	51.0				

2.2.1.3. Kinetics of staining of Gram-positive bacteria with THIA in the presence of TWEEN

The kinetics of the emission-enhancement from the introduction of the Gram-positive *B. subtilis* cells into a THIA solutions gave a saturation curves which had some apparent differences in shape and slope from the kinetics of staining of the two Gram-negative species. The *B. subtilis* staining kinetics curves were fitted to a mono-exponential rise functions (equation 5 snd Figure 39).

The values of the time constants (Table 33-34) ranged between 1.8-5.3 s. The fluctuations between the time constants values for the different repeats of the same data points, resulted in considerable uncertainly. Two-factor ANOVA examing the

concentration dependence of the kinetics, produced $p = 0.03$ and $p = 0.45$ for the cell density and for the dye concentration. Therefore, we cannot reject the null hypothesis (stating a lack of concentration dependence) even for the cell density dependence.

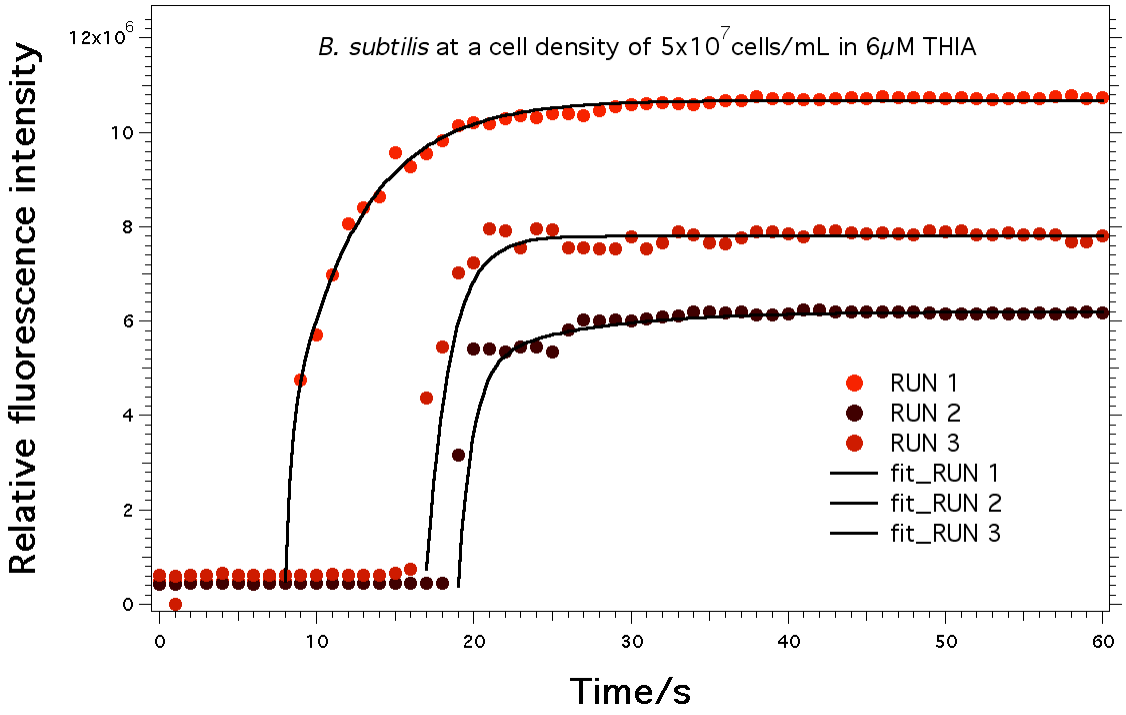

Figure 39. Kinetic curves resulting from the introduction of *B. subtilis* cells into a 6 μM THIA in Tris buffer with and without cells at a cell density of $5x10^7$ cells mL^{-1}. The red points represent discrete data points collected every tenth of a second while the black curves represent best-fit lines that were extracted by regressing on the experimental data.

Table 25. ANOVA table for a two-way ANOVA analysis for time constants from *B. subtilis*.

ANOVA

Source of Variation	*SS*	*df*	*MS*	*F*	*P-value*	*F crit*
Sample	6.40	2.00	3.20	4.38	0.03	3.55
Columns	1.64	2.00	0.82	1.12	0.35	3.55
Interaction	10.9	4.00	2.72	3.71	0.02	2.93
Within	13.2	18.0	0.73			
Total	32.1	26.0				

The kinetic curves representing the staining of the other Gram-positive species we tested, *B. sphaericus*, revealed a bi-exponential character with timecontants of the slow component exceeding the timeconstants for the other investigated species. The spread of the timeconstant values resulted in *p*-valeus from two-factor ANOVA that were 0.01 and 0.08 for testing the cell density and the dye concentration dependence (Table 26). A concervative assumption for critical *p-value* of 0.01 cannot allow us to reject the null hypotheses. Concurrently, the small *p*-value, especiallt for the cell-density dependence, makes our finding inconclusive: i.e., we cannot state if the kinetics of staining of *B. sphaericus* with THIA depends or does not depend on the cell density of the tested samples.

Although the rejection of the null hypotheses from this two-factor analysis depended on the arbitrary selection of the critical *p*-values: e.g., 0.01 – 0.10, one-way ANOVA indicated that the time constants for *B. sphaericus* manifested statistically significant difference from the timeconstants measured for the other three species. The *p*-values from the one-factor ANOVA comparing the

timeconstants for *B. sphaericus* with the time constants for *E. coli*, *E. aerogenes*, and *B. subtilis* were 1.7×10^{-10}, $<10^{-16}$, and $<10^{-16}$, respectively (Tables 25, 24 and 23, respectively). These small *p*-values clearly allow for rejection of the hypotheses that the timeconstants are identical for the different species, and demonstrate the species-specificity of the staining kinetics.

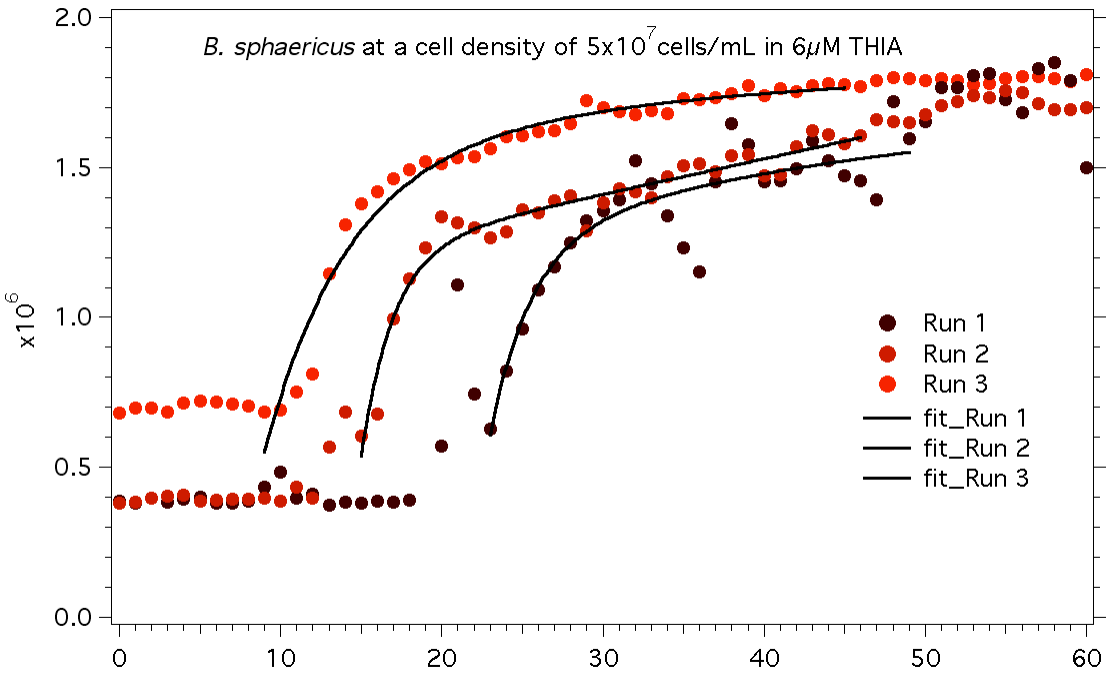

Figure 40. Kinetic curves resulting from the introduction of *B. sphaericus* cells into a 6 μM THIA in Tris buffer with and without cells at a cell density of $5x10^7$ cells mL^{-1}. The red points represent discrete data points collected every tenth of a second while the black curves represent best-fit lines that were extracted by regressing on the experimental data.

Table 26. ANOVA table for a two-way ANOVA analysis analyzing time constants from *B. sphaericus*.

ANOVA

Source of Variation	*SS*	*df*	*MS*	*F*	*P-value*	*F crit*
Sample	4.68E2	2.00	2.34E2	3.24	0.06	3.55
Columns	5.50E3	2.00	2.75E3	38.1	0.00	3.55
Interaction	1.25E3	4.00	3.12E2	4.32	0.01	2.93
Within	1.30E3	18.0	7.23E1			
Total	8.52E3	26.0				

The *p-value*, being slightly larger than 0.05, indicated that the time constants were weakly dependent on the dye concentrations; however, a column *p-value* smaller than 0.05 indicated that the time constants were dependent on the cell density. The interaction of the dye concentration and the bacterial cell density gave a *p-value* of less than 0.05, indicating that the interaction of the dye concentration and cell density does not impact the time constants.

2.2.1.4. Kinetics of staining of *Bacillus* endospores with THIA in the presence of TWEEN

The kinetics of the emission enhancement from the introduction of the Gram-positive *B. globigii* endospores into a THIA solution gave a saturation curve that differed from the kinetics for the vegetative bacterial cells, *B. subtilis*, a closely related but phylogenetically distinct bacillus species (Figure 37 and Figure 39).[116] The saturation curve for *B. globigii* was compared to the kinetic curve of *B. thuringiensis*. There were some obvious differences in shape and slope from the previous two Gram-positive vegetative cells. The kinetics curves were fitted to bi-

exponential functions, and time constants were extracted. There experiments were therefore performed on identical time scales to all previous experiments. There was high fidelity from run to run. The kinetic curves can be seen in (Figure 41 and 42).

The kinetics curves for *B. globigii* were compared to the kinetics curves of *B. thuringeinsis* and some differences in the shapes of the emission enhancement were observed. The data was fitted to a bi-exponential function and the time constants extracted (Tables 37-39).

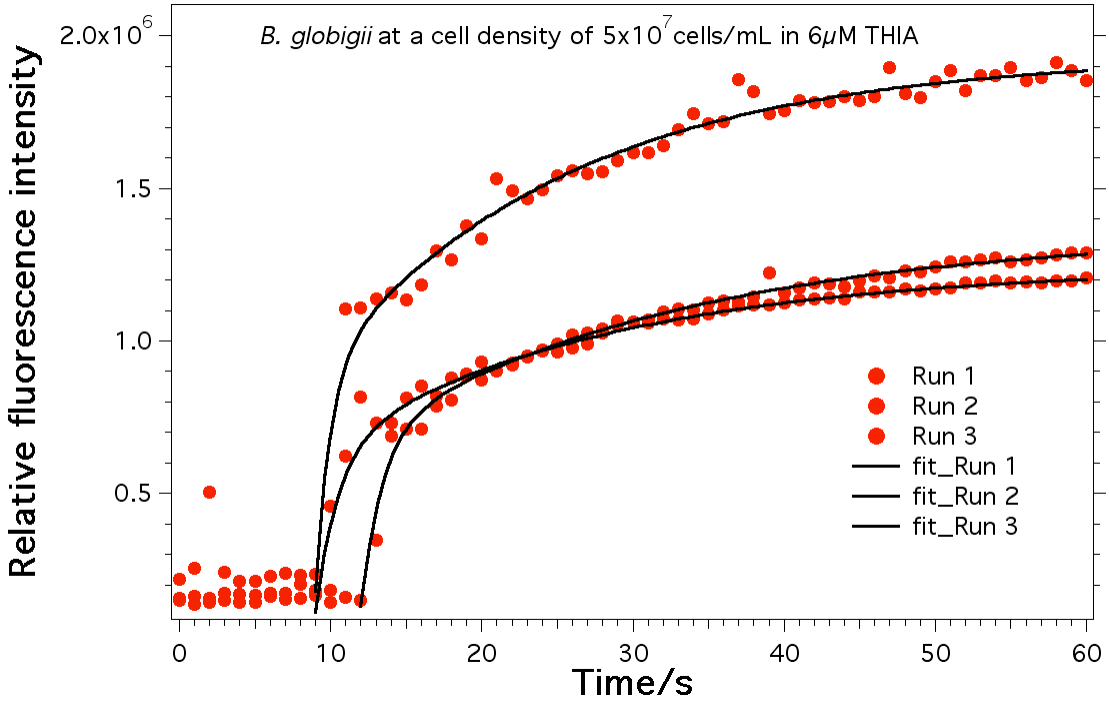

Figure 41. Kinetic curves resulting from the introduction of *B. globigii* endospores into a 6 μM THIA in Tris buffer with and without endospores at a cell density of $5x10^7$ cells mL^{-1}. The red points represent discrete data points collected every tenth of a second while the black curves represent best-fit lines that were extracted by regressing on the experimental data.

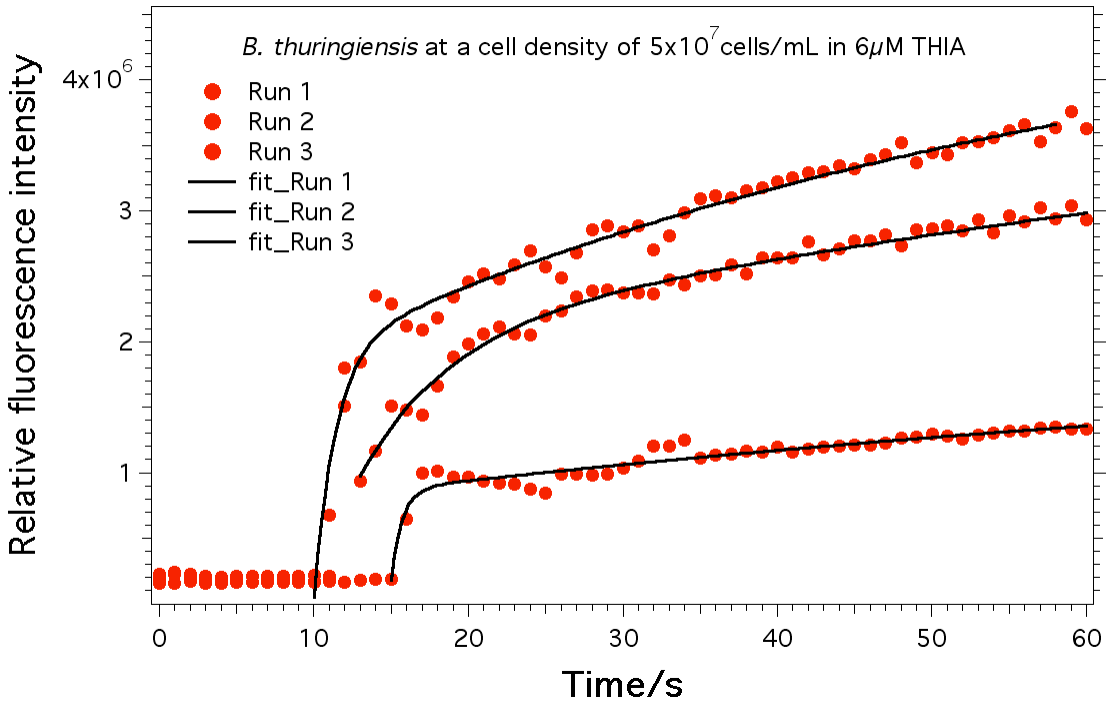

Figure 42. Kinetic curves resulting from the introduction of *B. thuringiensis* endospores into a 6 μM THIA in Tris buffer with and without endospores at a density of $5x10^7$ cells mL^{-1}. The red points represent discrete data points collected every tenth of a second while the black curves represent best-fit lines that were extracted by regressing on the experimental data.

The time constants for the emission enhancement of a THIA solution with 565 μM TWEEN 40 after the introduction of bacterial endospores were evaluated. We saw that the two *Bacillus* species, *B. globigii* and *B. thuringiensis*, had fitted time constants that were quite different. The time constants were in a narrow range for both endospores (16.9–21.6 s for *B. globigii* and 54.4–81.5 s for *B. thuringiensis*). ANOVA analysis confirmed that these values were different for the endospores of the two different species. Single-factor ANOVA analysis revealed that the time constants are unique (Tables 27-28).

Table 27. Time constants for *Bacillus* endospores.

Cell density (cells mL^{-1})	*B. globigii*	*B. thur*
5.0E+07	22	55
5.0E+07	20	60
5.0E+07	17	54
5.0E+07	25	58
5.0E+07	19	57
5.0E+07	22	67
5.0E+07	20	71
5.0E+07	22	72
5.0E+07	17	82

Table 28. Single-factor ANOVA analysis using the time constants from *Bacillus* endospores at a spore density of 10^6–10^8 cells mL^{-1} and dye concentration of 600 nM–60 μM THIA.

ANOVA

Source of Variation	*SS*	*df*	*MS*	*F*	*P-value*	*F crit*
Sample	1.48E2	2.00	7.41E1	4.25	0.02	3.26
Columns	2.45E4	5.00	4.90E3	281	0.00	2.48
Interaction	7.90E2	10.0	7.90E1	4.53	0.00	2.11
Within	6.28E2	36.0	1.74E1			
Total	2.60E4	53.0				

2.2.1.5. Comparison between the kinetic characteristics of the different bacterial species in the presence of TWEEN 40

We investigated the dynamics of the emission enhancement of THIA upon uptake by bacterial cells in the presence of TWEEN 40. We saw that the introduction of bacterial cells into a THIA solution resulted in emission enhancement (Figure 36-

41). The exponential fits of the emission-enhancement data, allowed us to extract the time constants for describing the interaction of the dye and the bacterial species.

Table 29. Time constants for emission enhancement of THIA with TWEEN 40 added at 565 μM and *E. coli* cells.

Conc	$\rho_{E.coli}$	τ_1	A	τ_2	B	ΔF
600 nM	$5x10^6$ cells mL^{-1}	3.1	$2.1x10^4$	35	$2.1x10^4$	$2.5x10^5$
600 nM	$5x10^6$ cells mL^{-1}	0.04	$1.7x10^6$	31	$7.5x10^4$	$5.2x10^5$
600 nM	$5x10^6$ cells mL^{-1}	13	$8.6x10^5$	35	$8.6x10^5$	$2.2x10^5$
600 nM	$5x10^7$ cells mL^{-1}	0.05	$8.2x10^4$	35	$1.0x10^5$	$1.5x10^6$
600 nM	$5x10^7$ cells mL^{-1}	4.9	$5.0x10^5$	28	$7.8x10^5$	$1.3x10^6$
600 nM	$5x10^7$ cells mL^{-1}	0.20	$3.7x10^4$	35	$5.3x10^5$	$1.4x10^6$
600 nM	$5x10^8$ cells mL^{-1}	3.0	$1.5x10^6$	19	$8.4x10^5$	$2.2x10^6$
600 nM	$5x10^8$ cells mL^{-1}	5.4	$1.6x10^6$	20	$8.2x10^5$	$2.2x10^6$
600 nM	$5x10^8$ cells mL^{-1}	3.1	$9.3x10^5$	27	$5.8x10^5$	$1.9x10^6$
6 μM	$5x10^6$ cells mL^{-1}	16	$3.8x10^5$	28	$9.9x10^5$	$1.3x10^6$
6 μM	$5x10^6$ cells mL^{-1}	23	$4.0x10^5$	26	$4.0x10^5$	$1.3x10^6$
6 μM	$5x10^6$ cells mL^{-1}	3.4	$8.6x10^5$	28	$8.6x10^5$	$9.3x10^5$
6 μM	$5x10^7$ cells mL^{-1}	13	$8.2x10^6$	23	$3.9x10^5$	$8.7x10^6$
6 μM	$5x10^7$ cells mL^{-1}	2.3	$3.9x10^5$	27	$6.4x10^5$	$7.8x10^6$
6 μM	$5x10^7$ cells mL^{-1}	9.0	$3.6x10^6$	30	$2.9x10^6$	$6.6x10^6$
6 μM	$5x10^8$ cells mL^{-1}	4.2	$2.1x10^4$	32	$2.1x10^4$	$8.1x10^6$
6 μM	$5x10^8$ cells mL^{-1}	4.5	$1.7x10^6$	28	$1.7x10^6$	$7.7x10^6$
6 μM	$5x10^8$ cells mL^{-1}	5.5	$8.6x10^5$	28	$8.6x10^5$	$7.5x10^6$
60 μM	$5x10^6$ cells mL^{-1}	1.0	$1.0x10^5$	35	$7.8x10^4$	$1.5x10^5$
60 μM	$5x10^6$ cells mL^{-1}	1.3	$3.4x10^4$	29	$1.7x10^4$	$2.6x10^4$
60 μM	$5x10^6$ cells mL^{-1}	4.3	$6.4x10^3$	29	$6.9x10^3$	$1.2x10^4$
60 μM	$5x10^7$ cells mL^{-1}	2.5	$1.9x10^4$	35	$8.5x10^4$	$6.0x10^4$
60 μM	$5x10^7$ cells mL^{-1}	2.7	$2.7x10^5$	39	$2.6x10^5$	$4.8x10^5$
60 μM	$5x10^7$ cells mL^{-1}	2.7	$2.7x10^5$	34	$2.6x10^4$	$3.6x10^5$
60 μM	$5x10^8$ cells mL^{-1}	2.6	$2.1x10^4$	26	$2.1x10^4$	$9.7x10^6$
60 μM	$5x10^8$ cells mL^{-1}	1.8	$1.7x10^6$	26	$1.7x10^6$	$1.0x10^7$
60 μM	$5x10^8$ cells mL^{-1}	1.8	$8.6x10^5$	27	$8.6x10^5$	$1.1x10^7$

Table 30. Mean time constants for emission enhancement of THIA with TWEEN 40 added at 565 μM and *E. coli* cells.

Conc	$\rho_{E.coli}$	τ_1	τ_2
64 μM	2x10^8 cells mL	2.3 ± 1	31 ± 4.9 s
6 μM	2x10^7 cells mL	3.7 ± 4	28 ± 6.4 s
600 nM	2x10^6 cells mL	10 ± 7	26 ± 5.3 s

Table 31. Time constants for emission enhancement of THIA with TWEEN 40 added at 565 μM and *E. aerogenes* cells.

Conc	$\rho_{E.coli}$	τ_1	A	τ_2	B	ΔF
600 nM	5x10^6 cells mL^{-1}	15	5.3 x10^5	24	5.9 x10^5	4.0 x 10^4
600 nM	5x10^6 cells mL^{-1}	7.9	1.1 x10^5	16	3.9 x10^6	6.7 x 10^4
600 nM	5x10^6 cells mL^{-1}	3.4	4.7 x10^5	24	8.9 x10^5	5.8 x 10^4
600 nM	5x10^7 cells mL^{-1}	2.4	1.0 x10^5	23	4.0 x10^5	1.5 x 10^5
600 nM	5x10^7 cells mL^{-1}	1.6	1.3 x10^5	17	4.5 x10^5	1.5 x 10^5
600 nM	5x10^7 cells mL^{-1}	2.0	2.0 x10^5	18	3.0 x10^5	2.3 x 10^5
600 nM	5x10^8 cells mL^{-1}	6.8	5.7 x10^5	24	6.9 x10^4	7.2 x 10^5
600 nM	5x10^8 cells mL^{-1}	2.2	4.7 x10^5	24	8.9 x10^4	8.4 x 10^5
600 nM	5x10^8 cells mL^{-1}	10	8.6 x10^5	12	3.0 x10^4	7.3 x 10^5
6 μM	5x10^6 cells mL^{-1}	1.5	1.5 x10^5	17	1.5 x10^4	1.6 x 10^5
6 μM	5x10^6 cells mL^{-1}	1.6	1.1 x10^5	18	2.9 x10^4	1.3 x 10^5
6 μM	5x10^6 cells mL^{-1}	1.0	1.0 x10^5	15	2.2 x10^4	1.2 x 10^5
6 μM	5x10^7 cells mL^{-1}	5.9	2.5 x10^6	17	9.8 x10^5	9.7 x 10^5
6 μM	5x10^7 cells mL^{-1}	16	3.2 x10^5	16	1.2 x10^6	9.4 x 10^5
6 μM	5x10^7 cells mL^{-1}	12	4.9 x10^6	18	9.1 x10^5	5.4 x 10^5
6 μM	5x10^8 cells mL^{-1}	1.9	5.7 x10^5	24	6.9 x10^4	8.0 x 10^6
6 μM	5x10^8 cells mL^{-1}	3.1	3.4 x10^6	21	2.6 x10^6	4.7 x 10^6
6 μM	5x10^8 cells mL^{-1}	22	1.7 x10^6	20	2.8 x10^6	7.4 x 10^6
60 μM	5x10^6 cells mL^{-1}	5.6	1.9 x10^5	18	5.6 x10^4	2.5 x 10^5
60 μM	5x10^6 cells mL^{-1}	3.6	7.7 x10^4	22	2.2 x10^5	1.2 x 10^5
60 μM	5x10^6 cells mL^{-1}	2.5	9.6 x10^4	20	5.5 x10^5	1.4 x 10^5
60 μM	5x10^7 cells mL^{-1}	1.2	3.2 x10^6	15	1.2 x10^6	5.0 x 10^5
60 μM	5x10^7 cells mL^{-1}	3.0	2.5 x10^4	17	1.0 x10^6	4.9 x 10^5
60 μM	5x10^7 cells mL^{-1}	5.5	1.9 x10^5	20	5.9 x10^4	2.5 x 10^5
60 μM	5x10^8 cells mL^{-1}	0.0	8.0 x10^4	17	2.1 x10^4	1.4 x 10^5
60 μM	5x10^8 cells mL^{-1}	4.9	1.0 x10^3	19	1.3 x10^5	1.5 x 10^5
60 μM	5x10^8 cells mL^{-1}	4.4	2.0 x10^5	24	4.5 x10^4	1.4 x 10^5

Table 32. Mean time constants for emission enhancement of THIA with TWEEN 40 added at 565 μM and *E. aerogenes* cells.

Conc	$\rho_{E.coli}$	τ_1	τ_2
64 μM	5x10^8 cells mL	6.8 ± 10	18 ± 3.0 s
6 μM	5x10^7 cells mL	6.1 ± 5	18 ± 5.8 s
600 nM	5x10^6 cells mL	7.2 ± 8	18 ± 3.0 s

Table 33. Time constants for emission enhancement of THIA with TWEEN 40 added at 565 μM and *B. subtilis* cells.

Conc	$\rho_{E.coli}$	τ_1	A	ΔF
600 nM	5x10^6 cells mL^{-1}	2.1	-4.7E6	7.3 x 10^6
600 nM	5x10^6 cells mL^{-1}	5.3	-7.3E6	7.6 x10^6
600 nM	5x10^6 cells mL^{-1}	1.8	-2.3E6	4.6 x 10^6
600 nM	5x10^7 cells mL^{-1}	2.7	-9.8E6	9.0 x 10^6
600 nM	5x10^7 cells mL^{-1}	2.2	-4.2E6	3.1 x 10^6
600 nM	5x10^7 cells mL^{-1}	1.8	-3.3E6	3.0 x 10^6
600 nM	5x10^8 cells mL^{-1}	3.0	-4.2E6	7.3 x 10^6
600 nM	5x10^8 cells mL^{-1}	3.7	-5.4E6	7.6 x10^6
600 nM	5x10^8 cells mL^{-1}	4.6	-9.5E6	4.6 x 10^6
6 μM	5x10^6 cells mL^{-1}	4.4	-9.5E4	2.5 x10^5
6 μM	5x10^6 cells mL^{-1}	4.1	-3.1E5	8.5 x 10^4
6 μM	5x10^6 cells mL^{-1}	3.3	-4.8E4	1.2 x 10^5
6 μM	5x10^7 cells mL^{-1}	2.8	-1.4E6	1.4 x 10^6
6 μM	5x10^7 cells mL^{-1}	4.4	-9.6E5	1.3 x 10^6
6 μM	5x10^7 cells mL^{-1}	4.4	-9.4E6	1.3 x 10^6
6 μM	5x10^8 cells mL^{-1}	3.5	-6.8E6	9.9 x 10^6
6 μM	5x10^8 cells mL^{-1}	2.5	-6.3E6	7.4 x 10^6
6 μM	5x10^8 cells mL^{-1}	2.4	-8.2E6	5.7 x 10^6
60 μM	5x10^6 cells mL^{-1}	5.3	-9.6E4	5.5 x 10^6
60 μM	5x10^6 cells mL^{-1}	4.5	-4.5e4	7.1 x 10^6
60 μM	5x10^6 cells mL^{-1}	5.6	-1.9E4	8.9 x 10^6
60 μM	5x10^7 cells mL^{-1}	2.9	-4.2E6	3.1 x 10^6
60 μM	5x10^7 cells mL^{-1}	2.4	-4.3E6	3.5 x 10^6
60 μM	5x10^7 cells mL^{-1}	2.6	-3.7E6	3.7 x 10^6
60 μM	5x10^8 cells mL^{-1}	2.9	-8.5E6	4.6 x 10^4
60 μM	5x10^8 cells mL^{-1}	2.7	-9.9E6	2.6 x 10^4
60 μM	5x10^8 cells mL^{-1}	3.1	-6.8E6	1.0 x 10^4

Table 34. Mean time constants for emission enhancement of THIA with TWEEN 40 added at 565 μM and *B. subtilis* cells.

Conc	$\rho_{E.coli}$	τ_1
64 μM	$5x10^8$ cells mL	4.6 ± 2
6 μM	$5x10^7$ cells mL	3.6 ± 2
600 nM	$5x10^6$ cells mL	3.0 ± 3

Table 35. Time constants for emission enhancement of THIA with TWEEN 40 added at 565 μM and *B. sphaericus* cells.

Conc	$\rho_{E.coli}$	τ_1	A	τ_2	B	ΔF
600 nM	$5x10^6$ cells mL^{-1}	5.8	-1.5e5	54	-6.9e4	5.3×10^5
600 nM	$5x10^6$ cells mL^{-1}	5.0	-3.4e5	45	-2.5e5	3.9×10^5
600 nM	$5x10^6$ cells mL^{-1}	5.9	-1.4e5	55	-7.0e4	4.0×10^5
600 nM	$5x10^7$ cells mL^{-1}	5.3	-1.2e6	67	-5.9e5	5.0×10^6
600 nM	$5x10^7$ cells mL^{-1}	2.8	-1.2e6	55	-6.4e5	4.1×10^6
600 nM	$5x10^7$ cells mL^{-1}	1.9	-8.2e5	54	-6.2e5	4.4×10^6
600 nM	$5x10^8$ cells mL^{-1}	3.4	-6.6e5	63	-4.9e5	8.6×10^6
600 nM	$5x10^8$ cells mL^{-1}	5.0	-6.2e6	58	-7.6e6	7.6×10^6
600 nM	$5x10^8$ cells mL^{-1}	1.9	-8.2e5	54	-4.2e6	6.2×10^6
6 μM	$5x10^6$ cells mL^{-1}	3.7	-2.4e7	19	-1.4e10	4.0×10^5
6 μM	$5x10^6$ cells mL^{-1}	2.7	-1.9e7	12	-8.3e6	4.5×10^5
6 μM	$5x10^6$ cells mL^{-1}	4.0	-1.1e7	52	-4.1e6	3.2×10^5
6 μM	$5x10^7$ cells mL^{-1}	5.8	-6.6e6			2.0×10^6
6 μM	$5x10^7$ cells mL^{-1}	6.2	-8.0e6			2.0×10^6
6 μM	$5x10^7$ cells mL^{-1}	6.4	-9.7e6			1.6×10^6
6 μM	$5x10^8$ cells mL^{-1}	5.3	-1.0e6	35	-3.1e5	8.0×10^6
6 μM	$5x10^8$ cells mL^{-1}	2.2	-2.6e5	33	-2.4e5	5.9×10^6
6 μM	$5x10^8$ cells mL^{-1}	7.2	-8.8e5	47	-1.0e6	7.2×10^6
60 μM	$5x10^6$ cells mL^{-1}	14	-1.7e6	57	-3.1e5	4.6×10^4
60 μM	$5x10^6$ cells mL^{-1}	0.10	2.1e4	50	2.2e6	2.6×10^4
60 μM	$5x10^6$ cells mL^{-1}	5.4	-8.6e5	56	-1.0e6	1.0×10^4
60 μM	$5x10^7$ cells mL^{-1}	3.1	-8.0e5	48	-1.0e6	3.1×10^6
60 μM	$5x10^7$ cells mL^{-1}	2.7	-9.0e6	49	-3.1e5	3.5×10^6
60 μM	$5x10^7$ cells mL^{-1}	4.1	-7.0e4	57	2.0e6	3.7×10^6
60 μM	$5x10^8$ cells mL^{-1}	3.4	-8.6e5	50	-1.0e6	5.5×10^6
60 μM	$5x10^8$ cells mL^{-1}	10	-8.8e5	49	-1.0e6	7.1×10^6
60 μM	$5x10^8$ cells mL^{-1}	4.2	-2.0e6	52	-3.0e5	8.9×10^6

Table 36. Mean time constants for emission enhancement of THIA with TWEEN 40 added at 565 μM and *B. sphaericus* cells.

Conc	$\rho_{E.coli}$	τ_1	τ_2
64 μM	$5x10^8$ cells mL	5.1 ± 4	51.8 ± 2.9 s
6 μM	$5x10^7$ cells mL	4.1 ± 3	52.4 ± 5.6 s
600nM	$5x10^6$ cells mL	2.4 ± 2	55.1 ± 4.0 s

Table 37. Time constants for bacterial solution with TWEEN 40 added at 565 μM TWEEN 40 for *B. globigii* endospores.

Conc	$\rho_{B.globigii}$	τ_1	A	τ_2	B	ΔF
6 μM	$5x10^6$ cells mL^{-1}	1.4	$5.6x10^5$	22	$6.7x10^5$	$1.0x10^6$
6 μM	$5x10^6$ cells mL^{-1}	20	$2.8x10^5$	20	$2.6x10^6$	$1.1x10^6$
6 μM	$5x10^6$ cells mL^{-1}	1.0	$7.2x10^5$	17	$1.0x10^6$	$1.7x10^6$
6 μM	$5x10^7$ cells mL^{-1}	27	$4.4x10^4$	25	$1.4x10^5$	$2.0x10^5$
6 μM	$5x10^7$ cells mL^{-1}	19	$1.2x10^5$	19	$1.1x10^5$	$2.9x10^5$
6 μM	$5x10^7$ cells mL^{-1}	21	$7.7x10^4$	22	$5.1x10^4$	$1.8x10^5$
6 μM	$5x10^8$ cells mL^{-1}	1.9	$2.8x10^5$	20	$2.6x10^5$	$5.5x10^4$
6 μM	$5x10^8$ cells mL^{-1}	22	$5.6x10^5$	22	$6.7x10^5$	$1.0x10^5$
6 μM	$5x10^8$ cells mL^{-1}	1.5	$7.2x10^5$	17	$1.0x10^6$	$1.2x10^5$

Table 38. Time constants for bacterial solution with TWEEN 40 added at 565 μM TWEEN 40 for *B. thuringiensis* endospores.

Conc	$\rho_{B.\ thuringiensis}$	τ_1	A	τ_2	B	ΔF
6 μM	$5x10^6$ cells mL^{-1}	1.4	$3.3x10^5$	55	$4.6x10^5$	3.5×10^6
6 μM	$5x10^6$ cells mL^{-1}	0.56	$4.6x10^5$	60	$3.4x10^6$	1.1×10^6
6 μM	$5x10^6$ cells mL^{-1}	4.7	$6.1x10^5$	54	$4.7x10^6$	2.0×10^6
6 μM	$5x10^7$ cells mL^{-1}	10	$3.4x10^5$	58	$3.1x10^5$	3.4×10^5
6 μM	$5x10^7$ cells mL^{-1}	6.5	$5.2x10^5$	57	$4.2x10^5$	4.0×10^5
6 μM	$5x10^7$ cells mL^{-1}	1.1	$4.7x10^4$	67	$4.7x10^5$	4.0×10^5
6 μM	$5x10^8$ cells mL^{-1}	94	$3.8x10^5$	71	$3.3x10^5$	2.2×10^5
6 μM	$5x10^8$ cells mL^{-1}	11	$3.6x10^5$	72	$3.7x10^5$	1.9×10^5
6 μM	$5x10^8$ cells mL^{-1}	1.4	$4.2x10^5$	82	$4.0x10^6$	1.2×10^5

Table 39. Mean time constants for bacterial solution with TWEEN 40 added at 565 μM TWEEN 40 for *Bacillus* endospores.

Conc	$\rho_{B.globigii}$	τ_1	τ_2
6 μM	$5x10^7$ cells mL	13 ± 11	22 ± 6 s
Conc	$\rho_{B.\ Thuringiensis}$	τ_1	τ_2
6 μM	$5x10^7$ cells mL	15 ± 30	64 ± 9 s

The emission-enhancement time constants appeared to cluster into a range of values. To confirm that these values were not simply due to random chance, we performed ANOVA tests were performed on the data. See Appendix C for a description of ANOVA.

ANOVA analysis was performed for the four vegetative bacterial species while the endospore samples were analyzed separately. A factorial number of analysis were performed to compare time constants from the experimental data; that is, we performed (n-1)! test to obtain a complete analysis of the data set. Since we had four vegetative bacterial species, we needed to perform (4 – 1)! = 3! or 1 x 2 x 3 = 6 tests (Tables 40-45).

Table 40. List of time constants and bacterial-cell densities for vegetative bacterial cells.

Cell density	*E. coli*	*E. aerogenes*	*B. subtilis*	*B. sphaericus*
2.00E+06	19.3	24.0	3.0	62.6
2.00E+06	19.5	24.3	3.7	58.0
2.00E+06	27.0	12.0	4.6	54.0
2.00E+06	35.0	23.0	2.7	66.6
2.00E+06	28.4	16.7	2.2	54.8
2.00E+06	34.9	18.4	1.8	54.1
2.00E+06	35.4	24.0	2.1	54.6
2.00E+06	31.0	16.0	5.3	45.3
2.00E+06	35.2	24.0	1.8	54.6
2.00E+07	32.2	24.0	3.5	35.2
2.00E+07	28.1	21.1	2.5	32.7
2.00E+07	27.5	20.2	2.4	46.5
2.00E+07	23.4	17.3	2.8	5.8
2.00E+07	27.3	15.5	4.4	6.2
2.00E+07	30.2	18.1	4.4	6.4
2.00E+07	27.8	16.9	4.4	19.1
2.00E+07	26.1	17.6	4.1	12.2
2.00E+07	27.8	14.6	3.3	52.2
2.00E+08	25.9	16.9	2.9	50.5
2.00E+08	26.1	19.0	2.7	48.9
2.00E+08	27.0	23.8	3.1	52.1
2.00E+08	35.3	15.0	2.9	48.4
2.00E+08	39.2	17.3	2.4	49.4
2.00E+08	34.0	20.0	2.6	57.2
2.00E+08	34.8	18.0	5.3	57.3
2.00E+08	29.0	22.0	4.5	49.8
2.00E+08	29.0	20.0	5.6	56.0

Table 41. ANOVA output for a single-parameter ANOVA analysis analyzing time constants from *B. subtilis* and *B. sphaericus*.

SUMMARY

Groups	*Count*	*Sum*	*Average*	*Variance*
3.00	26.0	8.80E1	3.38	1.28
62.6	26.0	1.13E3	43.4	326

ANOVA

Source of Variation	*SS*	*df*	*MS*	*F*	*P-value*	*F crit*
Between Groups	2.08E4	1.00	2.08E4	127	0.00	4.03
Within Groups	8.20E3	50.0	1.64E2			
Total	2.90E4	51.0				

Table 42. ANOVA output for a single-parameter ANOVA analysis analyzing time constants from *E. coli* and *B. subtilis*.

SUMMARY

Groups	*Count*	*Sum*	*Average*	*Variance*
19.3	26.0	777	29.9	20.5
24.0	26.0	496	19.1	11.5
3.00	26.0	88.0	3.38	1.28

ANOVA

Source of Variation	*SS*	*df*	*MS*	*F*	*P-value*	*F crit*
Between Groups	9.23E3	2.00	4.62E3	415	0.00	3.12
Within Groups	8.33E2	75.0	1.11E1			
Total	1.01E4	77.0				

Table 43. ANOVA output for a single-parameter ANOVA analysis analyzing time constants from *E. coli* and *B. sphaericus*.

SUMMARY

Groups	*Count*	*Sum*	*Average*	*Variance*
19.3	26.0	7.77E2	29.9	20.5
24.0	26.0	4.96E2	19.1	11.5
3.00	26.0	8.80E1	3.38	1.28
62.6	26.0	1.13E3	43.4	327

ANOVA

Source of Variation	*SS*	*df*	*MS*	*F*	*P-value*	*F crit*
Between Groups	2.24E4	3.00	7.45E3	82.8	0.00	2.70
Within Groups	9.00E3	100	90.0			
Total	3.14E4	103				

Table 44. ANOVA output for a single-parameter ANOVA analysis analyzing time constants from *E. aerogenes* and *B. subtilis*.

SUMMARY

Groups	*Count*	*Sum*	*Average*	*Variance*
Column 1	27.0	520	19.3	12.0
Column 2	27.0	91.0	3.37	1.23

ANOVA

Source of Variation	*SS*	*df*	*MS*	*F*	*P-value*	*F crit*
Between Groups	3.40E3	1.00	3.40E3	514	0.00	4.03
Within Groups	3.44E2	52.0	6.62E0			
Total	3.75E3	53.0				

Table 45. ANOVA output for a single-parameter ANOVA analysis analyzing time constants from *E. aerogenes* and *B. sphaericus*.

SUMMARY

Groups	*Count*	*Sum*	*Average*	*Variance*
24.0	26.0	4.96E2	19.1	11.5
3.00	26.0	8.80E1	3.38	1.28
62.6	26.0	1.13E3	43.4	326

ANOVA

Source of Variation	*SS*	*df*	*MS*	*F*	*P-value*	*F crit*
Between Groups	2.11E4	2.00	1.06E4	93.3	0.00	3.12
Within Groups	8.48E3	75.0	1.13E2			
Total	2.9E4	77.0				

The six one-factor ANOVA tests yielded *p*-values that were significantly smaller than 0.01. These resuts indicated that the kinetics of staining with THIA for the four vegetative species were discernible from one another with statistical level of significance exceeding 99% .

Similarly, we observed statistically significant difference between the values of the timeconstants for the two endospores. Althoguh, imaging will clearly allow the distinction between vegetative bacterial cels and bacterial endospores, some of the overlap between the timeconstants of the endospores and vegetative cells demonstrates the shortcomings for using a single stain for the development of dynamic assays. Expanding the choice of fluorescence stains to several dyes with different staining kinetics for each of the species can potentially allow for robust

statistically significant discernibility of a broad range of bacterial species in their vegetative and spore forms.

2.2.2. Kinetics of bacterium-induced fluorescence enhancement of THIA in the absence of a surfactant

The kinetics of staining for the four vegetative bacterial species did not have rates that differed significantly from one another without the addition of any additives. This can be seen in the similarities of the time constants extracted from the kinetics curves (Table 46). Therefore, the use of TWEEN 40 for the kinetic measurements of the fluorescence staining proved to be essential for attaining discernibility between the time constants for the different bacterial species.

Table 46. Time constants for emission enhancement of THIA without TWEEN 40 added with *E. coli* cells.

E. coli density	THIA concentration in 2mM tris buffer / μM		
Cell mL^{-1}	0.6		0.6
2×10^6	3.7 ± 0.8	2×10^6	3.7 ± 0.8
2×10^7	4.4 ± 0.3	2×10^7	4.4 ± 0.3
2×10^8	4.6 ± 0.1	2×10^8	4.6 ± 0.1
E. aerogenes density	THIA concentration in 2mM tris buffer / μM		
Cell mL^{-1}	0.6	6	60
1×10^6	11 ± 4.0	15 ± 3.0	6.7 ± 1.7
1×10^7	7.9 ± 1.3	10 ± 4.0	15 ± 1.0
1×10^8	12 ± 1.0	9.8 ± 5.3	12 ± 1.0
B. subtilis density	THIA concentration in 2mM tris buffer / μM		
Cell mL^{-1}	0.6	6	60
4×10^6	8.6 ± 1.7	4.4 ± 2.3	5.1 ± 0.4
4×10^7	9.5 ± 1.6	3.8 ± 0.8	4.4 ± 0.4
4×10^8	4.6 ± 1.4	4.6 ± 1.3	4.9 ± 0.2
B. sphaericus density	THIA concentration in 2mM tris buffer / μM		
Cell mL^{-1}	0.6	6	60
6×10^6	8.3 ± 1.0	7.4 ± 0.6	6.9 ± 0.9
6×10^7	7.6 ± 1.4	6.4 ± 0.2	7.6 ± 0.4
6×10^8	7.2 ± 0.2	7.6 ± 0.3	7.3 ± 0.5

2.2.3. Kinetics of fluorescence enhancement of other cyanine dyes

We explored the kinetics of emission enhancement of two other thiacyanine dyes. THO and THC both displayed emission enhancement, induced by addition of *E. coli* (Figure 45). The emission-enhancement kinetic curves were significantly different from the curves we observed for THIA. The time constants for the emission enhancement of THO, THC and THIA induced by *E. coli*, were sufficiently different

that it provided a means for generating dynamic patterns for species identification (Figure 43 (a) and (b), Figure 36).

The initial emission enhancement of THC was followed by a rapid decay. The observed decay provides an explanation for the observed decrease in the intensity of the spectra of THC measured seconds after the addition of bacterial cells.

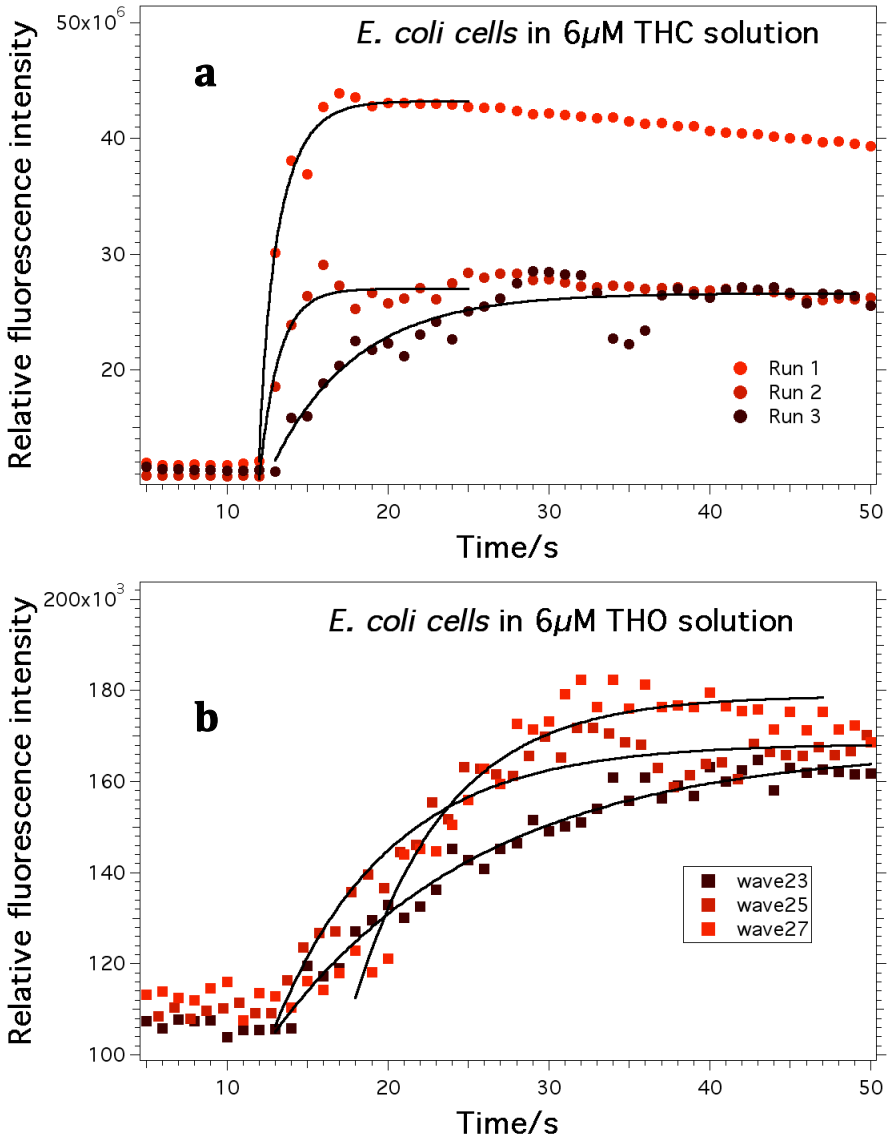

Figure 43. Kinetic curves for $5x10^7$ cell mL^{-1} of *E. coli* in 6 mM of (a) THC and (b) THO solutions dissolved in 2 mM Tris buffer at pH 8.5.

Table 47. Time constants for bacterial solution with TWEEN 40 added at 565 μM TWEEN 40 for *E. coli*, all three thiacyanine dyes.

THC	$\rho_{E.coli}$	τ_1	A	ΔF
6 μM	$5x10^7$ cells mL^{-1}	4.7	$4.0x10^7$	$1.5x10^7$
6 μM	$5x10^7$ cells mL^{-1}	1.4	$3.9x10^7$	$1.5x10^7$
6 μM	$5x10^7$ cells mL^{-1}	1.2	$2.4x10^7$	$1.5x10^7$
THO	$\rho_{E.coli}$	τ_1	A	ΔF
6 μM	$5x10^7$ cells mL^{-1}	7.5	$4.2x10^6$	$7.5x10^4$
6 μM	$5x10^7$ cells mL^{-1}	7.2	$3.6x10^6$	$6.1x10^4$
6 μM	$5x10^7$ cells mL^{-1}	11	$4.0x10^6$	$5.7x10^4$

Table 48. Mean time constants for *E. coli* solution with TWEEN 40 added at 565 μM TWEEN 40 in thiacyanine dye solutions.

Conc	$\rho_{E.coli}$	τ_1
6 μM THC	$5x10^7$ cells mL	2.4 ± 2.0
Conc	$\rho_{E.coli}$	τ_1
6 μM THO	$5x10^7$ cells mL	8.6 ± 2.2

2.3. Conclusions

The dynamics of the staining process for six model bacterial species using three thiacyanine dyes was investigated. The thiacyanine dye THIA was primarily focus of this study. We found that the time constants show no dependence on the dye concentration and on the cell density. Therefore, if we have a single dye and a single bacterial species, we should observe similar time constants. The time constants in the presence of TWEEN 40 show statistically significant difference for the different

bacterial species. In the absence of the surfactant, the difference between most of the time constants for the different bacterial species was statistically insignificant.

The preliminary data in this spectroscopy study can potentially be used to help develop an assay for rapid identification of bacterial species. The findings from the exploratory research presented in this and the previous chapter require further exploration to prove feasible for the development of working assays.

2.4. Experimental

2.4.1. Materials

E. coli TOP 10 (Invitrogen) and *E. aerogenes, B. subtilis, B. sphaericus* (Carolina Biologicals) strains were used for all experiments. Propidium iodide and SYTO 9 were obtained from Invitrogen. LB broth, LB Agar, 3,3'-diethylthiacyanine iodide, 3,3'-diethylthiacarbocyanine iodide (THIA-CARB) (Sigma), eosin Y disodium salt, methylviologen dichloride hydrate and alcohols (methanol, ethanol, 1-propanol, 1-butanol, ethylene glycol and glycerol: all spectroscopic grade) were purchased from Sigma-Aldrich. Tris(hydroxylmethyl) aminomethane was obtained from Acros Organics. Sodium hydroxide was purchased from Fisher Scientific. For all aqueous solutions, we used Milli-Q water (from an in-house purification system).

2.4.2. Methods

2.4.2.1. Bacterial sample preparation.

The bacterial cultures for two Gram-positive species, *Bacillus subtilis* and *Bacillus sphaericus*, and two Gram-negative species, *Escherichia coli* and *Enterobacter aerogenes*, were prepared on solid Luriebroth (LB) agar media. Colonies from these cultures were transferred to liquid media and allowed to grow overnight, up to 24 hours. The solid LB agar with bacterial culture was stored at -4 ^{o}C in a refrigerator. Prior to use in the experiment, the liquid cultures were centrifuged, pellet, washed

twice and re-suspended in 2 mM Tris buffer solution. Stock solutions were prepared by suspending spores in 2 mM Tris buffer, then stored at 4 ^{o}C and used completely within 24 hours (to prevent contamination). Cells were grown overnight at 37 ^{o}C in liquid media with shaking at 200 rpms in LB Broth cultures. Prior to analysis, the cell media were changed from LB Broth to Tris buffer at pH 8.5 (2 mM) by centrifuging the bacteria to a pellet, decanting the LB Broth and re-suspending the cells in Tris buffer. Cell counting was performed using an improved Neubauer counting chamber positioned on a MicroMaster microscope stage (Fisher Scientific) and observed using a 40x (0.40 NA) objective and a 10x eyepiece (400x magnification). To ensure that all bacteria used in our experiments were in their growth phase, we constructed growth curves for the bacterial strains being investigated. The curves revealed that bacteria in liquid cultures, grown 18-24 hours, are within their growth phases. All bacterial strains were maintained at room temperature during all experiments conducted.

2.4.2.2. Spectroscopy measurements

The absorption spectra were recorded using an UV/Vis spectrophotometer (Varian Cary 50 Bio), at a wavelength range between 350 and 700 nm. All measurements were taken in an 1-cm plastic cuvette. The excitation and emission spectra, as well as the emission enhancement kinetics, were recorded with a fluorescence spectrophotometer (Fluorolog 3-22). For the emission spectra and the kinetics

measurements, the excitation wavelength was set near the absorption maximum of the dye, λ_{ex} = 420 nm.

In our experiments, TWEEN surfactant was added to each stock solution at a concentration of 565 μM in order to modulate the uptake of dye by the cells. In another experiment, TWEEN was added to the bacteria solution. The density of both the vegetative bacterial cells were determined using a hemocytometer at 400x magnification using an optical microscope. Fluorescence cuvettes were filled with dye solution containing aqueous THIA solution for absorption and emission measurements. Measurements of the fluorescence intensity at the spectral maximum were colleted over a five-minute period. These experiments were performed as described previously, introducing cells to a THIA solution in 2 mM Tris buffer.

Control experiments were performed using Tris buffer (no cells), Tris buffer (with cells) and THIA in buffer (no cells). The quantum yield of each dye was determined by measuring the fluorescence emission and the absorption in different solvents. See Appendix H for details.

2.4.2.3. Data analysis.

Statistical data analysis was performed using IgorPro (version 6.02) with the

ANOVA method adopted from Samuels and Witmer, 3rd Ed.

Two-factor and one-factor ANOVA were used to evaluate whether the data were statistically significant within a 95% confidence limit.

2.4.2.4. Calculating the quantum yield of each dye

The quantum yield of each dye was determined by measuring the fluorescence emission and the absorption in different solvents. We calculated the quantum yield by:[58]

$$\Phi = \Phi_0 \frac{S}{S} \frac{1-10^{-A_0}}{1-10^{-A}} \left(\frac{n}{n_0} \right)^2 \qquad \textbf{Equation 7.}$$

Where S is the area under the fluorescence spectra, A is the absorption at the excitation wavelength and n is the medium refractive index. The subscript "0" indicates the quantities for the fluorescence standard, coumarin 151 in ethanol.

References

1. Klevens, R. M.; Morrison, M. A.; Nadle, J.; Petit, S.; Gershman, K.; Ray, S.; Harrison, L. H.; Lynfield, R.; Dumyati, G.; Townes, J. M.; Craig, A. S.; Zell, E. R.; Fosheim, G. E.; McDougal, L. K.; Carey, R. B.; Fridkin, S. K.; Investigators, A. M.; , Invasive methicillin-resistant Staphylococcus aureus infections in the United States. *Jama-Journal of the American Medical Association* **2007,** 298, (15), 1763-1771.

2. Cheng, J. C.; Huang, C. L.; Lin, C. C.; Chen, C. C.; Chang, Y. C.; Chang, S. S.; Tseng, C. P., Rapid detection and identification of clinically important bacteria by high-resolution melting analysis after broad-range ribosomal RNA real-time PCR. *Clin Chem* **2006,** 52, (11), 1997-2004.

3. Klevens, R. E., J; Richards, C; Horan, T; Gaynes, R; Pollack, D; Cardo, D;, Estimating Health Care-Associated Infections and Death in U.S. Hospitals, 2002. *Public Health Reports, National Center for Infectious Disease, CDC* **2007,** 122.

4. Clark CD, J. K., Jones JL, et al. , Incidence of hand infections and their bacterial flora. *Presented at the American Academy of Orthopaedic Surgeons 74th Annual Meeting. Feb. 14-18, 2007. San Diego.* **2007**.

5. Bond, P. L.; Erhart, R.; Wagner, M.; Keller, J.; Blackall, L. L., Identification of some of the major groups of bacteria in efficient and nonefficient biological phosphorus removal activated sludge systems. *Applied and Environmental Microbiology* **1999,** 65, (9), 4077-4084.

6. Sakata, H., [Comparative study on bacterial eradication rate and clinical efficacy of CDTR, CFPN, and FRPM for treatment of children with otitis media and lower respiratory tract infection due to Streptococcus pneumoniae and Haemophilus influenzae]. *Jpn J Antibiot* **2001,** 54 Suppl B, 96.

7. Tambic, A., [Methicillin-resistant Staphylococcus aureus (MRSA), a predictor of the end of the antibiotic era--diagnosis, epidemiology, therapy and dissemination prevention]. *Lijec Vjesn* **1997,** 119, (5-6), 166-71.

8. Thorell, E. A.; Jackson, M. A.; Harrison, C.; Selvarangan, R., Methicillin-resistant Staphylococcus aureus (MRSA) in healthy children: Risk factor (RF) analysis and pulsed field gel electrophoresis (PFGE) of colonizing and invasive strains. *Pediatric Research* **2006,** 60, (4), 498-498.

9. Fogarty, C. M.; Greenberg, R. N.; Dunbar, L.; Player, R.; Marrie, T. J.; Kojak, C. M.; Morgan, N.; Williams, R. R., Effectiveness of levofloxacin for adult community-

acquired pneumonia caused by macrolide-resistant Streptococcus pneumoniae:integrated results from four open-label, multicenter, phase III clinical trials. *Clin Ther* **2001,** 23, (3), 425-39.

10. Hadley, J. A., The Microbiology and Management of Acute and Chronic Rhinosinusitis. *Curr Infect Dis Rep* **2001,** 3, (3), 209-216.

11. Kashani, H.; Dahlin, C.; Alse'n, B., Influence of different prophylactic antibiotic regimens on implant survival rate: a retrospective clinical study. *Clin Implant Dent Relat Res* **2005,** 7, (1), 32-5.

12. Kruger, A. J.; Raptis, S.; Fitridge, R. A., Management practices of Australian surgeons in the treatment of venous ulcers. *ANZ J Surg* **2003,** 73, (9), 687-91.

13. Madridejos-Mora, R.; Amado-Guirado, E.; Perez-Rodriguez, M. T., Effectiveness of the combination of feedback and educational recommendations for improving drug prescription in general practice. *Med Care* **2004,** 42, (7), 643-8.

14. Manfredi, R., [Antibiotic resistance and community-acquired infections]. *Recenti Prog Med* **2002,** 93, (3), 149-56.

15. Rossi, C.; Sternon, J., [Flouroquinolones of the third and fourth generations]. *J Pharm Belg* **2001,** 56, (6), 137-48.

16. Rossi, C.; Sternon, J., [Third and fourth generation fluoroquinolones]. *Rev Med Brux* **2001,** 22, (5), 443-56.

17. Rutschmann, O. T.; Domino, M. E., Antibiotics for upper respiratory tract infections in ambulatory practice in the United States, 1997-1999: does physician specialty matter? *J Am Board Fam Pract* **2004,** 17, (3), 196-200.

18. Sternon, J.; Glupczynski, Y., [Overprescribing of antibiotics outside the hospital]. *Rev Med Brux* **1999,** 20, (1), 43-7.

19. Alberts, B., From the National Academies. *Cell Biol Educ* **2002,** 1, (4), 109-10.

20. Kaplan, M. L.; Kaplan, L., The Gram Stain and Differential Staining. *J Bacteriol* **1933,** 25, (3), 309-21.

21. Baddiley, J., Teichoic acids in cell walls and membranes of bacteria. *Essays Biochem* **1972,** 8, 35-77.

22. Beveridge, T. J.; Graham, L. L., Surface layers of bacteria. *Microbiol Rev* **1991,** 55, (4), 684-705.

23. Todar, K.; , Todar's Online Textbook of Bacteriology. **2008**.

24. Nakae, T., Permeability properties of the outer membrane of gram-negative bacteria--a discover of porin. *Kitasato Arch Exp Med* **1984,** 57, (1), 1-20.

25. Nikaido, H.; Nakae, T., The outer membrane of Gram-negative bacteria. *Adv Microb Physiol* **1979,** 20, 163-250.

26. Raetz, C. R. H.; Whitfield, C., Lipopolysaccharide endotoxins. *Annual Review of Biochemistry* **2002,** 71, 635-700.

27. Smit, J.; Nikaido, H., Outer membrane of gram-negative bacteria. XVIII. Electron microscopic studies on porin insertion sites and growth of cell surface of Salmonella typhimurium. *J Bacteriol* **1978,** 135, (2), 687-702.

28. Tono, H.; Kornberg, A., Biochemical studies of bacterial sporulation. IV. Inorganic pyrophosphatase of vegetative cells and spores of Bacillus megaterium. *J Bacteriol* **1967,** 93, (6), 1819-24.

29. Dubos, R. J.; Hotchkiss, R. D., The Production of Bactericidal Substances by Aerobic Sporulating Bacilli. *J Exp Med* **1941,** 73, (5), 629-640.

30. Kubitschek, H. E., Growth during the bacterial cell cycle: analysis of cell size distribution. *Biophys J* **1969,** 9, (6), 792-809.

31. Pooley, H. M., Layered distribution, according to age, within the cell wall of bacillus subtilis. *J Bacteriol* **1976,** 125, (3), 1139-47.

32. Forbes, B. A.; Sahm, D. F.; Weissfeld, A. S.; Bailey, W. R. Bailey & Scott's diagnostic microbiology.

33. Gillespie, S. H.; Hawkey, P. M., *Principles and practice of clinical bacteriology*. 2nd ed.; John Wiley & Sons: Chichester, West Sussex, England ; Hoboken, NJ, 2006; p viii, 605 p.

34. Henriques, A. O.; Moran, C. P., Jr. , Structure, assembly, and function of the spore surface layers. *Annu Rev Microbiol* **2007,** 61, 555-88.

35. Klotz, L. C., Overproduction of proteins in recombinant organisms. *Ann N Y Acad Sci* **1983,** 413, 1-11.

36. Nicholson, W. L.; Fajardo-Cavazos, P.; Rebeil, R.; Slieman, T. A.; Riesenman, P. J.; Law, J. F.; Xue, Y., Bacterial endospores and their significance in stress resistance. *Antonie Van Leeuwenhoek* **2002,** 81, (1-4), 27-32.

37. Peck, M. W., Biology and genomic analysis of Clostridium botulinum. *Adv Microb Physiol* **2009,** 55, 183-265, 320.

38. Dixon, T. C.; Fadl, A. A.; Koehler, T. M.; Swanson, J. A.; Hanna, P. C., Early Bacillus anthracis-macrophage interactions: intracellular survival survival and escape. *Cell Microbiol* **2000,** 2, (6), 453-63.

39. Iandolo, J. J.; Ordal, Z. J., Germination System for Endospores of Sarcina Ureae. *J Bacteriol* **1964,** 87, 235-6.

40. Kobayashi, N.; Bauer, T. W.; Sakai, H.; Togawa, D.; Lieberman, I. H.; Fujishiro, T.; Procop, G. W., The use of newly developed real-time PCR for the rapid identification of bacteria in culture-negative osteomyelitis. *Joint Bone Spine* **2006,** 73, (6), 745-7.

41. Kotilainen, P.; Jalava, J.; Meurman, O.; Lehtonen, O. P.; Rintala, E.; Seppala, O. P.; Eerola, E.; Nikkari, S., Diagnosis of meningococcal meningitis by broad-range bacterial PCR with cerebrospinal fluid. *Journal of Clinical Microbiology* **1998,** 36, (8), 2205-2209.

42. Rudi, K.; Kleiberg, G. H.; Heiberg, R.; Rosnes, J. T., Rapid identification and classification of bacteria by 16S rDNA restriction fragment melting curve analyses (RFMCA). *Food Microbiology* **2007,** 24, (5), 474-481.

43. Jonasson, J.; Monstein, H. J., Classification, identification and subtyping of bacteria based on pyrosequencing and signature matching of 16s rDNA fragments - Commentary. *Apmis* **2007,** 115, (5), 678-679.

44. Struthers, J. K.; Westran, R. P. Clinical bacteriology.

45. Denis, O.; Deplano, A.; De Beenhouwer, H.; Hallin, M.; Huysmans, G.; Garrino, M. G.; Glupczynski, Y.; Malaviolle, X.; Vergison, A.; Struelens, M. J., Polyclonal emergence and importation of community-acquired methicillin-resistant Staphylococcus aureus strains harbouring Panton-Valentine leucocidin genes in Belgium. *Journal of Antimicrobial Chemotherapy* **2005,** 56, (6), 1103-1106.

46. Berney, M.; Hammes, F.; Bosshard, F.; Weilenmann, H. U.; Egli, T., Assessment and interpretation of bacterial viability by using the LIVE/DEAD BacLight Kit in combination with flow cytometry. *Appl Environ Microbiol* **2007,** 73, (10), 3283-90.

47. Deka, C.; Steinkamp, J. A., Time-resolved fluorescence-decay measurement and analysis on single cells by flow cytometry. *Applied Optics* **1996,** 35, (22), 4481-4489.

48. Eray, M.; Matto, M.; Kaartinen, M.; Andersson, L.; Pelkonen, J., Flow cytometric analysis of apoptotic subpopulations with a combination of annexin V-FITC, propidium iodide, and SYTO 17. *Cytometry* **2001,** 43, (2), 134-42.

49. Hofmann, O.; Murray, K.; Wilkinson, A. S.; Cox, T.; Manz, A., Laser induced disruption of bacterial spores on a microchip. *Lab on a Chip* **2005,** 5, (4), 374-377.

50. van Baar, B. L. M., Characterisation of bacteria by matrix-assisted laser desorption/ionisation and electrospray mass spectrometry. *Fems Microbiology Reviews* **2000,** 24, (2), 193-219.

51. Friedlander, C. Die Mikrokokken der Pneumonie. Fortschr.

52. Gram, H. C., Über die isolirte Färbung der Schizomyceten in Schnitt- und Trockenpräparaten. . *Fortschritte der Medizin* **1884,** 2, (186).

53. Romero, S.; Schell, R. F.; Pennell, D. R., Rapid Method for the Differentiation of Gram-Positive and Gram-Negative Bacteria on Membrane Filters. *Journal of Clinical Microbiology* **1988,** 26, (7), 1378-1382.

54. Stahl, C.; Olsen, E., Gram-negative staining of gram-positive intestinal bacteria with particular reference to examinations of faeces in infants. *Acta Paediatr* **1950,** 39, (6), 372-80.

55. Bronk, B. V.; Reinisch, L., Variability of Steady-State Bacterial Fluorescence with Respect to Growth-Conditions. *Applied Spectroscopy* **1993,** 47, (4), 436-440.

56. Marlon Thomas, E. Z., Valentine Vullev A method and device for real-time fluorescence detection of bacterial pathogens. *Provisional patent* **2007**.

57. Elizabeth Zeilins, M. T. G. s. a., Valentine Vullev, Bacterium-Induced Fluorescence-Enhancement Kinetics: Breaking 100-Year Old Traditions of Staining Bioanalyses. *Undergraduate Research Journal, University of California-Riverside* **June 2008,** II.

58. Lakowicz, J. R.; SpringerLink (Online service), *Principles of fluorescence spectroscopy*. 3rd ed.; Springer: New York, 2006; p xxvi, 954 p.

59. Albani, J. R., *Principles and applications of fluorescence spectroscopy*. Blackwell Science: Oxford ; Ames, Iowa, 2007; p viii, 255 p., [4] p. of plates.

60. Grabowski, Z. R.; Dobkowski, J., Twisted Intramolecular Charge-Transfer (Tict) Excited-States - Energy and Molecular-Structure. *Pure and Applied Chemistry* **1983,** 55, (2), 245-252.

61. Cooper, M.; Ebner, A.; Briggs, M.; Burrows, M.; Gardner, N.; Richardson, R.; West, R., Cy3B: improving the performance of cyanine dyes. *J Fluoresc* **2004,** 14, (2), 145-50.

62. Carreon, J. R.; Stewart, K. M.; Mahon, K. P., Jr.; Shin, S.; Kelley, S. O., Cyanine dye conjugates as probes for live cell imaging. *Bioorg Med Chem Lett* **2007,** 17, (18), 5182-5.

63. Esposito, A.; Wouters, F. S., Fluorescence lifetime imaging microscopy. *Curr Protoc Cell Biol* **2004,** Chapter 4, Unit 4 14.

64. Taatjes, D. J.; Mossman, B. T., *Cell imaging techniques : methods and protocols*. Humana Press: Totowa, N.J., 2006; p xiv, 490 p.

65. Jones, G., 2nd; Yan, D.; Hu, J.; Wan, J.; Xia, B.; Vullev, V. I., Photoinduced electron transfer in arylacridinium conjugates in a solid glass matrix. *J Phys Chem B* **2007,** 111, (24), 6921-9.

66. Grabowski, Z. R.; Rotkiewicz, K.; Rettig, W., Structural changes accompanying intramolecular electron transfer: Focus on twisted intramolecular charge-transfer states and structures. *Chemical Reviews* **2003,** 103, (10), 3899-4031.

67. Grabowski, Z. R., Electron-Transfer in Flexible Molecules and Molecular-Ions. *Pure and Applied Chemistry* **1993,** 65, (8), 1751-1756.

68. Grabowski, Z. R., Electron-Transfer and the Structural-Changes in the Excited-State. *Pure and Applied Chemistry* **1992,** 64, (9), 1249-1255.

69. Brooker, L. G., Chemistry of the cyanine dyes. *Ann N Y Acad Sci* **1948,** 50, (21-26), 108.

70. Harvey, B. J.; Levitus, M., Nucleobase-specific enhancement of Cy3 fluorescence. *J Fluoresc* **2009,** 19, (3), 443-8.

71. Chibisov, A. Z. G. G. H. S. Y. T. A., Photorelaxation Processes in Covalently Linked Indocarbocyanine and Thiacarbocyanine Dyes. *Journal of Physical Chemistry* **1995,** 99, (3), 886-893.

72. Potter, C. A. S.; Brown, R. G.; Vollmer, F.; Rettig, W., Role of Twisted Intramolecular Charge-Transfer States in the Decay of 2-(2'-Hydroxyphenyl)Benzothiazole Following Excited-State Intramolecular Proton-Transfer. *Journal of the Chemical Society-Faraday Transactions* **1994,** 90, (1), 59-67.

73. Roth, B. L.; Poot, M.; Yue, S. T.; Millard, P. J., Bacterial viability and antibiotic susceptibility testing with SYTOX green nucleic acid stain. *Appl Environ Microbiol* **1997,** 63, (6), 2421-31.

74. Busso, D.; Stierle, M.; Thierry, J. C.; Moras, D., Automated recombinant protein expression screening in Escherichia coli. *Methods Mol Biol* **2008,** 426, 175-86.

75. Kang, C. I.; Kim, S. H.; Park, W. B.; Lee, K. D.; Kim, H. B.; Oh, M. D.; Kim, E. C.; Choe, K. W., Bloodstream infections caused by Enterobacter species: predictors of 30-day mortality rate and impact of broad-spectrum cephalosporin resistance on outcome. *Clin Infect Dis* **2004,** 39, (6), 812-8.

76. Ballou, B.; Fisher, G. W.; Waggoner, A. S.; Farkas, D. L.; Reiland, J. M.; Jaffe, R.; Mujumdar, R. B.; Mujumdar, S. R.; Hakala, T. R., Tumor labeling in vivo using cyanine-conjugated monoclonal antibodies. *Cancer Immunol Immunother* **1995,** 41, (4), 257-63.

77. Antelmann, H.; Scharf, C.; Hecker, M., Phosphate starvation-inducible proteins of Bacillus subtilis: proteomics and transcriptional analysis. *J Bacteriol* **2000,** 182, (16), 4478-90.

78. Meador-Parton, J.; Popham, D. L., Structural analysis of Bacillus subtilis spore peptidoglycan during sporulation. *J Bacteriol* **2000,** 182, (16), 4491-9.

79. Hansen, M. E.; Wangari, R.; Hansen, E. B.; Mijakovic, I.; Jensen, P. R., Engineering of Bacillus subtilis 168 for increased nisin resistance. *Appl Environ Microbiol* **2009,** 75, (21), 6688-95.

80. Klein D, U. I., Braun S, Tightly Bound Binary Toxin in the Cell Wall of Bacillus sphaericus. *Applied and Environmental Microbiology* **2002,** 68, (7), 3300-3307.

81. de Boer, A. S.; Diderichsen, B., On the safety of Bacillus subtilis and B. amyloliquefaciens: a review. *Appl Microbiol Biotechnol* **1991,** 36, (1), 1-4.

82. Zhou, B.; Wirsching, P.; Janda, K. D., Human antibodies against spores of the genus Bacillus: a model study for detection of and protection against anthrax and the bioterrorist threat. *Proc Natl Acad Sci U S A* **2002,** 99, (8), 5241-6.

83. Turnbull, P. C., Anthrax vaccines: past, present and future. *Vaccine* **1991,** 9, (8), 533-9.

84. Gaur, R.; Gupta, P. K.; Banerjea, A. C.; Singh, Y., Effect of nasal immunization with protective antigen of Bacillus anthracis on protective immune response against anthrax toxin. *Vaccine* **2002,** 20, (21-22), 2836-9.

85. Pena, G.; Miranda-Rios, J.; de la Riva, G.; Pardo-Lopez, L.; Soberon, M.; Bravo, A., A Bacillus thuringiensis S-layer protein involved in toxicity against Epilachna varivestis (Coleoptera: Coccinellidae). *Appl Environ Microbiol* **2006,** 72, (1), 353-60.

86. Farrell, S.; Halsall, H. B.; Heineman, W. R., Immunoassay for B. globigii spores as a model for detecting B. anthracis spores in finished water. *Analyst* **2005,** 130, (4), 489-97.

87. Elizabeth Zeilins, M. S. T., Valentine Vullev Bacterium-Induced Fluorescence-Enhancement Kinetics: Breaking 100-Year Old Traditions of Staining Bioanalyses. *Undergraduate Research Journal* **2008,** II.

88. Mandal A, P. M., Principal Component Analysis of the Absorption Spectra of the Dye Thiacyanine in the Presence of the Surfactant AOT: Precise Identification of the Dye–Surfactant Aggregates. *Journal of Colloid and Interface Science* **1997,** 192, (1), 83-93.

89. Yamaguchi, A.; Kometani, N.; Yonezawa, Y., Luminescence properties of the mixed J-aggregate of oxacyanine dye and thiacyanine dye. Formation of a persistence-type aggregate. *J Phys Chem B* **2005,** 109, (4), 1408-14.

90. Patist A., B. S., Penfield K., Aikens P., Shah D., On the Measurement of Critical Micelle Concentrations
of Pure and Technical-Grade Nonionic Surfactants. *Journal of Surfactants and Detergents* **2000,** 3, (1), 53.

91. Vogt, G.; Krampert, G.; Niklaus, P.; Nuernberger, P.; Gerber, G., Optimal Control of Photoisomerization. *Physical Review Letters* **2005,** 94, (6), 068305/1-068305/4.

92. Tolmachev, A. C. G. Z. H. G. Y. S. A. Photorelaxation Processes in Covalently Linked Indocarbocyanine and Thiacarbocyanine Dyes.

93. Anikovsky M, T. A., Kuzmin V Fluorescent Properties of Some Thia- and Oxacarbbocyanine Dyes in the Presence of DNA.

94. Malicka, J.; Gryczynski, I.; Fang, J.; Lakowicz, J. R., Fluorescence spectral properties of cyanine dye-labeled DNA oligomers on surfaces coated with silver particles. *Anal Biochem* **2003,** 317, (2), 136-46.

95. Sun, Y.; Phipps, J.; Elson, D. S.; Stoy, H.; Tinling, S.; Meier, J.; Poirier, B.; Chuang, F. S.; Farwell, D. G.; Marcu, L., Fluorescence lifetime imaging microscopy: in vivo application to diagnosis of oral carcinoma. *Opt Lett* **2009,** 34, (13), 2081-3.

96. Pawley, J. B., *Handbook of biological confocal microscopy*. 2nd ed.; Plenum Press: New York, 1995; p xxiii, 632 p.

97. Phipps, J.; Sun, Y.; Saroufeem, R.; Hatami, N.; Marcu, L., Fluorescence lifetime imaging microscopy for the characterization of atherosclerotic plaques. *Proc Soc Photo Opt Instrum Eng* **2009,** 7161, 71612G.

98. Bhatta, H.; Goldys, E. M., Quantitative characterization of different strains of Saccharomyces yeast by analysis of fluorescence microscopy images of cell populations. *J Microbiol Methods* **2009,** 77, (1), 77-84.

99. Coling, D.; Kachar, B., Principles and application of fluorescence microscopy. *Curr Protoc Mol Biol* **2001,** Chapter 14, Unit 14 10.

100. Jung, G.; Gerharz, S.; Schmitt, A., Solvent-dependent steady-state fluorescence spectroscopy for searching ESPT-dyes: solvatochromism of HPTS revisited. *Phys Chem Chem Phys* **2009,** 11, (9), 1416-26.

101. Preffer, F.; Dombkowski, D., Advances in complex multiparameter flow cytometry technology: Applications in stem cell research. *Cytometry B Clin Cytom* **2009**.

102. Sharpe, J. C.; Evans, K. M., Advances in flow cytometry for sperm sexing. *Theriogenology* **2009,** 71, (1), 4-10.

103. Jennings, C. D.; Foon, K. A., Recent advances in flow cytometry: application to the diagnosis of hematologic malignancy. *Blood* **1997,** 90, (8), 2863-92.

104. Landay, A. L., Advances in flow cytometry for diagnostic pathology. *Lab Invest* **1994,** 70, (1), 134.

105. Hwang, L. C.; Wohland, T., Recent advances in fluorescence cross-correlation spectroscopy. *Cell Biochem Biophys* **2007,** 49, (1), 1-13.

106. Heuff, R. F.; Swift, J. L.; Cramb, D. T., Fluorescence correlation spectroscopy using quantum dots: advances, challenges and opportunities. *Phys Chem Chem Phys* **2007,** 9, (16), 1870-80.

107. Thompson, N. L.; Lieto, A. M.; Allen, N. W., Recent advances in fluorescence correlation spectroscopy. *Curr Opin Struct Biol* **2002,** 12, (5), 634-41.

108. McConnell, G., Confocal laser scanning fluorescence microscopy with a visible continuum source. *Optics Express* **2004,** 12, (13), 2844-2850.

109. Fazii, P.; Ciancaglini, E.; Sforza, G. R., Differential fluorescent staining method for detection of bacteria in blood cultures, cerebrospinal fluid and other clinical specimens. *European Journal of Clinical Microbiology & Infectious Diseases* **2002,** 21, (5), 373-378.

110. Biggerstaff, J. P.; Le Puil, M.; Weidow, B. L.; Prater, J.; Glass, K.; Radosevich, M.; White, D. C., New methodology for viability testing in environmental samples. *Molecular and Cellular Probes* **2006,** 20, (2), 141-146.

111. Gaforio, J. J.; Serrano, M. J.; Ortega, E.; Algarra, I.; Alvarez de Cienfuegos, G., Use of SYTOX green dye in the flow cytometric analysis of bacterial phagocytosis. *Cytometry* **2002,** 48, (2), 93-6.

112. Haase, S. B., Cell cycle analysis of budding yeast using SYTOX Green. *Curr Protoc Cytom* **2004,** Chapter 7, Unit 7 23.

113. Anaya, C.; Church, N.; Lewis, J. P., Detection and identification of bacterial cell surface proteins by fluorescent labeling. *Proteomics* **2007,** 7, (2), 215-9.

114. Ballou, B.; Ernst, L. A.; Waggoner, A. S., Fluorescence imaging of tumors in vivo. *Curr Med Chem* **2005,** 12, (7), 795-805.

115. Biver T, D. B. A., Secco F, Venturini M, Yarmoluk S, *Cyanine Dyes as Intercalating Agents: Kinetic and Thermodynamic Studies on the DNA/Cyan40 and DNA/CCyan2 Systems*. Biophysicsal Journal: 2005.

116. Burke, S. A.; Wright, J. D.; Robinson, M. K.; Bronk, B. V.; Warren, R. L., Detection of molecular diversity in Bacillus atrophaeus by amplified fragment length polymorphism analysis. *Appl Environ Microbiol* **2004,** 70, (5), 2786-90.

117. Marchioni, F.; Venturi, M.; Credi, A.; Balzani, V.; Belohradsky, M.; Elizarov, A. M.; Tseng, H.-R.; Stoddart, J. F., Polyvalent Scaffolds. Counting the Number of Seats Available for Eosin Guest Molecules in Viologen-Based Host Dendrimers. *Journal of the American Chemical Society* **2004,** 126, (2), 568-573.

Appendices

Appendix A: Mixing conditions for the kinetic studies

Investigation of whether pipetting is the time-limiting step for the homogeneous mixing of bacterial species with the thiacyanine dye solution was performed. To assure that the observed kinetics represent the dye-cell interactions rather than the dynamics of sample mixing, we conducted a series of fluorescence-quenching studies involving diffusion-limited bimolecular processes. Replicating the addition and mixing of the bacterial suspensions to the THIA solutions, we introduced methyl viologen (MV^{2+}) to solutions of 4.5 μM eosin Y (EY^{2-}) solution under identical mixing conditions. The quenching of the fluorescence of EY^{2-}, due the formation of charge-transfer complexes with MV^{2+} (100 μM),[117] exhibited time constants smaller than one second (Figure 48 a & b). The measured time constants for the bacterium-induced fluorescence enhancement of THIA, on the other hand, were in the order of seconds (Table 35-41). Therefore, the sample mixing and the diffusion of the cyanine dye to the bacterial exterior are not the rate-limiting steps of the observed fluorescence-enhancement processes.

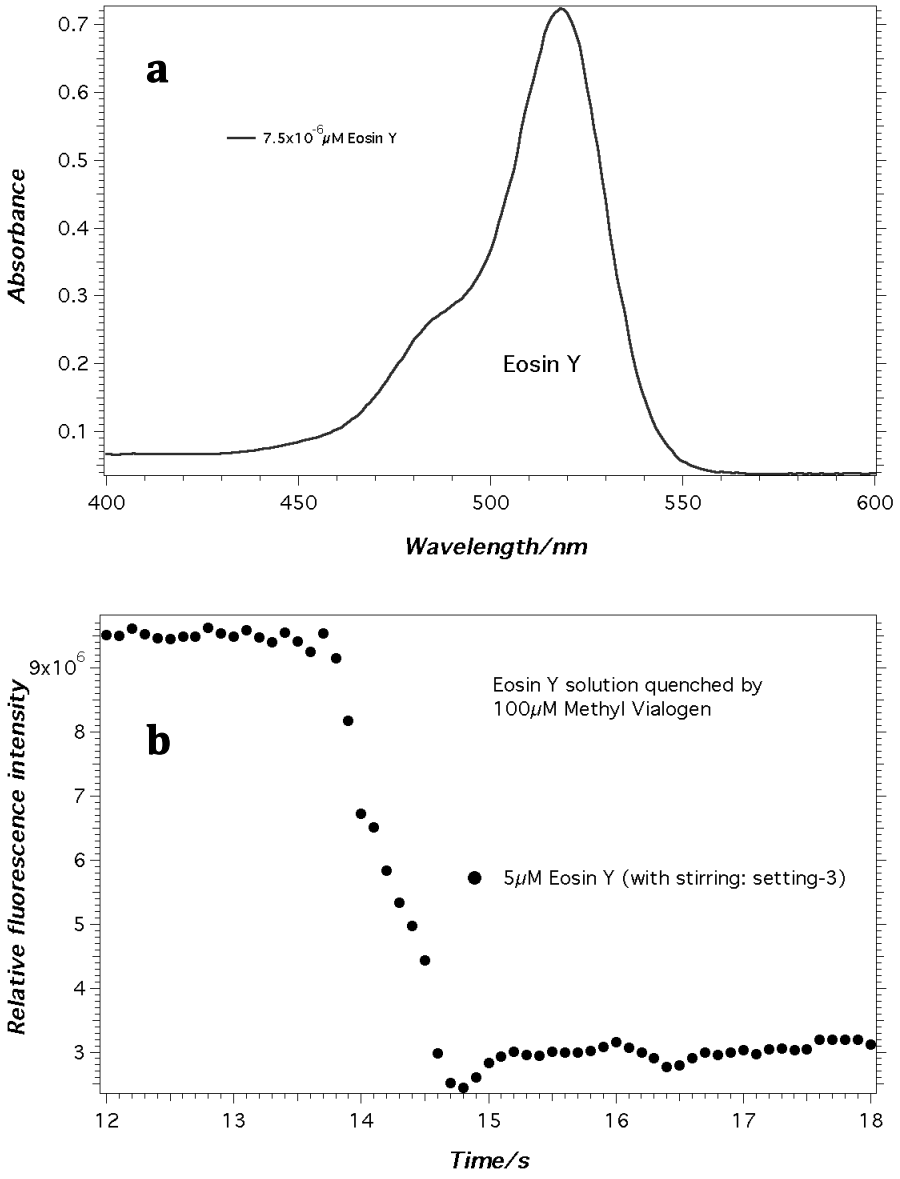

Figure 44. Plot of (a) the absorption spectra of 7.5 μM EY and (b) the dynamics of the quenching of the fluorescence of eosin Y (EY) with methyl viologen (MV) under conditions identical to the conditions of the kinetic measurements of the emission enhancement of THIA. Quenching exhibited time constants smaller than one second.

Appendix B: Growth rate and cell counting of bacterial species

To ensure that the bacterial cultures that we used for the sample preparation were in their growth phase, we constructed growth curves for the investigated bacterial species. The curves revealed that the investigated bacteria, cultured for 18–24 hours, were still in their active growth phase.

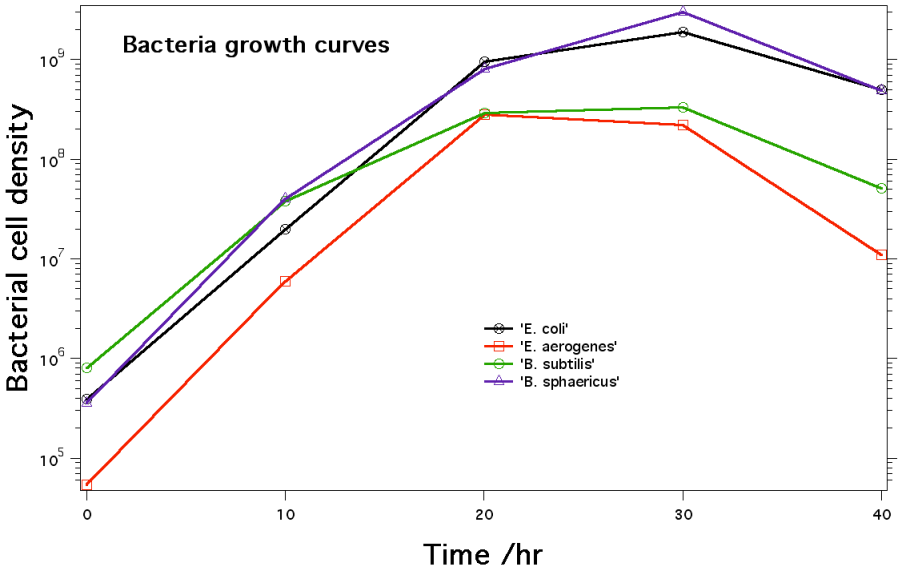

Figure 45. Growth curves for the investigated bacterial species *E. coli*, *E. aerogenes*, *B. subtilis* and *B. sphaericus* in Luria-Bertani (LB) broth at 37^{o} C

Appendix C: Cell imaging and vitality tests

C.1. Cell count

An improved Neubauer counting chamber was used to count the *E. coli*, *E. aerogenes* cells, *B. subtilis* and *B. sphaericus* samples (Paul Marienfeld GmbH & Co. KG) while imaging was done using a MicroMaster microscope with a 40x, NA = 0.65 (Fisher Scientific).

C.2. Vitality tests

Propidium iodide (Invitrogen) and SYTO 9 (Invitrogen) were used as the viability testing kit. Eosin Y (Sigma) and Methyl viologen (Aldrich) were used to evaluate the dependence of diffusion of mixing in the sample cuvette.

Viability testing was performed on the cell cultures to determine if the cell preparation had any negative impact on cell vitality. We conducted viability tests by adding cell suspensions to a 1-ml centrifuge tube containing a mixed solution with a final concentration of 1 μM Propidium iodide and 5 μM SYTO 9 in Tris buffer at pH 8.5 (2 mM).

C.3. Imaging cells

Bright-field micrographs were recorded using a CCD camera on an Accu-scope inverted microscope using a 40x objective, NA 0.4 (Accu-scope).

Fluorescent micrographs were recorded using a CCD camera on an Accu-scope inverted microscope illuminated with a 30-watt mercury arch lamp and fitted with filter cubes to block the broad-band excitation light and transmit the emitted

light (green light). Confocal micrographs were recorded using a Photo Multiplier Tube (PMT) (Zeiss LSM520) using a 63x water immersion objective (Images were zoomed in at approximately 630x magnification).

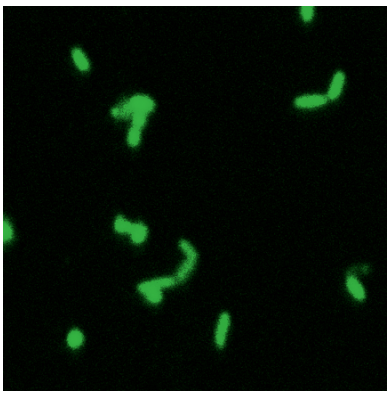

Figure 46. Confocal microscope image of *E. coli* cells stained with THIA in 2mM tris buffer. Image taken at 630x magnification.

Appendix D: Saturation fluorescence intensities for different dye concentrations and cell densities

We evaluated the fluorescence intensity as a function of bacterial cell density. The study revealed saturation of the bacterial species except for samples with a dye concentration of 60 μM. It is believed that the high dye concentration prevents light from penetrating the samples and so light can only interact with solution at a superficial depth close to the wall of the cuvette. Therefore, we believe that there is significant error in measurements from this sample.

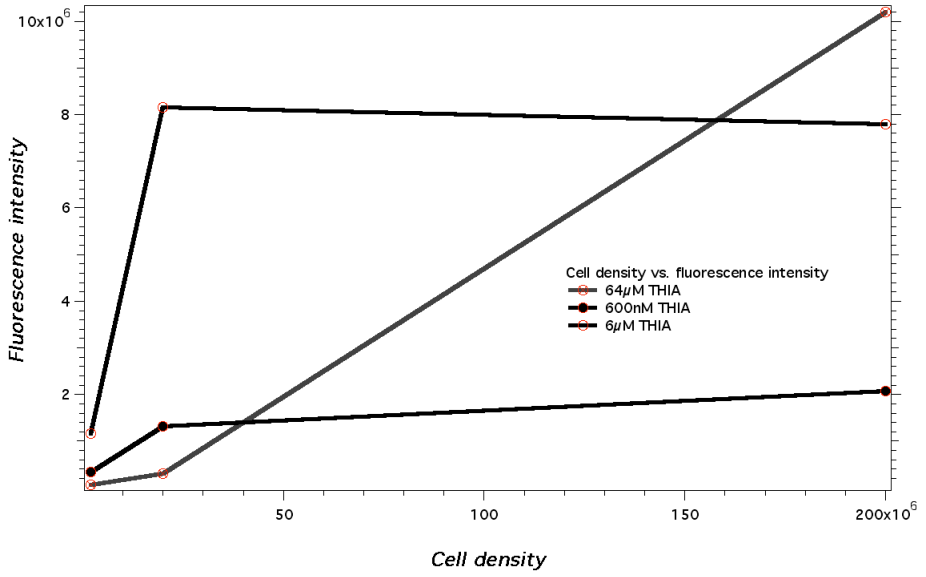

Figure 47. Plot of fluorescence intensity as a function of cell density for different cell densities.

Appendix E: Analysis of Variance (ANOVA)

Analysis of Variance or ANOVA is a statistical test that allows you to compare the means of three or more groups. The main question asked by an ANOVA analysis is as follows: Do the means of the quantitative variables depend on which group the sample is in?

There are several varieties of AVONA, including single-parameter ANOVA (or single-factor ANOVA) and two-parameter ANOVA (or two-way ANOVA). One-way ANOVA is used to test for differences among three or more independent groups. When there are only two means to compare, the t-test and the F-test are equivalent; the relation between ANOVA and t is given by $F = t^2$. Two-way ANOVA is used for repeated measurements. In this case, the same groups are used for each treatment.

ANOVA measures two sources of variation in the data and compares their relative sizes: variation BETWEEN groups and Variation WITHIN groups. The ANOVA F-statistic is a ratio of the Between-Group Variation divided by the Within-Group Variation. The fundamental technique is a partitioning of the total sum of squares (which is abbreviated SS) into components related to the effects used in the model. For example, we show the model for a simplified ANOVA with one type of treatment at different levels.

The number of degrees of freedom (abbreviated df) can be partitioned in a similar way and specifies the chi-square distribution, which describes the associated sums of squares. Below is an output from an ANOVA analysis performed using Excel.

Figure 48. Input data: Time constant from mono-exponential fits

60	4.6	2.0E+06
60	4.3	2.0E+06
60	4.7	2.0E+06
6.0	4.3	2.0E+07
6.0	4.8	2.0E+07
6.0	5.1	2.0E+07
0.6	3.7	2.0E+08
0.6	4.4	2.0E+08
0.6	4.6	2.0E+08

Table 49. Single-Factor ANOVA Analysis of data from Table 48.

Anova: Single Factor

SUMMARY

Groups	Count	Sum	Average	Variance
Column 1	7.0	2.0E2	28	8.8E2
Column 2	7.0	3.2E1	4.5	2.0E-1
Column 3	7.0	2.7E8	3.8E7	5.2E+15

ANOVA

Source of Variation	SS	df	MS	F	P-value	F crit
Between Groups	6.7E+15	2.0	3.4E+15	1.9	0.17	3.5
Within Groups	3.1E+16	18	1.7E+15			
Total	3.8E+16	20				